

Sunniva Vold

Zirconia-Supported Catalysts for Oxidation of NO to NO₂ in the Production of Nitric Acid

Master's thesis in Chemical Engineering and Biotechnology

Supervisor: Magnus Rønning

Co-supervisor: Jithin Gopakumar, Bjørn Christian Enger

June 2021

Sunniva Vold

Zirconia-Supported Catalysts for Oxidation of NO to NO₂ in the Production of Nitric Acid

Master's thesis in Chemical Engineering and Biotechnology
Supervisor: Magnus Rønning
Co-supervisor: Jithin Gopakumar, Bjørn Christian Enger
June 2021

Norwegian University of Science and Technology
Faculty of Natural Sciences
Department of Chemical Engineering



Preface

This project is a part of industrial Catalysis Science and Innovation (iCSI), a project initiated in 2015 in collaboration with Yara, Sintef, and NTNU under the name *Catalytic oxidation of NO to NO₂ for nitric acid production*. The work aims to find an efficient catalyst for oxidation of NO to NO₂ at favorable conditions, and several materials have been studied since the project started. Ata ul Rauf Salman was the first Ph.D candidate on the project, and published his Ph.D thesis summer 2019 after four years in the project. Several master students have contributed in the project, among them Beate Meisland Østrådt, who wrote her thesis: *Supported Manganese Oxide Catalysts for NO Oxidation in Nitric Acid Production* (2018). The promising results motivated to further investigation on manganese oxide catalysts supported on zirconium. Jithin Gopakumar joined the project in 2020, and is the present the doctoral candidate in the project.

The work has been supervised by Vice Dean and Professor Magnus Rønning and co-supervised by Jithin Gopakumar (Ph.D candidate) and Bjørn Christian Enger (Senior Research Scientist, SINTEF).

Declaration of Compliance

I, Sunniva Vold, hereby declare that this is an independent work according to the exam regulations of the Norwegian University of Science and Technology (NTNU).

Signature:

Trondheim, Norway 14.06.21



Sunniva Vold

Acknowledgement

This master thesis is the final work of the five-year integrated master program Chemical Engineering and Biotechnology at the Norwegian University of Science and Technology (NTNU). The master thesis is written for the Catalysis group, a part of the Chemical Engineering department at NTNU.

I want to express my gratitude to my supervisor Magnus Rønning for his continuous guidance, support, and encouragement during the year. He has been available to help whenever it was needed. I appreciate the opportunity to be a part of this project.

Secondly, I would like to thank my co-supervisor, Jithin Gopakumar, who is the doctoral candidate for the project. He has been available whenever needed, patient, and has been a driving force in the project. He has my sincerest gratitude for the continuous help, motivation, and guidance. Without him and his hard work, I would not have had an experimental rig to obtain results. We have worked in close cooperation, and it has been a pleasure. I wish him all the best in the continuation of the project. I would also like to thank Bjørn Christian Enger, Senior Research Scientist at Sintef, who attended weekly meetings throughout the year to support and contribute valuable help.

I would like to thank the Catalysis group engineers Estelle Vanhaecke, Karin Wiggen Dragsten and Anne Hoff. They have been giving great help and guidance inside and outside the laboratories and attributed to the great work atmosphere in the catalysis group.

Finally, I will thank my fellow students writing a master's for the catalysis group and the other Ph.D. candidates and postdoctoral researchers in the catalysis group. It has been a great working atmosphere in the group, and I am very grateful for all the good conversations and help.

Contents

Preface	iii
Acknowledgement	iv
List of Figures	xiii
List of Tables	xvii
Nomenclature	xix
Abstract	xxiii
Sammendrag	xxv
1 Introduction	1
1.1 Background	1
1.2 State of the art	1
1.3 Motivation	2
1.4 Strategy	3
2 Nitric Acid Production	5
2.1 History	5
2.2 Ostwald Process	5
3 Catalytic Oxidation of NO	9
3.1 Manganese Based Catalyst	9
3.2 Bimetallic catalyst	10
3.3 Zirconium Oxide as Support	12
4 Theory	13

4.1 Catalyst Preparation	13
4.1.1 Incipient Wetness Impregnation	13
4.1.2 Calcination	14
4.2 Characterization	14
4.2.1 Thermogravimetric analyses	14
4.2.2 Nitrogen Adsorption	15
4.2.3 Hydrogen temperature programmed reduction	17
4.2.4 X-ray diffraction	18
4.3 Activity Measurement	19
4.3.1 Fourier-transform infrared spectroscopy Gas Analyzer	19
5 Materials and Methods	21
5.1 Catalyst preparation	21
5.2 Catalyst Characterization before Activity Testing	22
5.2.1 Thermogravimetric analyses	22
5.2.2 Nitrogen Adsorption	22
5.2.3 Temperature Programmed Reduction	22
5.2.4 X-ray Diffraction	23
5.3 Activity Testing	23
5.4 Catalyst Characterization after Activity Testing	27
5.4.1 X-ray Diffraction	27
6 Results and Discussion	29
6.1 Characterization Before Activity Testing	29
6.1.1 TGA	29
6.1.2 Nitrogen Adsorption	30
6.1.3 Temperature programmed reduction	31
6.1.4 XRD	33
6.2 Catalytic Activity	35

6.2.1 Blank Run	35
6.2.2 Zirconia	36
6.2.3 Conversion and Experimental Challenges	37
6.2.4 Effect of Temperature	38
6.2.5 Steady-state Conditions	51
6.3 Characterization After Activity Testing	59
7 Conclusion and future work	63
7.1 Conclusions	63
7.2 Future Work	64
A Catalyst Preparation	I
A.1 Preparation Calculations	I
A.2 Used Measurements	III
B Characterization Results	V
B.1 Nitrogen Adsorption	V
B.2 TPR	VI
B.3 XRD	VII
C Catalytic Activity Measurements	IX
C.1 Amounts used in Activity Measurements	IX
C.2 Total NO conversion	IX
C.3 Catalytic Conversion	XI
C.3.1 Effect of Temperature	XII
C.3.2 Temperature Dependency	XV
C.4 Steady-state conditions	XVI
C.5 Characterization after Activity Measurements	XIX
C.5.1 XRD	XIX
D Flow Scheme of Rig 2.1	XXIII

List of Figures

2.1	The Ostwald process, illustrated in a block diagram. Step 1: Catalytic oxidation of ammonia with air, 2: NO oxidation and 3: NO ₂ react with water. Adapted from Thiemann, Scheibler, and Wiegand [17].	6
2.2	Obtained from G. D Honti, <i>The Nitrogen Industry</i> , 1976 [12].	7
3.1	The suggested mechanism of NO oxidation over supported manganese oxide catalysts in partially simulating nitric acid condition, suggested and illustrated by Salman <i>et al.</i> [28].	10
3.2	Crystal structures of α -, β -, γ - and δ -MnO ₂ catalysts, illustrated by Chen <i>et al.</i> [11].	10
3.3	The reaction routes on Mn/TiO ₂ and Mn/ZrO ₂ catalysts proposed by Zhao <i>et al.</i> [44].	12
4.1	Transport phenomena involved in incipient wetness impregnation. The solute migrates into the pore from the left to the right in the figure. Reprinted from [50].	14
4.2	Illustration of different layers during physical adsorption. Adapted from Chorkendorff and Niemantsverdriet [46].	15
4.3	Types of physisorption isotherms and hysteresis loops, obtained from Sing <i>et al.</i> , 1985 [60].	17
4.4	X-rays are scattered by the atoms in an ordered lattice. The spacing between the lattice planes can be calculated using the angles of maximum intensity and allowing further identification of phases in a sample. Diffractograms are measured as a function of the angle 2θ and formed by a small fraction of the particles. Reprinted from [46, 63].	18
5.1	A illustration of the reactor used in the activity testing of the catalysts in nitric acid plant conditions. a) represents the reactor after modifications and b) is before modifications. Drafted by Jithin Gopakumar.	24
5.3	The complete temperature program each catalyst were analyzed at. WHSV = 24 000 $Nml/h g_{cat}$ during all the experiments.	25

5.2 A simplified flow scheme of Rig 2.1 in Chemistry Hall D at NTNU in Trondheim, drafted by Jithin Gopakumar.	28
6.1 TGA curves for 20Mn with the relative differential plots, presenting the difference in DSC signal, mass percent and temperature as a function of time. The temperature was increased to 400 °C with a ramp rate of 10 °C/min and held for 6 hours before the temperature was increased to 900 °C with the same ramp rate.	29
6.2 The TPR curves for the zirconia-supported manganese catalysts.	32
6.3 The H ₂ -TPR profile of two zirconia-supported manganese oxide catalysts with 5 and 20 wt% manganese loading with promotion of 1 wt% silver and one zirconia supported silver catalyst with 5wt% silver loading.	33
6.4 XRD patterns of ZrO ₂ , 5Mn, 20Mn and 5Ag in two separate plots. The settings were 40 kV and 40 mA with a wavelength of 1.54060 Å employing Cu K α radiation.	34
6.5 The NO conversion as a function of temperature for gas-phase reaction and SiC in two different particle fractions and a mix of the two particle sizes from 50-400 °C in dry conditions and 110-400 °C in wet conditions. The ramp rate was 5 °C/min and pressure at 1 bar with WHSV = 24000 Nml/h · g _{cat} . The NO ₂ level considering the thermodynamic equilibrium of this reaction is represented as a grey line.	36
6.6 The NO conversion as a function of temperature for the zirconium oxide support, both dry and wet temperature ramp from 50 to 400 °C and 110 to 400 °C with a ramp rate of 5 °C/min at 1 bar with WHSV = 24000 Nml/h · g _{cat} . SiC in 30 mesh fraction is presented in both plots, and SiC in a mixed fraction in addition in the wet run.	37
6.7 The catalytic NO conversion (%), $x_{NO,c}$, of 5Mn Dry 1 and 2 compared with 5Ag Dry 1 and 2 from 50-400 °C with a ramp rate of 5 °C/min. The WHSV = 24000 Nml/h · g _{cat} , and pressure at 1 bar.	39
6.8 The catalytic NO conversion (%), $x_{NO,c}$, from 50-400 °C with a ramp rate of 5 °C/min. The WHSV = 24000 Nml/h · g _{cat} , and pressure is 1 bar.	40
6.9 The temperature dependency of the catalytic activity for 5Ag and 5Mn presented as the slope of catalytic NO conversion $x_{NO,c}$ as a function of temperature in the range from 250 to 350°C.	41
6.10 The NO conversion (%) of 5Mn, 5Mn-1Pt and 5Mn-1Ag in dry and wet conditions from 50-400 °C and 110-400 °C with a ramp rate of 5 °C/min. WHSV = 24000 Nml/h · g _{cat} at 1 bar.	42
6.11 The temperature dependency of the catalytic activity for 5Mn, 5Mn-1Pt and 5Mn-1Ag presented as the slope of catalytic NO conversion $x_{NO,c}$ as a function of temperature in the range from 250 to 350 °C.	43

6.12 The NO conversion (%) of 5Mn and 20Mn in dry and wet conditions from 50-400 °C and 110-400 °C with a ramp rate of 5 °C/min respectively. $WHSV = 24000 \text{ Nml/h} \cdot g_{cat}$ and pressure at 1 bar.	44
6.13 The temperature dependency of the catalytic activity for 5M and 20Mn presented as the slope of catalytic NO conversion $x_{NO,c}$ as a function of temperature in the range from 250 to 350 °C.	45
6.14 The total NO conversion of 5Mn and 20Mn as a function of temperature and the TPR spectrum of the same catalysts to see the correlation between the onset temperature of catalytic activity and reduction temperature.	45
6.15 The NO conversion (%) of 20Mn, 20Mn-1Pt and 20Mn-1Ag in dry and wet conditions from 50-400 °C and 110-400 °C with a ramp rate of 5 °C/min. $WHSV = 24\ 000 \text{ Nml/h} \cdot g_{cat}$ at 1 bar.	46
6.16 The temperature dependency of the catalytic activity for 20Mn, 20Mn-1Pt and 20Mn-1Ag presented as the slope of catalytic NO conversion $x_{NO,c}$ as a function of temperature in the range from 250 to 350°C.	47
6.17 The temperature dependency of the catalytic activity for the catalysts presented as the slope of catalytic NO conversion $x_{NO,c}$ as a function of temperature in the range from 250 to 350 °C.	48
6.18 The NO conversion (%) of 5Mn Dry 1, water-pretreatment (5Mn 1h H ₂ O Dry 1), pre-oxidized (5Mn 2h O ₂ Dry 1) and 5Mn Dry 2 from 50 to 400 °C with a ramp rate of 5 °C/min. $WHSV = 24\ 000 \text{ Nml/h} \cdot g_{cat}$, and pressure at 1 bar.	49
6.19 The NO conversion (%) of 20Mn-1Pt with and without pretreatment in H ₂ (20Mn-1Pt vs 20Mn-1Pt Reduced) in dry and wet conditions from 50-400 °C and 110-400 °C with a ramp rate of 5 °C/min. $WHSV = 24\ 000 \text{ Nml/h} \cdot g_{cat}$ at 1 bar.	50
6.20 The temperature dependency of the catalytic activity for 20Mn, 20Mn-1Pt, 20Mn-1Pt Reduced and 20Mn-1Ag presented as the slope of catalytic NO conversion $x_{NO,c}$ as a function of temperature in the range from 250 to 350°C.	51
6.21 The steady-state runs at 250 °C (in dashed lines) and 350 °C for 5Ag and 5Mn, where the temperature program follows dry-wet-dry-wet conditions with two hours each test run. The gas-phase contribution is shown as SiC. $WHSV = 24\ 000 \text{ Nml/h} \cdot g_{cat}$, and pressure at 1 bar.	52
6.22 The steady-state runs at 250 °C (in dashed lines) and 350 °C for 5Mn, 5Mn-1Pt and 5Mn-1Ag, where the temperature program follows dry-wet-dry-wet conditions with two hours each test run. The gas-phase contribution is shown as SiC. $WHSV = 24000 \text{ Nml/h} \cdot g_{cat}$, and pressure at 1 bar.	53
6.23 The steady-state runs at 250 °C (in dashed lines) and 350 °C for 5Mn and 20Mn, where the temperature program follows dry-wet-dry-wet conditions with two hours each test run. The gas-phase contribution is shown as SiC. $WHSV = 24\ 000 \text{ Nml/h} \cdot g_{cat}$, and pressure at 1 bar.	54

6.24	The steady-state runs at 250 °C (in dashed lines) and 350 °C for 20Mn, 20Mn-1Pt and 20Mn-1Ag, where the temperature program follows dry-wet-dry-wet conditions with two hours each test run. The gas-phase contribution is shown as SiC. $WHSV = 24\ 000\ Nml/h \cdot g_{cat}$, and pressure at 1 bar.	56
6.25	The total conversion, x_{NO} , is presented at 250 and 350 °C for each catalyst. SiC is displayed, presenting the gas-phase reaction conversion The conversion is an average calculated from the last hour within each steady-state experiment.	57
6.26	The reaction rate, r_{NO} [$\mu mol/(g_{cat}s)$], calculated from total NO conversion of the zirconia-supported manganese catalysts during the second wet temperature scan at 250 °C (blue line) and 350 °C (red line).	58
6.27	The %-change within each steady-state experiment is displayed in 6.27a and 6.27b at 250 and 350 °C for each catalyst.	59
6.28	The settings were 40 kV and 40 mA with a wavelength of 1.54060 Å employing Cu $K\alpha$ radiation. γ -MnO ₂ (●) is indicated with a dot and Mn ₂ O ₃ (★) is indicated with a star.	60
6.29	XRD patterns of 20Mn-1Pt (with pretreatment in H ₂) before and after catalytic activity measurements. The settings were 40 kV and 40 mA with a wavelength of 1.54060 Å employing Cu α radiation. γ -MnO ₂ (●) is indicated with a dot and Mn ₂ O ₃ (★) is indicated with a star. The peak indicated with a square is assumed to be Mn _{0.5} Pt _{0.5} O ₂ (■).	62
B.1	The isotherm linear plot and BET surface area plot for the zirconia support.	V
B.2	The BJH desorption average pore size distribution for zirconia.	VI
B.3	The H ₂ -TPR profile of the zirconia-supported manganese oxide catalysts.	VI
B.4	XRD patterns of zirconia support and two manganese on zirconia with 20 and 5 wt%. The specific MnO ₂ peaks are indicated with a dot.	VII
C.1	The total NO conversion (%) of the manganese catalysts from 110 – 400°C with a ramp rate of 5 °C/min. $WHSV = 24\ 000\ Nml/h \cdot g_{cat}$ and pressure at 1 bar.	X
C.2	The total NO conversion (%) of the manganese catalysts from 110 – 400°C with a ramp rate of 5 °C/min. $WHSV = 24000\ Nml/h \cdot g_{cat}$ and pressure at 1 bar.	X
C.3	The total NO conversion (%) of 20Mn-1Pt with and without pretreatment in the first and second temperature scan in dry conditions from 50 – 400°C with a ramp rate of 5 °C/min. $WHSV = 24000\ Nml/h \cdot g_{cat}$ and pressure at 1 bar.	XI
C.4	The catalytic NO conversion of the catalysts at 250°C extracted from the temperature dependency experiments.	XII
C.5	The catalytic NO conversion of the catalysts at 350°C extracted from the temperature dependency experiments.	XIII

C.6 The total NO conversion (%) of the 5 wt% manganese oxide catalysts from 110 – 400°C with a ramp rate of 5 °C/min. $WHSV = 24000 \text{ Nml/h} \cdot g_{cat}$ and pressure at 1 bar.	XIII
C.7 The catalytic NO conversion (%) of the 20 wt% manganese oxide catalysts from 110 – 400°C with a ramp rate of 5 °C/min. $WHSV = 24000 \text{ Nml/h} \cdot g_{cat}$ and pressure at 1 bar.	XIV
C.8 The NO conversion (%) of 20Mn-1Pt Dry 1 and 2 compared with 5Mn-1Pt Dry 1 and 2 from 50 – 400°C with a ramp rate of 5°C/min in dry conditions at 1 bar. $WHSV = 24000 \text{ Nml/h} \cdot g_{cat}$	XIV
C.9 The NO conversion (%) of 20Mn-1Ag Dry 1 and 2 compared with 5Mn-1Ag Dry 1 and 2 from 50 – 400°C with a ramp rate of 5°C/min in dry conditions at 1 bar. $WHSV = 24000 \text{ Nml/h} \cdot g_{cat}$	XV
C.10 The catalytic NO conversion is extracted from the temperature scan test runs at 250°C and 350°C.	XV
C.11 XRD patterns of ZrO ₂ and 5Ag before and after catalytic activity measurements. The settings were 40 kV and 40 mA with a wavelength of 1.54060 Å employing Cu α radiation. Ag ⁰ (●) is indicated with a hexagon.	XX
C.12 XRD patterns of 5Mn and 20Mn before and after catalytic activity measurements. The settings were 40 kV and 40 mA with a wavelength of 1.54060 Å employing Cu α radiation. γ-MnO ₂ (●) is indicated with a dot and Mn ₂ O ₃ (★) is indicated with a star.	XX
C.13 XRD patterns of 5Mn-1Ag and 20Mn-1Ag before and after catalytic activity measurements. The settings were 40 kV and 40 mA with a wavelength of 1.54060 Å employing Cu α radiation. γ-MnO ₂ (●) is indicated with a dot and Mn ₂ O ₃ (★) is indicated with a star.	XXI
C.14 XRD patterns of 5Mn-1Pt and 20Mn-1Pt before and after catalytic activity measurements. The settings were 40 kV and 40 mA with a wavelength of 1.54060 Å employing Cu α radiation. γ-MnO ₂ (●) is indicated with a dot and Mn ₂ O ₃ (★) is indicated with a star.	XXI

List of Tables

5.1	List of the different catalysts prepared by incipient wetness method. The number represents the weight percent, and all the manganese is present as a metal oxide.	21
5.2	The name of each temperature program performed in nitric acid plant conditions with dry and wet feed. In all the test runs the WHSV of 24 000 Nml/h_{cat} at 1 bar.	25
5.3	Different pretreatments tested on 5Mn and 20Mn-1Pt.	26
5.4	Amount of different particle sizes in the test runs with SiC in the reactor.	26
6.1	Structural data from N_2 physisorption giving the BET surface area, the BJH desorption cumulative pore volume and BJH desorption average pore diameter for the catalysts.	30
6.2	The Scherrer equation was used to calculate the crystallite size, $d_p = \frac{K\lambda}{B_p(2\theta)\cos(\theta)}$, where λ , $B_p(2\theta)$ and θ is given in radians. The specific peak for MnO_2 is where 2θ equals 37.3° , and for this peak the crystalline size of MnO_2 is calculated. θ is half of the diffraction angle, and the wavelength λ equals 1.54060 Å. The shape factor was chosen to be 0.9, and the dispersion was calculated from the crystalline size by the formula $D = \frac{1}{d_p}$.	35
6.3	The temperature dependency, represented as the slope from the temperature interval between 250-350 °C of each catalyst during the temperature scans in dry and wet conditions.	48
6.4	The first deactivation for 5Ag and 5Mn when water is added, the regenerability from Dry 1 to Dry 2, the second deactivation with water introduced and the regenerability between the wet test runs at 350 and 250 °C.	53
6.5	The first deactivation for 5Mn, 5Mn-1Pt and 5Mn-1Ag when water is added in the feed, the regenerability from Dry 1 to Dry 2, the second deactivation with water introduced and the regenerability between the wet test runs at 350 and 250 °C.	54

6.6	The first deactivation of 5Mn and 20Mn when water is added in the feed, the regenerability from Dry 1 to Dry 2, the second deactivation with water introduced and the regenerability between the wet test runs at 350 °C and 250 °C.	55
6.7	The first deactivation of the catalyst when water is added, the regenerability from Dry 1 to Dry 2, the second deactivation with water introduced and the regenerability between the wet test runs for 20Mn, 20Mn-1Pt and 20Mn-1Ag at 350 and 250 °C.	56
6.8	The reaction rate, r_{NO} [$\mu\text{mol} \cdot \text{g}_{\text{cat}}^{-1} \cdot \text{s}^{-1}$] for the different catalysts at 250 °C and 350 °C.	57
6.9	The Scherrer equation was used to calculate the crystallite size, $d_p = \frac{K\lambda}{B_p(2\theta)\cos(\theta)}$, where λ , $B_p(2\theta)$ and θ is given in radians. The specific peak for MnO_2 is where 2θ equals 37.3° , and for this peak the crystalline size of MnO_2 is calculated. θ is half of the diffraction angle, and the wavelength λ equals 1.54060 Å. The shape factor was chosen to be 0.9, and instrumental line broadening is 0.05. <i>Before</i> is crystallite size before catalytic activity testing, and <i>After</i> is the crystallite size after approximately 20 hours on stream.	61
A.1	Total weight of prepared catalyst and incipient wetness point for the used zirconia.	I
A.2	Molar mass of chemicals used in the preparation of the catalysts.	I
A.3	An overview of the catalysts, the wt% of active material and promoter, and the support as % of the total weight.	II
A.4	Amounts of zirconia, metal precursor and deionized water used in catalyst preparation for 5Mn catalysts.	III
A.5	Amounts of zirconia, metal precursor and deionized water used in catalyst preparation for 20Mn catalysts.	III
A.6	Amounts of zirconia, metal precursor and deionized water used in catalyst preparation for 5Ag.	IV
B.1	The results of the different manganese oxide catalysts from TPR show the temperatures where reduction peaks occurs in Figure B.3. $T_{\text{o,red}}$ indicates the onset temperature, where the catalyst starts the consumption of H_2 . $T_{\text{M}0}$ gives information about the first reduction appearing before the highest peak. $T_{\text{M}1}$ indicates the temperature occurring at the highest peak, while the remaining $T_{\text{M}2}$, $T_{\text{M}3}$ and $T_{\text{M}4}$ indicate high temperature peaks.	VII
C.1	Mass of catalyst, zirconia and SiC used in activity measurements, and weight after the activity experiments.	IX
C.2	An overview of which background used to subtract NO conversion from the total NO conversion. SiC mix contained 2.75 g of 30 mesh particle size and 0.5 g 53-90 μm article fraction.	XII

-
- C.3 The temperature dependency for each catalyst in the four temperature programs in dry and wet conditions presented as the slope of catalytic conversion as a function of temperature, the R^2 and p-value of each regression calculation. XVI
- C.4 NO conversion during two hours at 250°C and 350°C at 1 bar with $WHSV = 24000 Nm^3 \cdot h^{-1} \cdot g_{cat}^{-1}$ where $t_0 = 0$ min , $t_1 = 60$ min and $t_2 = 120$ min. The %-change between the time increments are presented together with the overall %-change from t_0 to t_2 XVII
- C.5 The %-change within each steady-state experiment at 350° where t_0 represent the start time and t_1 is the final time at 120 minutes. The NO conversion is total conversion, and the gas-phase contribution is included in the conversion. XVIII
- C.6 The %-change within each steady-state experiment at 350° where t_0 represent the start time and t_1 is the final time at 120 minutes. The NO conversion is total conversion, and the gas-phase contribution is included in the conversion. XIX

Nomenclature

BET	Brunauer Emmett and Teller
BJH	Barrett-Joyner-Halenda
CEM	Control-Evaporation-Mixing
DRIFTS	Diffuse Reflectance Infrared Fourier Transform Spectroscopy Analysis
DSC	Differential Scanning Calorimetry
FTIR	Fourier Transform Infrared
FWHM	Full Width at Half Maximum
HRTEM	High-resolution transmission electron microscopy
LHHW	Langmuir-Hinselwood-Hougen-Watson
MvK	Mars van Krevelen
PFR	Plug Flow Reactor
SEM	Scanning Electron Microscopy
TCD	Thermal Conductivity Detector
TGA	Thermogravimetric analyses
TPR	Temperature Programmed Reduction
TPX	Temperature Programmed Techniques
VOC	Volatile Organic Compounds
WHSV	Weight Hourly Space Velocity
XRD	X-Ray Diffraction

Symbols

<i>Symbol</i>	<i>Description</i>
C	Constant in BET equation
p	Partial pressure
p_0	Saturation pressure
V	Volume
V_m	Adsorption volume
D	Metal dispersion
d	Distance between lattice planes
d_p	Average Crystallite size
K	Shape factor in Scherrer equation
ΔH_{r298}	Enthalpy of reaction at 289 K
a.u	Arbitrary unit
Ca	Carberry number
h	Hour
J	Joule
k	Rate constant
mol	Mole
min	Minute
NO _x	Nitrogen oxides
ppm	Parts per million
r_{NO}	Reaction rate of NO oxidation
SiC	Silicon Carbide
t	Time
wt%	Weight percentage
$x_{NO,c}$	Catalytic NO conversion
x_{NO}	Total NO conversion
Å	Ångstrom

Abstract

Nitric acid is primarily consumed to produce nitrate fertilizer and is a necessary chemical for modern agriculture produced using the Ostwald process. One of the three chemical steps in the process is the homogeneous gas-phase oxidation of nitric oxide (NO) to nitrogen dioxide (NO₂). If the bulky homogeneous reaction used in current state-of-art technology is displaced with a heterogeneous catalytic reaction, the oxidation process can be accelerated, and process intensification can be achieved.

Six zirconia-supported manganese oxide catalysts with two different loadings of manganese (5 and 20 wt%) and two promoters (1 wt% Pt and Ag) were synthesized by incipient wetness impregnation. In addition, one zirconia-supported silver catalyst was prepared by the same method. The catalysts were investigated as a function of temperature and time to evaluate their catalytic performance for NO oxidation in partially simulating nitric acid plant conditions with and without water at atmospheric pressure. Catalytic performance at 250 and 350 °C was highlighted due to favored working conditions at a nitric acid plant. The results revealed that 20 wt% manganese with 1 wt% silver on zirconia exhibited the best catalytic activity during the temperature scan test runs and at approximate steady-state condition experiments at 250 and 350 °C in dry and wet feed.

A minor difference in catalytic activity was observed comparing the unpromoted 5 and 20 wt% manganese catalysts, considering results from steady-state period of the experiments for two hours, indicating that the catalytic activity does not scale with the amount of manganese loaded on the catalyst. The molar ratio between Ag/Mn appears to affect the catalyst's reactivity, and 20 wt% manganese with 1 wt% silver on zirconia exhibited higher NO conversion than zirconia supported 5 wt% manganese with 1 wt% silver.

The inhibition effect of water occurred for the manganese oxide catalysts. However, the inhibition effect was reversible, and the activity was fully recovered upon returning to dry conditions. The zirconia-supported silver catalyst exhibits catalytic activity in the oxidation of NO but performed unsuccessfully relative to the manganese oxide catalysts. However, the inhibition effect of water is not observed for the silver catalyst as it achieves the same or higher catalytic activity in a wet feed.

Factors potentially affecting the catalytic activity were investigated by different characterization mechanisms involving N₂-adsorption, H₂-TRP, TGA, and XRD. The characterizations confirmed the presence of γ -MnO₂ after preparation and were obtained after the catalytic activity experiments. Results from XRD indicate that the high oxygen content in the feed regenerates the preferred oxidized state of the active MnO₂ phase resulting in good catalytic stability in the time frame studied. A possible deactivation was assumed to be due to a partially phase-transition of manganese and was observed for the unpromoted 20 wt% manganese catalyst detected in XRD. However, the partial phase-transition of manganese observed for the 20 wt% manganese with 1 wt% silver on zirconia did, in contrast, did not deactivate the catalyst but possibly enhanced catalytic activity. For the unpromoted catalysts, a correlation between reduction temperature from H₂-TPR and the onset temperature of catalytic activity, indicating that oxidation of NO over manganese oxide proceeds via a Mars van Krevelen mechanism.

Sammendrag

Salpetersyre er et viktig kjemisk produkt som hovedsakelig blir brukt til å produsere kunstgjødning av nitrater. Den industrielle prosessen for framstilling av salpetersyre foregår i tre hovedtrinn, kald Ostwaldprosessen. I det andre steget av denne prosessen skjer det en homogen gassfase reaksjon hvor nitrogen monoksid (NO) blir oksidert til nitrogen dioksid (NO₂). Om denne homogene reaksjonen endres til en heterogen katalytisk reaksjon, kan oksidasjonen akselereres og en mer effektiv og lønnsom prosess i framstilling av salpetersyre kan oppnås.

I dette arbeidet ble seks manganoksid på zirkoniumdioksid katalysatorer fremstilt ved *incipient wetness impregnation* metoden med to forskjellige belastninger av mangan, henholdsvis 5 og 20 vekt%, og to promotorer (1 vekt% sølv og platina). I tillegg ble en sølvkatalysator på zirkoniumdioksid fremstilt etter samme metode. Katalysatorene ble undersøkt som en funksjon av temperatur og tid for å evaluere deres katalytiske ytelse for NO-oksidasjon ved delvis simulering av salpetersyreanleggsforhold med og uten vann ved atmosfæretrykk. Katalytisk ytelse på 250 og 350 ° C ble undersøkt når dette er ønskelige temperaturforhold ved et salpetersyreanlegg. Resultatene avdekket at 20 vekt% mangan med 1 vekt% sølv på zirkoniumdioksid viste den beste katalytiske aktiviteten under temperaturskanningen og ved konstante forhold ved 250 og 350°C.

Det ble observert en minimal forskjell i katalytisk aktivitet ved sammenlikning av katalysatorene med 5 og 20 vekt% mangan, noe som indikerer at den katalytiske aktiviteten ikke skalerer med mengden aktivt materialet på katalysatoroverflaten. Det molare forholdet mellom sølv og mangan ser ut til å spille en rolle når 20 vekt% mangan med 1 vekt% sølv viser høyere katalytisk aktivitet enn 5 vekt% mangan med 1 vekt% sølv.

Når vann introduseres, hindres den katalytiske aktiviteten for mangankatalysatorene. Denne hindrende effekten er regenerert når vann igjen fjernes, og katalysatorene opptrer like godt som før vann var introdusert. Sølv på zirkoniumdioksid viser noe katalytisk aktivitet, men lavt i forhold til mangan-katalysatorene. Det er allikevel verdt å merke seg at sølv-katalysatorens aktivitet ikke blir hindret av vann.

Faktorene som trolig påvirket den katalytiske aktiviteten ble undersøkt med ulike karakteriseringsmetoder inkludert N₂-adsorpsjon, temperatur programmert reduksjon (H₂-TPR), termogravimetrisk analyse (TGA) og røntgen diffraksjon (XRD). Resultatene fra XRD gjorde det klart at den ønskelige fasen av mangan (γ-MnO₂) var oppnådd i synteseprosessen, og forble i den fasen også etter den katalytiske aktiviteten var testet. En mulig deaktivering ble antatt å være på grunn av en delvis faseovergang av mangan og ble observert for den ikke-promoterte 20 vekt% mangankatalysatoren, påvist i XRD. I motsetning har den delvise faseovergang av mangan observert for 20 vekt% mangan med 1 vekt% sølv, ikke deaktivert katalysatoren, men trolig forbedret katalytisk aktivitet.

Det ble funnet en korrelasjon mellom reduksjonstemperaturen fra TPR analysen og temperaturen mangan katalysatorene uten promotering viste katalytisk aktivitet. Funnet tyder på at oksidasjonen av NO over manganoksid går via en Mars-van Krevelen mekanisme.

Chapter 1

Introduction

1.1 Background

One of the UN's main goals is to end hunger, achieve food security, improve nutrition, and promote sustainable agriculture [1]. The goal includes reaching high standards of human welfare while maintaining long-term sustainability of the environment [2]. The increased focus on the global population growth leads to concerns that food production capacity will be insufficient to meet future demand [3]. According to FAO's predictions, food production needs to increase by approximately 70% by 2050 [4]. Farm land is a strictly limited resource, and as food demand increases a solution is to improve existing agriculture's productivity by applying fertilizers [3, 2, 5].

Balancing the nutrients in the ground by adding fertilizers is a possible way to gain higher crop yields and ensure healthy and robust growth [6]. The three main components of fertilizers are nitrogen, phosphorus, and potassium. The nitrogen comes from ammonium (NH_4^+) and nitrates (NO_3^-) produced from nitric acid. Approximately 70% of the annual global production of nitric acid is used for fertilizer production [7]. Yara, is one such fertilizer-producing company, which dominates the nitric acid market [8]. During the past century, they have continuously improved solutions to increase global food production.

Yara produces nitric acid by the Ostwald Process, where the nitric acid is obtained from ammonia in three steps, starting with catalytic oxidation of ammonia. The second step is the oxidation of nitric oxide (NO), and finally, the NO_2 reacts with water to yield nitric acid [9]. The second step is a gas-phase, third-order reaction, favored by low temperature and high pressure [10]. A more energy-efficient and economical production of nitric acid may be achieved by using a catalyst to oxidize NO.

1.2 State of the art

At the desired industrial boundary conditions in a modern pressurized nitric acid plant, no catalyst has yet been discovered for the NO oxidation. The main challenges is the high concentration of nitric oxide and the presence of water in the feed. There exists a wide range of studies at conversion levels below equilibrium regarding NO oxidation over a catalyst, primarily in research concerning NO_x emissions where NO is present in ppm-levels.

The current and broadly used catalysts for the NO oxidation for low concentration of NO include noble metals like Pt with its low activation temperature. Unfortunately, these metals are highly costly, and the availability is limited, leading to the search for noble-metal-free options [11].

Alternatives have been studied and exhibited catalytic activity involving transition metal oxide catalysts like copper, cobalt, and manganese [12]. Materials like asbestos and coke have also shown catalytic activity. When using cobalt, unwanted reactions occur with nitric acid, and the catalytic activity of coke is wholly inhibited when water is present [12]. None of the mentioned materials have shown enough promising results to be used under industrial conditions.

Manganese oxide supported by zirconia is less costly and has revealed good catalytic activity for converting NO in partially simulating nitric acid production conditions in research previously done in the project by Salman [13]. The results motivate for further research on zirconia-supported manganese oxide catalysts.

1.3 Motivation

The primary motivation for this research lies within the process intensification potential for industrial nitric acid production. The aim is to find an efficient catalyst for NO oxidation at conditions applicable to a nitric acid plant. If the bulky homogeneous reaction is replaced with a heterogeneous catalytic reaction, the oxidation process can be accelerated.

The effect of the catalyst enables an improvement in the recovery of high-quality heat in a compact system at 200-300 °C, as compared to the none-recoverable heat loss taking place by the homogeneous reaction in tubing downstream and between existing heat exchangers. The NO oxidation has a negative temperature dependency and the reaction rate decreases with increased temperature. Without the use of catalyst, the forward reaction is promoted by extracting heat in a series of heat exchangers and giving adequate residence time. As a result, there is a potential to decrease capital expenditure (CAPEX) when building new plants for nitric acid production [13].

Finally, this work aims to understand how the oxidation of NO is affected over zirconia-supported manganese catalysts regarding metal loading and promotion of platinum and silver in dry and wet partially simulating nitric acid plant conditions. The relevant positions of the envisaged catalytic unit in the industrial process defines the conditions of catalytic studies with a feed composition of 10 vol% NO, 6 vol% O₂, 15 vol% H₂O (when present), 1 bar and from 50 to 400°C.

To summarize, the motivation is to:

- Accelerate the NO oxidation reaction in the industrial production of nitric acid.
- Increase the potential for high-quality heat recovery.
- Substantial decrease in capital expenditure (CAPEX) for new nitric acid plants.
- Better understand the NO conversion over a catalyst regarding the amount of active material on the catalyst support in partially simulating nitric acid plant conditions.

- Better understand the NO conversion concerning the addition of reduction promoter (platinum and silver) to the zirconium-supported manganese catalysts in partially simulating nitric acid plant conditions.

1.4 Strategy

This work aims to continue investigating a new cost-efficient catalyst for NO oxidation under resembling nitric acid plant conditions, after promising results from the research done by Salman and Østrådt at an earlier stage of the project [13, 14]. They studied unpromoted manganese catalysts on different supports. In this work zirconia-supported manganese oxide catalysts without and with the promotion of silver and platinum have been studied under high concentrations of NO (10%).

During the autumn of 2020, six zirconia-supported manganese oxide catalysts and one zirconia-supported silver oxide catalyst were made and characterized in the course TKP4580 - *Chemical Engineering, Specialization Project*. The catalysts were prepared by the incipient wetness impregnation method and characterized by N₂ adsorption along with X-ray diffraction (XRD), temperature-programmed reduction (TPR), and Thermogravimetric analyses (TGA).

This master thesis is a continuation of the master project described above. Catalytic activity was studied as a function of temperature and time in a dedicated setup. Water is a fundamental part of the reaction mixture in the nitric acid plant. However, catalytic analyses were conducted both in the absence and presence of water to clarify the effect of water on the catalyst activity and structure. N₂ adsorption and XRD were repeated in this master, and the catalysts were further characterized after the catalytic activity experiment with X-ray diffraction.

Several challenges exist when studying an industrial process in the laboratory. It is essential to reduce the gas phase contribution favored by the higher concentration and residence time when studying the catalytic activity. The NO oxidation reaction is sensitive to small pressure drops and temperature gradients which is challenging to fully eliminate. A dedicated rig was already existed for this project [15], tailored to study the catalytic activity at atmospheric pressure. Before the catalytic activity experiments in this work, the rig was modified to optimize the experimental conditions where the reactor design was changed and lines before the gas-analyzer were shortened. The catalytic investigation was limited to nitric acid plant conditions with a feed containing 10 vol% NO, 6 vol% O₂, 15 vol% H₂O (when present) at 1 bar and from 50 to 400 °C and 110 to 400 °C (with water present).

Chapter 2

Nitric Acid Production

2.1 History

The beginning of nitric acid production dates back to the eighth century when Abū Mūsā Jābir ibn Hayyān prepared it from cyprus vitol, saltpeter, and alum [16]. Later, in 1658, Glauber distilled niter with oil of sulfuric acid to obtain nitric acid. It took another 100 years to prove oxygen in nitric acid, and not before 1816, the complete chemical position was found. Until 1924, nitric acid production resulted from Chile saltpeter and concentrated sulfuric acid [16].

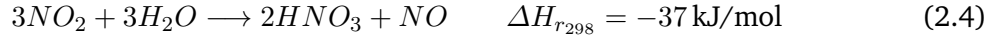
At the beginning of the twentieth century, there was a global need for more efficient farming. When the chemical industry started developing in Norway, the entrepreneur and engineer Sam Eyde had a central role. In 1903 Eyde met the Norwegian physicist and inventor Kristian Olaf Bernhard Birkeland. Together, they created an industrial process developing nitrate fertilizers. The nitrogen oxides were obtained by passing air through an electric arc, known to be the Birkeland-Eyde electric arc process for nitrogen fixation. A problem with the process was the low yield of nitric oxide and the vast need for electricity. Around 1910, Fritz Haber and Carl Bosch developed more efficient and less energy-intensive technology for nitrogen fixation, known as the Haber-Bosch process for ammonia production. Around the same time, the German scientist Wilhelm Ostwald invented a way to make nitric acid based on the catalytic oxidation of ammonia. When the Haber-Bosch process made ammonia commercially available and cheaper, the Birkeland-Eyde process was replaced with the Haber-Bosch and Ostwald process. Today, this is still the production process for all nitric acid [7].

2.2 Ostwald Process

The Ostwald process's overall reaction is presented in Equation 2.1 and is highly exothermic.



The Ostwald process contains three main chemical reactions, starting with a catalytic burning of ammonia, followed by NO oxidation, and finally NO₂ reacting with water [12]. The reaction equations are presented in Equation 2.2, 2.3 and 2.4 respectively.



In Equation 2.2 the optimal producing conditions are high temperature, and ammonia is oxidized with air over a platinum gauze catalyst with rhodium added for strengthening properties [10]. Two side reactions occur during the catalytic oxidation of ammonia, resulting in undesired products involving the formation of nitrous oxide (N_2O), a potent greenhouse gas. In the chemical industry, nitric acid production is the largest source of nitrous oxide as a pollutant [7]. Being one of the leading nitric acid producers, YARA has developed a cobalt-alumina spinel catalyst that reduces the nitrous oxide levels by 80% [7].

The following step in the Ostwald process, NO oxidation, is a homogeneous gas-phase reaction favored by low temperature and high pressure being in equilibrium with its dimer N_2O_4 . Finally, nitric acid is achieved when NO_2 react with water, favored by high pressure [12].

A schematic presentation of the Ostwald process is illustrated in Figure 2.1

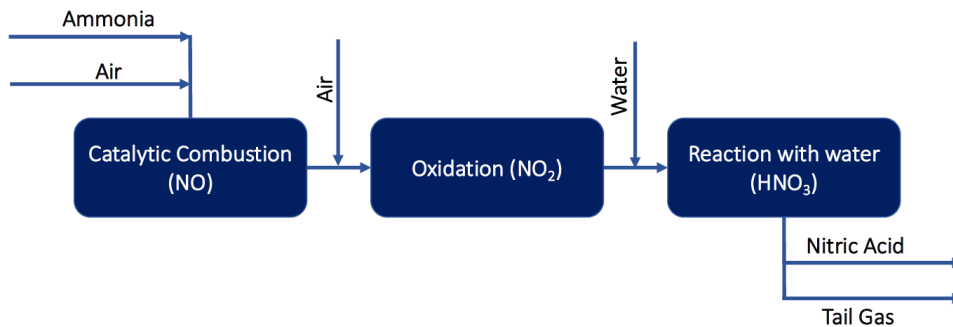


Figure 2.1: The Ostwald process, illustrated in a block diagram. Step 1: Catalytic oxidation of ammonia with air, 2: NO oxidation and 3: NO_2 react with water. Adapted from Thiemann, Scheibler, and Wiegand [17].

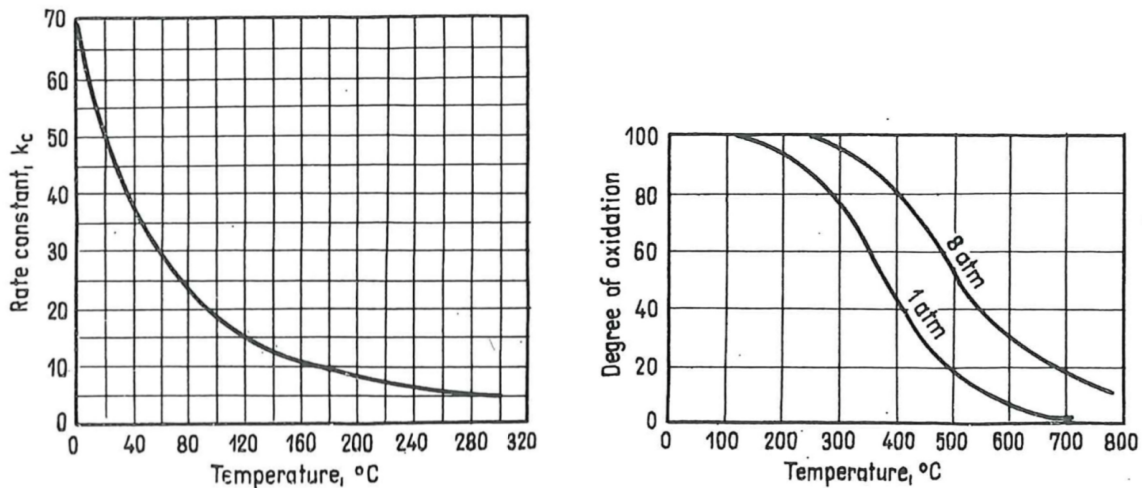
The non-catalyzed NO oxidation, favored by low temperature and high pressure is one of the few third-order reactions, making it special [10]. The reaction rate, r , is described as,

$$\frac{dp_{NO_2}}{d\tau} = -r_{NO} = k \cdot (p_{NO})^2 \cdot p_{O_2} \quad (2.5)$$

where p_{NO} , p_{O_2} and p_{NO_2} are the partial pressure of NO, O_2 and NO_2 respectively. The reaction rate constant, k , increases with decreasing temperature, making it favored by low temperatures both thermodynamically and kinetically [10]. The reaction rate is dependent on the oxygen content and the second power of the NO content, meaning the oxidation happens

faster the higher the initial concentration of either active component [12]. When the oxidation approaches equilibrium at high temperatures, the reaction will slow down considerably due to the low NO concentration.

Illustrated in Figure 2.2a in 2.2, the NO oxidation is greatly temperature-dependent, and the rate constant drops rapidly when the temperature increases. In Figure 2.2b in 2.2 the degree of oxidation is plotted as a function of temperature, at 1 and 8 atm [12]. The equilibrium shifts towards oxidation when pressure increases and temperature decreases.



(a) Rate constant of NO oxidation as a function of temperature. (b) Equilibrium degree of oxidation of NO as a function of the temperature for 1 and 8 atm.

Figure 2.2: Obtained from G. D Honti, *The Nitrogen Industry*, 1976 [12].

When water is present in the gas feed, generated by the combustion of ammonia, the reaction will consume NO_2 and produce NO. Consequently, the gas mixture's degree of oxidation decreases [12].

In a typical nitric acid plant, the gas composition of the exit gas after the first ammonia oxidation step, shown in Figure 2.1, is approximately 10 vol% NO, 6 vol% O_2 and 15 vol% H_2O . As mentioned, the different steps in the Ostwald process favor high and low pressure. When designing a nitric acid production plant, the operating pressure is important, resulting in two main applied process designs: single-pressure and dual-pressure plants. The single-pressure processes are generally operated at high pressure (7-12 bar), and higher ammonia oxidation catalyst temperature, making the energy recovery more efficient. In the dual-pressure process, a compressor is placed between the ammonia oxidation and when NO_2 reacts with water to yield nitric acid. The oxidation of ammonia is performed at 4-5 bar and the water-reaction with NO_2 at 10-15 bar [10].

Since Ostwald patented the process in 1902, efforts have been carried out to find a suitable catalyst for the NO oxidation under nitric acid plant conditions [12]. The slowness of the reaction rate before reaching equilibrium is one of the main challenges in this research. According to the Arrhenius law, catalytic activity is often favored by higher temperatures, but as explained, thermodynamically the NO conversion is higher at lower temperatures. It is desired to find an active catalyst at low temperatures, such that maximum NO conversion is achieved [13].

Chapter 3

Catalytic Oxidation of NO

3.1 Manganese Based Catalyst

Manganese oxide presents an intriguing class of heterogeneous catalysis because of the wide range of functional domains. For instance, utilization in both gas and liquids phase reactions, as well as in electrochemical devices. Manganese oxide has high chemical stability, and the redox performance enables various intermediate Mn oxidation states and crystalline phases [18, 19, 20, 21, 22, 23]. Over the last years, manganese oxide has been considered in the research based on diesel exhaust conditions. Mn is less expensive than the noble metals like Pt and has a low environmental impact.

For transition metal oxides, such as manganese oxide, it is trusted that the oxidation of organic molecules involves a Mars and van Krevelen (MvK) mechanism where the organic molecule is oxidized by lattice oxygen of metal oxide. The latter is being re-oxidized by adsorbed oxygen [24, 25, 26]. Manganese oxides show apparent oxygen storage/release ability when they easily undergo a rapid reduction-oxidation cycle through the interaction with reducing/oxidation agents. [25, 27].

Salman studied the catalytic oxidation of NO to NO₂ under partially simulating nitric acid production conditions. Different catalysts involving supported platinum, manganese oxides, and perovskites were examined. Catalytic oxidation was investigated over powdered catalyst using a feed of 10 vol% NO, 6 vol% O₂ and 15 vol% H₂O (when present) at atmospheric pressure. The effect of loading (5, 10 and 20 wt%) and support material (alumina, silica, and zirconia) was investigated considering the supported manganese oxide catalysts. For alumina- and silica-supported catalysts, the oxidation activity was found to be increasing with the loading of manganese. The zirconia-supported catalysts were found to be independent of manganese loading and were found to give the best activity for NO oxidation among the other tested supports. Water present in the feed inhibits the NO conversion, however manganese oxide on zirconia support shows promising results [13].

Salman found the onset temperature of catalytic conversion to match the onset temperature of reduction of surface manganese oxide in the research regarding the catalytic oxidation of NO for nitric acid production. The correlation between the reducibility of supported manganese oxide and catalytic activity lead to the suggestion that NO oxidation proceeded via a Mars-van Krevelen mechanism [13]. The illustration of the suggested mechanism is shown in Figure 3.1.

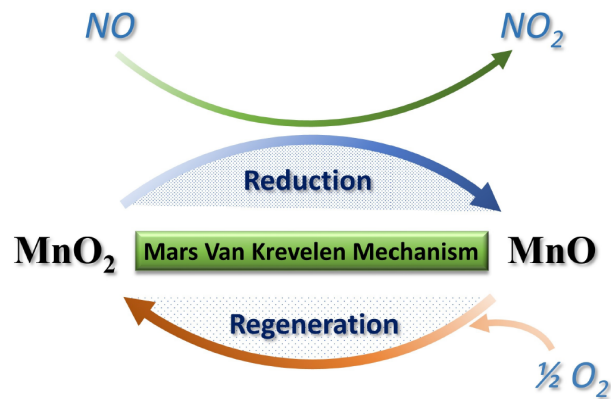


Figure 3.1: The suggested mechanism of NO oxidation over supported manganese oxide catalysts in partially simulating nitric acid condition, suggested and illustrated by Salman *et al.* [28].

The phase structure of MnO_x can significantly influence the catalytic activity for NO oxidation [11, 29, 30, 31]. Chen *et al.* published a paper in 2016 regarding the catalytic oxidation of NO over unsupported manganese oxide (MnO₂ with different crystal structures. α -, β -, γ - and δ -MnO₂ were prepared, and their catalytic properties for NO oxidation were examined. The catalytic activity were assessed with a feed consisting of 500 ppm NO, 5 vol% O₂, 200 ppm SO₂ (when present) and 10 vol% H₂O (when present) with the temperature from 100-400 °C. The catalysts with different crystal structures revealed significantly different catalytic activity for NO oxidation, where γ -MnO₂ presents the highest. γ -MnO₂ is a mix of the structures ramsdellite and pyrolusite, which leads to point defects in the structure and several vacancies, possibly explaining the high catalytic activity [11]. Chen *et al.* illustrated the different crystal structures, displayed in Figure 3.2

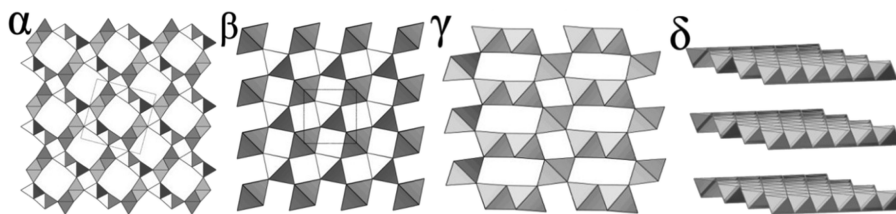


Figure 3.2: Crystal structures of α -, β -, γ - and δ -MnO₂ catalysts, illustrated by Chen *et al.* [11].

Wang *et al.*, investigated on the catalytic activity of unsupported manganese oxide in the NO oxidation (500 ppm NO, 5 vol% O₂, 200 ppm SO₂ (when used) and 15 vol% H₂O (when used)). MnO₂, Mn₂O₃ and Mn₃O₄ were made by hydrothermal synthesis, and the catalytic activity increased in the order of MnO₂ > Mn₂O₃ > Mn₃O₄ [32]. Chen *et al.* found that the amount of Mn⁴⁺ associated with the O-ligand is compatible with the activity of NO oxidation [33].

3.2 Bimetallic catalyst

Catalysts can be complex materials optimized by adding small amounts of elements to increase the overall reactivity, or selectivity of the catalyst [?]. A small addition of noble metals can lower the reduction temperature and improve dispersion while the mechanical properties

remain the same. Salman *et al.* suggested that NO oxidation over a supported manganese oxide catalyst proceeded via a Mars-van Krevelen mechanism in resembling nitric acid plant conditions [13]. Suppose the manganese oxide catalysts are promoted with a metal oxide that reduces at a lower temperature than manganese oxide. In that case, a possible outcome could be enhanced catalytic activity at a lower temperature.

Platinum reduces at a lower temperature than manganese oxide and a promotion to manganese oxide could possibly reduce the reduction temperature of manganese oxide. Ayastuy *et al.* investigated $\text{MnO}_x/\text{Pt}/\text{Al}_2\text{O}_3$ catalysts for CO oxidation in H_2 -rich streams over a temperature range of 25-250 °C. In their work, the presence of platinum lowered the reduction temperature of MnO_2 with increasing loading of Mn indicating a better contact between Pt and Mn with sufficient Mn [34].

Studies have determined that the lattice oxygen mobility of manganese oxides can be improved by doping other metal elements like CeO_2 , Cu and Ag [35, 36, 37]. Gac *et al.* discovered that the decrease of Mn-O bond strength due to the introduction of silver was helpful for the increase of the activity in research related to the decomposition of N_2O [38]. The improvement of lattice oxygen mobility of manganese oxygen distinctly increases the reactivity of Mn-Ag catalysts in a study regarding catalytic combustion of methane by Machocki *et al.* [37].

Silver reduces at a lower temperature than manganese and could work as a reduction agent to lower the reduction temperature [39]. Luo *et al.* studied the catalytic activity of Ag-Mn composite oxides supported by $\gamma\text{-Al}_2\text{O}_3$ for the oxidation of volatile compounds. Due to the silver promotion, the reduction temperature of manganese oxide decreased [39].

Qu *et al.* published a study on the improved reactivity of manganese catalysts by Ag in catalytic oxidation of toluene. It was found that Ag enters into MnO_2 phase, and the $\text{Ag}_{1.8}\text{Mn}_8\text{O}_{16}$ mixed phase forms. Meanwhile, Ag leads to parts of MnO_2 being changed into Mn_2O_3 . The Ag/Mn molar ratio greatly affects the molar ratio of the surface Mn^{4+} to Mn^{3+} and surface adsorbed oxygen (O_{ads}) to lattice oxygen (O_{latt}) through the interaction between silver and MnOx. The conjunction of MnO_2 , Mn_2O_3 , $\text{Ag}_{1.8}\text{Mn}_8\text{O}_{16}$, and the strong interactions between Ag and Mn species show a good synergetic interaction, promoting the reducibility of catalysts and the formation of plentiful active lattice oxygen, leading to the increased catalytic activity of toluene oxidation [26].

Several studies are published where the activity for lean NOx reduction over silver-catalysts are investigated, and rise the motivation to investigate the performance of silver and silver promotion in partially simulating nitric acid plant conditions. Männikkö, Skoglundh, and Ingelsten studied the selective catalytic reduction of NOx with methanol (500 ppm NO, 10% O_2 and varying concentrations of methanol) over silver catalysts supported on alumina and ZSM-5. They investigated parameters that can improve the NOx reduction performance, i.e., the C/N molar ratio and the addition of hydrogen. Essential factors to give higher NOx reduction were the support material, the preparation method, and a low Ag loading [40]. In another study by Männikkö *et al.*, characterization of the active species in the silver/alumina system for lean NOx reduction with methanol were published. The selectivity for lean NOx reduction over silver/alumina and the low-temperature activity is strongly dependent on the composition of surface silver species [41]. They revealed correlations between diffraction peaks from temperature-programmed desorption with NO and temperature for NOx reduction during methanol-SCR conditions.

3.3 Zirconium Oxide as Support

Zirconia (ZrO_2) is an interesting support material in catalysis when it can improve the activity of the supported metal oxide catalysts. The surface of ZrO_2 has bi-functional characteristics, both acidity and basicity [42]. ZrO_2 is found to have the capability to adsorb NO_x , and act in the oxidation of NO [43, 44]. Zirconia can occur in different crystallographic phases, where monoclinic is the most relevant for catalytic purposes. The phase is thermodynamically stable up to 1170°C , and consists of a well-developed mesoporous texture [45].

Zhao *et al.* compared Mn/TiO_2 and Mn/ZrO_2 catalysts for NO oxidation. The activity measurements for the catalytic oxidation of NO were performed at a temperature range of $30 - 700^\circ\text{C}$. The feed composition consisted of 500 ppm NO, 10% O_2 and balance N_2 . In the results, Mn/ZrO_2 exhibited better activity than Mn/TiO_2 . It is assumed that ZrO_2 abundant adsorption sites for the intermediate nitrates for this catalytic system accelerate the catalytic oxidation [44]. They illustrated the possible reaction route, displayed in Figure 3.3.

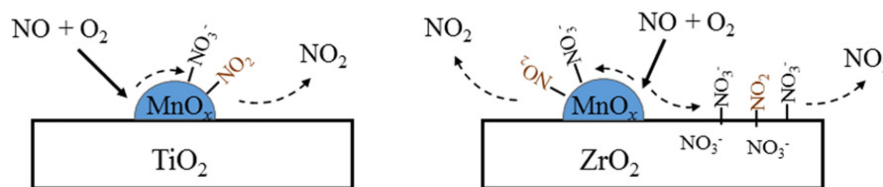


Figure 3.3: The reaction routes on Mn/TiO_2 and Mn/ZrO_2 catalysts proposed by Zhao *et al.* [44].

Salman observed that the zirconia-supported catalysts showed higher activity than alumina- and silica-supported manganese at partially simulating nitric acid plant conditions. The results from catalytic activity testing indicated the independence of manganese loading (5, 10, and 20 wt%) on the zirconia and NO conversion. Compared with alumina and silica as support, Mn/ZrO_2 catalysts presented the best features for industrial application in NO oxidation [13].

Chapter 4

Theory

4.1 Catalyst Preparation

There are different catalysts in heterogeneous catalysis, including supported or unsupported with diverse catalytically active materials. The numerous preparation methods can roughly be divided into dry and wet methods, and the choice between methods often depends on the cost of catalyst precursor. The optimum catalytic activity per unit volume of catalyst and high surface area can be obtained using coprecipitation. This method is preferable when the materials are cheap. With expensive materials like noble metals, when the active phase is favored deposited as nanometre-sized particles on the support, impregnation or precipitation from solution is a better alternative [46].

4.1.1 Incipient Wetness Impregnation

In the incipient wetness impregnation method a catalytically active phase is dispersed over a support material. The method is fast and inexpensive [47, 48]. The method involves introducing a volume of solution containing the precursor (V) equal to the pore volume (V_p), so $V = V_p$ [47]. The solution's volume is empirically determined by adding water until the sample looks wet with no excess of solution remaining outside of the pores [49, 48]. By capillary suction, the precursor solution is drawn into the pores of the support [47]. The liquid phase is replaced with the air in the pores because the capillary pressure is greater than the trapped air pressure inside the pore with a small radius. The physical model is illustrated in Figure 4.1

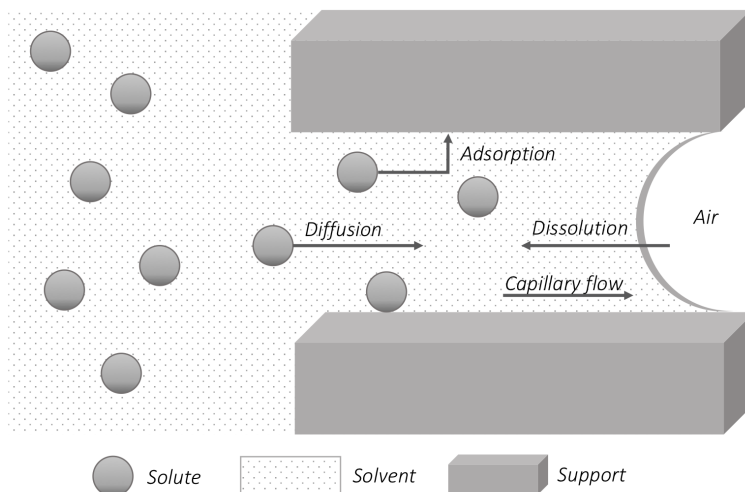


Figure 4.1: Transport phenomena involved in incipient wetness impregnation. The solute migrates into the pore from the left to the right in the figure. Reprinted from [50]

Several factors could affect the impregnation method, like temperature and concentration of the active metal. Heat is released when a solid/gas phase is replaced with a solid/liquid phase that can change the impregnation conditions if the precursor's solubility is sensitive to temperature changes. The time to wet and fill the support's pores will increase if the viscosity is too high. It is essential to consider that the precursor's loading is restricted by the precursor's solubility in the solution [48].

4.1.2 Calcination

Calcination is a heat treatment of the catalyst where the metal oxide catalyst is formed when the undesired species coming from the precursor evaporates. Several parameters should be considered in the calcination process, and the program performed can affect the properties of the catalyst. The calcination setup design enables a gas flow to go through the catalyst sample during the heat treatment. Air or oxygen can be used in cases when oxidation of the surface species is desired. In removing unwanted ligands, thermal decomposition of non-oxidic precursors and decomposition of salts calcination can be applied [51].

4.2 Characterization

4.2.1 Thermogravimetric analyses

Thermogravimetric analysis (TGA) is a microbalance technique where a sample is reduced or oxidized in a controlled environment while weight is measured. The method can provide information about the oxidation state of a component within a compound. By heating a sample and measuring the changes in physicochemical properties, phase changes of a species can be traced to a specific temperature [52]. While the temperature is increasing, different gases will escape from the sample.

A TGA can be equipped with a differential scanning calorimeter (DSC). In brief, DSC estimates how much energy a sample absorbs or releases during heating or cooling. The DSC can detect exothermic or endothermic reactions and give a signal shown in the DSC measurement curve [53].

4.2.2 Nitrogen Adsorption

Determination of physical properties is often desired in heterogeneous catalysis, including measuring surface area, pore size, and pore volume. With the possibility of defining a material's internal surface, the availability for active sites to accommodate can be determined. Information about these physical properties can also give knowledge about the accessibility of the reactant sites to reactants and how easily transporting reactants in bulk to the catalyst's surface can appear. The internal surface depends on the size and number of pores. A high surface area is often beneficial to maximize the dispersion of catalytic components, but not always as high porosity can lead to deactivation like sintering. When a solid mass of an object is created by heat or pressure without melting it into liquid, it is called sintering [54]. The pore structure and surface area need to be optimized for a given feedstock to maximize active catalytic sites [55].

The adsorption and desorption of N_2 usually determine the surface area of a mesoporous material at liquid nitrogen temperature in vacuum conditions. A mesoporous material is in the range where the surface area is greater than 1 or 2 m^2/g up to 1200 m^2/g [55]. The principle defining the surface area is determined by the number of N_2 -molecules needed to cover the surface by a complete monolayer. In practice, the nitrogen molecules may adsorb beyond the monolayer and will form multilayers [46]. This is illustrated in Figure 4.2.

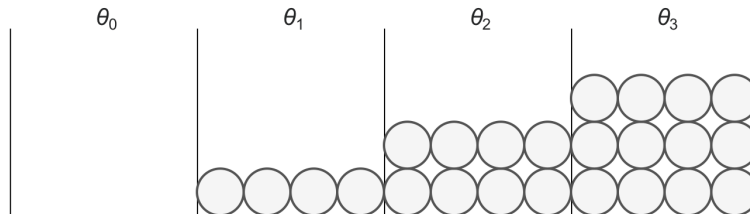


Figure 4.2: Illustration of different layers during physical adsorption. Adapted from Chorkendorff and Niemantsverdriet [46]

The relationship between the volume adsorbed at a given partial pressure and the volume adsorbed at monolayer coverage is described by Brunauer, Emmett, and Teller, known as the BET method [56]. The relationship is specified in Equation 4.1.

$$\frac{p_{N_2}}{V[p_0 - p_{N_2}]} = \frac{1}{CV_m} + \frac{(C - 1)p_{N_2}}{CV_m p_0} \quad (4.1)$$

In Equation 4.1, p_{N_2} is the partial pressure of N_2 , p_0 is the saturation pressure, V represent the volume of adsorbed N_2 and V_m is the adsorption volume at monolayer coverage. The rate of adsorption and desorption finds the constant C .

When Brunauer, Emmet, and Teller developed the method, they based the theory on numerous assumptions [55]:

- The equilibrium between adsorbate and adsorptive is dynamic. This means the rate of adsorption and desorption in any layer are equal.
- Molecules adsorb on comparable adsorption sites in the first layer.
- Molecules in the first layer constitute the adsorption sites for molecules in the second layer and higher layers.
- Interactions between adsorbate and desorption are disregarded.
- The adsorption-desorption requirements are the same for all layers except the first.
- The condensation energy equals the adsorption energy for molecules in the 2nd layer and higher.
- At saturation pressure ($p = p_0$), the multilayer builds to infinite thickness.

When molecules adsorb beyond the monolayer, the BET adsorption isotherm will not give the actual surface area. In practice, coverage beyond monolayer occurs. The most valid results are obtained at relative pressures between 0.05 and 0.3 [46, 55].

The pore size distribution can be determined with the same equipment used to measure BET. After the N_2 is adsorbed to the material's surface, the process is reversed by incrementally decreasing the pressure. Knowledge regarding the porous structure can be given from the gas adsorption isotherm [55]. The finer the pores, the more apparent the N_2 will condense in them. The Kelvin equation describes this phenomenon, called capillary pore condensation. This model determines the quantity of adsorbate removed from the sample material's pores while the relative pressure decreases [46]. Developed by Barrett, Joyner, and Halenda [57], the BJH method can determine the pore size distribution by measuring the capillary condensation occurring in the pores of the catalyst surface in accordance with the Kelvin equation,

$$\ln \frac{p}{p_0} = \frac{(-2\gamma \hat{V}_{liq} \cos \theta)}{r_k R T} \quad (4.2)$$

where γ is the surface tension of liquid nitrogen, \hat{V}_{liq} the molar volume of liquid nitrogen, θ the contact angle between liquid and solid, r_k the Kelvin radius or radius of the wetted pore, R the gas constant, T the absolute temperature, p the measured pressure, and p_0 the saturation pressure [55].

The shape of the N_2 adsorption isotherms could give information about the material analyzed. The classification of physisorption isotherms was originally grouped into six types according to the 1982 IUPAC recommendations [58]. The different isotherms are displayed in Figure 4.3a. Removal of the N_2 gas from the pores during the physisorption will show a hysteresis effect [46]. The classification of hysteresis loops was recommended by the IUPAC in 1984 and was based on observations of pore filling of N_2 by the use of the Kelvin equation (Equation 4.2) [59, 60]. The different hysteresis loops are displayed in Figure 4.3b, obtained from Sing *et al.*, 1985 [60].

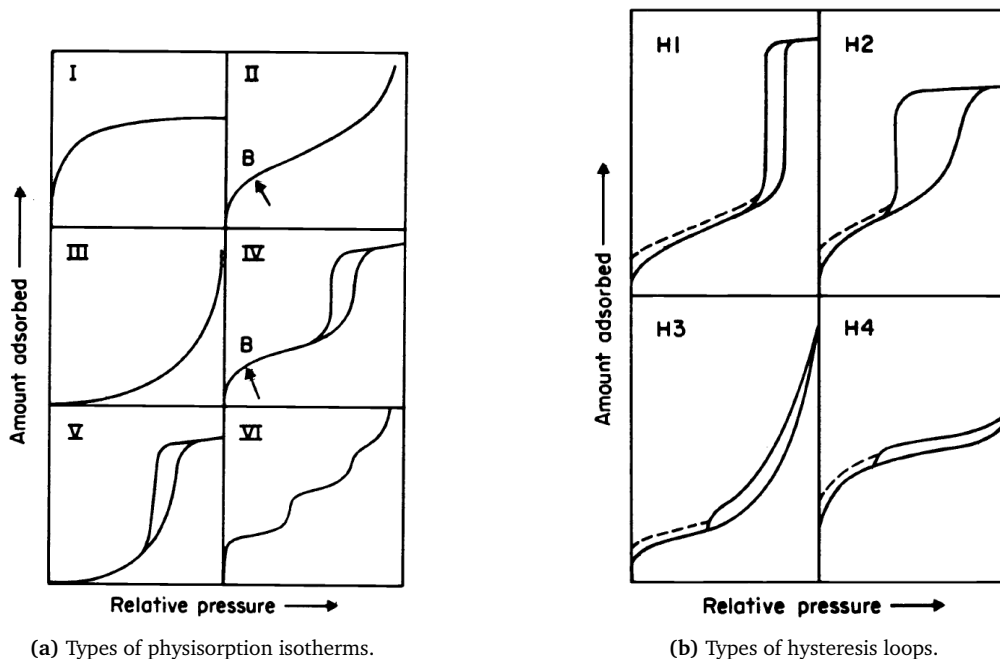


Figure 4.3: Types of physisorption isotherms and hysteresis loops, obtained from Sing *et al.*, 1985 [60].

The type H3 hysteresis loops in Figure 4.3b are typically given by the adsorption of non-polar gases by montmorillonite clays and the aggregates of other platy particles [59]. The shape of the H3 hysteresis loop follows the same shape as type II isotherm, shown in Figure 4.3a [60], which is correlated with the metastability of the adsorbed multilayer due to the low degree of pore curvature. As a consequence, the mesopore size distribution cannot be evaluated reliably from either branch of the loop for the H3 hysteresis loop [59].

4.2.3 Hydrogen temperature programmed reduction

Temperature-programmed (TP) reaction methods are techniques where a chemical reaction is observed while the temperature increases linearly in time [61, 62]. In TP reduction (TPR), one gets insight into the mechanism of the reduction process. The sample is exposed to H₂, typically 5 vol% H₂ in Ar. In the setup, a thermal conductivity detector (TCD) estimates the hydrogen content before and after the reaction [63], and the rate of reduction is followed at the outlet of the reactor [64]. The reduction of a metal oxide MO_n by H₂ is illustrated in Equation 4.3.



Only partial reduction to a lower oxide may be expected in several cases, like the reduction of Mn₂O₃ to MnO. The reduction is thermodynamically favorable at moderately high water content, but a further reduction to metallic manganese is unlikely [63].

TPR provides useful information about the temperature needed to reduce the catalyst completely. If the catalyst contains more than one metal, the TPR may suggest whether the metals

are in contact or not [63]. Supported catalysts may be more challenging to reduce when the carrier could prevent the reduction due to the nature of the oxide/support interactions [61].

4.2.4 X-ray diffraction

X-ray diffraction (XRD) is one of the most frequently applied techniques in catalyst characterization and identifies crystalline phases inside the material [46]. If the material is adequately crystalline to diffract X-rays, typically crystallites larger than 3 to 5 nm, and is present in quantity higher than 1%, XRD can be applied for chemical phase analysis, both qualitative and quantitative [65].

Crystal structures consist of planes formed by repetitive forms of atoms, which can diffract X-rays. The diffraction angles vary for the several planes within the crystal, and every element has its own moderately unique pattern. The variations in these patterns enable the differentiation of different planes in the catalyst [55]. In the elastic scattering of X-ray photons by atoms in a periodic pattern, the X-ray diffraction occurs [46]. The X-ray diffraction allows one to derive lattice spacing by Bragg's relation in Equation 4.4

$$n\lambda = 2d \sin(\theta) \quad n = 1, 2, \dots \quad (4.4)$$

The λ describes the wavelength of the X-rays while d is the distance between two different planes. The angle between the incoming X-ray and the normal to the reflecting lattice plane is presented in θ . In contrast, the n is the variable reflecting the order of the reflection. The interfering X-rays will leave the crystal at a specific angle, 2θ [46].

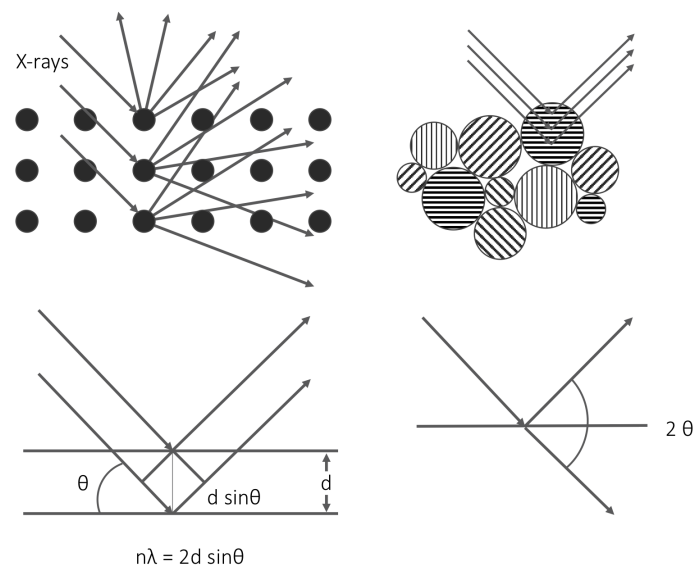


Figure 4.4: X-rays are scattered by the atoms in an ordered lattice. The spacing between the lattice planes can be calculated using the angles of maximum intensity and allowing further identification of phases in a sample. Diffractograms are measured as a function of the angle 2θ and formed by a small fraction of the particles. Reprinted from [46, 63]

The shape of the diffraction peak carries information about the dimensions of the reflecting planes. For crystallite sizes below 100 nm, the diffraction peak is broad enough for line broad-

ening to occur due to incomplete destructive interference in scattering directions where the X-rays are out of phase. XRD peak width is inversely related to the crystallite size of a given phase, and the crystallite size can be related to the breadth of the peak [55]. The Scherrer equation, displayed in Equation 4.5, relates the full width at half maximum (FWHM) $B_p(2\theta)$ and the size of the crystallites d_p .

$$d_p = \frac{K \lambda}{B_p(2\theta) \cos(\theta)} \quad (4.5)$$

K describes a dimensionless shape factor related to crystallite shape. For spherical-shaped crystals, 0.9 is often used [66]. λ is the wavelength of the X-ray and θ is the diffraction angle, both given in radians [46].

The Scherrer equation's calculations are only a relative measure, and gives a rough estimation of crystallite size [67, 68]. The calculations should not be used for absolute determinations when the analysis fails to account for microstrains' effects, and uncertainty in correcting instrumental broadening [69]. In the measurement of the peak broadening, the correction for instrumental broadening is considered by comparing the FWHM intensity of the X-ray reflection of the sample with the single-crystalline Si standard. Gaussian correction is applied to exclude the instrumental broadening to get a more precise crystal broadening with Equation 4.6

$$B_p^2(2\theta) = B_h^2(2\theta) - B_f^2(2\theta) \quad (4.6)$$

where $B_p^2(2\theta)$ is the corrected FWHM, and $B_h^2(2\theta)$ and $B_f^2(2\theta)$ are the FWHM of the sample and the single-crystalline Si standard [70].

It is possible to obtain a rough estimation of the dispersion, D with Equation 4.7 with the average bulk crystallite size, d_p , calculated from the Scherrer equation. The constant, k , changes with the assumption of the shape of the particle and is set to unity in order to do internal comparison of different catalysts in Equation 4.7 [71].

$$D = \frac{k}{d_p} \quad (4.7)$$

4.3 Activity Measurement

4.3.1 Fourier-transform infrared spectroscopy Gas Analyzer

Infrared spectra appear from transitions between quantized vibrational energy stated in a molecule. The range of molecular vibrations varies from a simple coupled motion of the two atoms of a diatomic molecule to more complex movement in a sizeable polyfunctional molecule. Every molecule has a unique vibrational mode, slightly different from all other molecules (except enantiomers). During the vibration, the motion is regularly expressed in terms of the normal coordinate, Q_i . Only if the molecule's dipole moment μ changes during the vibration, the molecule is promoted to the excited state ($\frac{\partial \mu}{\partial Q_i} \neq 0$). A common design used

for interferometers is based on the two-beam interferometer. It is a device that divides a beam of radiation into two paths and then recombines the two beams after a path difference has been introduced. Interference between the beams can occur, and conduction is created [72].

A Fourier-transform infrared-based gas analyzer (FT-IR) can be capable of ppb to % sensitivity for measuring multiple gases in various applications, such as catalysis and combustion process monitoring. The infrared beam is partially absorbed by the gas species present after the gas sample enters the gas cell. The spectral frequencies are absorbed, and the analyzer measures the adsorption spectra. By using pre-loaded calibrations, an analysis algorithm measures the concentration of each gas [73].

Chapter 5

Materials and Methods

5.1 Catalyst preparation

Seven zirconia-supported catalysts were synthesized by the incipient wetness impregnation method, shown in Table 5.1. Different preparation methods can, in theory, be used to prepare supported manganese oxide catalysts. However, Salman and Østrådt prepared the zirconia-supported manganese oxide catalysts by the incipient wetness method, and afterward, calcined [13, 14]. Their work showed promising results for the zirconia-supported catalysts, and the same method was chosen for the synthesis in this work.

The catalysts were made with two different loadings (5 and 20 wt%) of manganese and additionally promoted with 1 wt% silver and 1 wt% platinum. The loading is presented with the number, shown in Table 5.1.

Table 5.1: List of the different catalysts prepared by incipient wetness method. The number represents the weight percent, and all the manganese is present as a metal oxide.

Catalyst	Name
20 wt% Mn on ZrO ₂	20Mn
20 wt% Mn and 1 wt% Pt on ZrO ₂	20Mn-1Pt
20 wt% Mn and 1 wt% Ag on ZrO ₂	20Mn-1Ag
5 wt% Mn on ZrO ₂	5Mn
5 wt% Mn and 1 wt% Pt	5Mn-1Pt
5 wt% Mn and 1 wt% Ag	5Mn-1Ag
5 wt% Ag on ZrO ₂	5Ag

The zirconia (Alfa Aesar 1/8" pellets) was crushed before it was sieved to the fraction 53-90 μm . The zirconia was calcined at 650 °C in synthetic air with a ramp rate of 10 °C/min. The incipient wetness point was found experimentally to be 0.5 gram deionized water per gram zirconia.

Manganese nitrate precursor ($\text{Mn}(\text{NO}_3)_2 \cdot x\text{H}_2\text{O}$, where x is assumed 4), deionized water, and support were weighed out. Waters of crystallization in the precursor was considered when calculating the total amount of precursor solution. The manganese nitrate and water were

mixed until the salt was fully dissolved before adding drop-wise to the calcined support. The impregnated support was dried overnight in an oven with airflow at 120 °C to exclude the moisture. The catalyst was sieved again to obtain the fraction 53-90 μm and calcined at 400 °C for six hours in synthetic air with a ramp rate of 5 °C/min.

The bimetallic catalysts were synthesized by co-impregnation. Manganese nitrate and platinum nitrate (Alfa Aesar 15 wt% $\text{Pt}(\text{NO}_3)_4$ solution) was dissolved in deionized water corresponding to the incipient wetness point. The solution was added drop-wise to the support, mixed, and dried overnight at 120 °C. Finally, the catalyst was calcined at 400 °C for six hours in synthetic air with a ramp rate of 5 °C/min for the nitrates to evaporate. The exact same procedure was followed for the silver-promoted catalyst where manganese nitrate and silver nitrate (Alfa Aesar, 99 + % purity AgNO_3) was dissolved in deionized water corresponding to the incipient wetness point.

The preparation calculations, exact measurements, and the chemical used are found in Appendix [A](#). The risk assessment for the experiment is to be found in Appendix [E](#).

5.2 Catalyst Characterization before Activity Testing

The characterization methods TGA, N_2 adsorption, TPR, and XRD were used to determine the catalyst's physical and chemical properties, which is assumed to reflect in the performance in the conversion of NO [\[55\]](#).

5.2.1 Thermogravimetric analyses

TGA was performed with *Netzsch STA 449C* to identify the sample's weight loss with increasing temperature. For analysis, 100 mg of sample (before calcination) was used. The temperature was increased from room temperature to 400 °C with a ramp rate of 10 °C/min and held for 6 hours. During the final step, the temperature increased to 900 °C with the same ramp rate.

5.2.2 Nitrogen Adsorption

Nitrogen adsorption was used to determine the surface area, pore volume, and pore size of the zirconia support and the catalysts. The samples (\approx 100 mg) were degassed at 200 °C under vacuum overnight in a VacPrep 061 Degasser. Nitrogen adsorption was performed in the *Micrometrics TriStar II 3020 Surface Area And Porosity Analyzer* at 77 K. The program was set to measure the volume adsorbed at 90 different pressures, starting at 0.01 P/P_0 .

5.2.3 Temperature Programmed Reduction

The reduction temperature of the catalyst was analyzed using *Altamira BenchCat Hybrid 1000HP*. Approximately 100 mg of the catalyst was weight out and packed in a u-shaped quartz reactor with quartz wool over and under the sample. The reactor was placed into the equipment, and leak tests were conducted. The catalyst was pre-treated with a flow of argon (50 mL/min) at 150 °C for 30 minutes with a heating rate of 10 °C/min. The reduction was

performed in a temperature scan from 50 to 800 °C with a heating rate of 5 °C/min. This was done with a flow of 50 mL/min flow of 7% H₂ in Ar. After the reduction, a new treatment of the sample was executed, being the same as the pre-treatment.

5.2.4 X-ray Diffraction

Bruker D8 Advanced X-ray Diffractometer (D8 Davinci) was utilized to achieve XRD patterns. The settings were 40 kV and 40 mA with a wavelength of 1.54060 Å employing Cu K α radiation. The samples were analyzed using a crystallinity program, measuring at 5-75° for 120 minutes with a slit opening of 0.1 degrees. The same settings, program, and standard sample holders were used for all the catalysts. DIFFRAC.SUITE EVA software was used to analyze the diffraction patterns, and to find the crystallite size of manganese. With the same software, the background was subtracted in the presentation of the XRD patterns. The instrumental line broadening was taken into consideration in the calculation of crystallite size.

5.3 Activity Testing

The activity measurements were performed in Rig 2.1, a dedicated set up built to study NO oxidation at approaching nitric acid plant conditions, on the second floor in Chemistry Hall D at NTNU in Trondheim. The reactant gases involved were obtained from AGA AS (40% NO/Ar, 40% O₂/Ar) and argon 6.0 (AGA AS) as the inert gas. The five feed gas lines were connected to the ventilation network, implemented with a pressure-reducing valve, pressure gage, Bronkhorst electronic mass flow controller (MFC), and check valve. Each line was individually heated to 200 °C by using heating tapes controlled by tunable power sources (0-10 A, 230V). A Bronkhorst electronic Controlled-Evaporation-Mixing (CEM) unit was used to control the reactor's water amount and mix the oxygen, water, and argon when water was desired in the feed. A simplified flow scheme is displayed in Figure 5.2 placed at the end of this chapter, and a more detailed is found in Appendix D.

The reactor used for activity testing was a vertical stainless-steel tubular reactor with an inner diameter of 9.7 mm. Modifications were performed to minimize the gas phase NO conversion resulting in two separate tubes entering the top of the reactor instead of one. The reactor is illustrated graphically in Figure 5.1, illustrating the design before (b) and after (a) modifications. NO, entering the reactor in one of the tubes, was mixed with oxygen diluted with argon, entering through the other tube. The modification aimed to further reduce the gas-phase conversion upstream of the catalyst bed. When water was present, it entered the reactor together with oxygen and argon from the CEM.

The reactor was loaded with 500 mg of catalyst and 2.75 g of silicon carbide (SiC) with a particle size of 30 mesh (595 μ m). The SiC was added as an inert to decrease temperature gradients caused by the exothermic heat of reaction and gain isothermal conditions in the catalyst bed. The particle size fraction was chosen to be different to separate the catalyst and SiC after the reaction. Quartz wool was used above and below the sample to keep it intact in the reactor. The catalyst bed was placed on top of a cylinder-shaped hollow tube with length of \approx 1 cm, being placed closest to the outlet of the reactor to keep the catalyst bed in place. One end had a slightly smaller diameter, and this was facing up in the reactor. A thermocouple was placed inside the reactor entering from the top and extending through the catalyst bed. A cylindrical aluminum block equipped with up to six cartridges heaters embraced the reactor

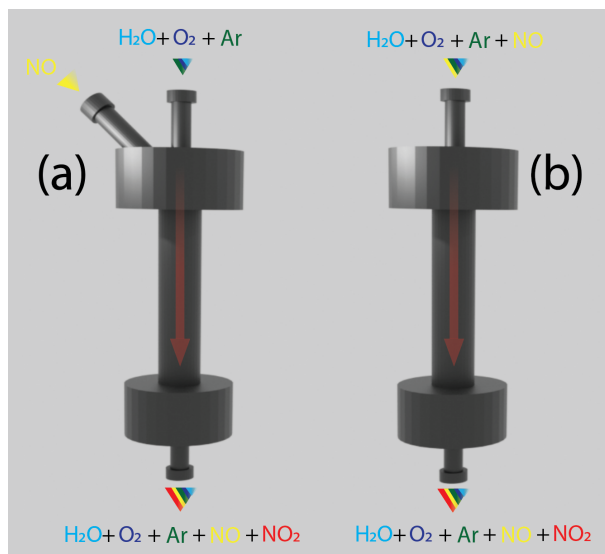


Figure 5.1: A illustration of the reactor used in the activity testing of the catalysts in nitric acid plant conditions. a) represents the reactor after modifications and b) is before modifications. Drafted by Jithin Gopakumar.

to ensure uniform and controlled heating.

The reactor's total feed flow rate was 200 Nml/min, corresponding to WHSV of 24 000 $Nml/h g_{cat}$. After the reaction, the products were diluted immediately with 800 Nml/min argon at the reactor outlet to minimize the gas-phase reactions and cool the product stream to 191 °C. Inlet and outlet gas concentrations were examined by a Fourier Transform Infrared (FT-IR) gas analyzer (MKS 2030HS, 5.11 m path length, 1 bar, and 191 °C).

The activity measurements were mainly performed without pretreatment to have the same basis of comparison. All catalysts were heated to 200 °C to evaporate potential water on the catalysts and cooled to 50 °C. The temperature program each catalyst were evaluated under is illustrated in Figure 5.3, including temperature scan test runs and approximate steady-state condition experiments in dry and wet conditions. When 15 vol% water was present in the feed, the temperature scan were performed from 110 °C to 400 °C. In a dry feed, the temperature scan started at 50 °C and went up to 400 °C. Between each temperature scan step, the catalysts were cooled down in 200 Nml/min flow of argon. The steady-state conditions were performed to analyze the stability and rate of initial deactivation during 2 hours steady-state with and without water at 250 and 350 °C.

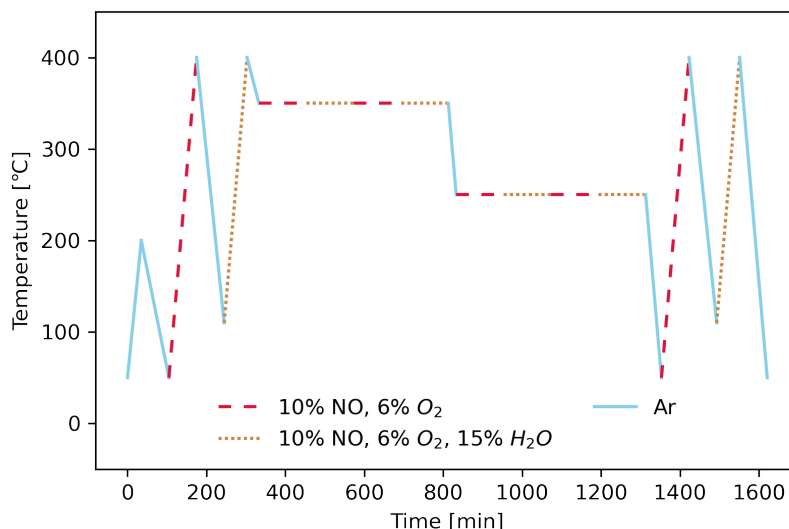


Figure 5.3: The complete temperature program each catalyst were analyzed at. $WHSV = 24\ 000\ Nml/h\ g_{cat}$ during all the experiments.

The explanation of each temperature program and the respective name for one catalyst in the order experimentally performed is described in Table 5.2. The temperature scans were named Dry and Wet 1. The following were four steady-state runs at 350 °C with and without water repeated, named SS350 Dry and Wet. Further, four steady-state runs were performed at 250 °C named SS250 Dry and Wet. The two last temperature scans were performed after the steady-state experiments and are named Dry and Wet 2.

Table 5.2: The name of each temperature program performed in nitric acid plant conditions with dry and wet feed. In all the test runs the $WHSV$ of $24\ 000\ Nml/h\ g_{cat}$ at 1 bar.

Name	Temperature [°C]	Ramp Rate [°C/min]	Condition
Heating	50-200	10	100% Ar
Dry 1	50-400	5	10% NO, 6% O ₂
Wet 1	110-400	5	10% NO, 6% O ₂ , 15% H ₂ O
350SS Dry 1	350	-	10% NO, 6% O ₂
350SS Wet 1	350	-	10% NO, 6% O ₂ , 15% H ₂ O
350SS Dry 2	350	-	10% NO, 6% O ₂
350SS Wet 2	350	-	10% NO, 6% O ₂ , 15% H ₂ O
250SS Dry 1	250	-	10% NO, 6% O ₂
250SS Wet 1	250	-	10% NO, 6% O ₂ , 15% H ₂ O
250SS Dry 2	250	-	10% NO, 6% O ₂
250SS Wet 2	250	-	10% NO, 6% O ₂ , 15% H ₂ O
Dry 2	50-400	5	10% NO, 6% O ₂
Wet 2	110-400	5	10% NO, 6% O ₂ , 15% H ₂ O

Some activity measurements were carried out with pretreatment of the catalyst to see potential activation effects. The pretreatments are displayed in Table 5.3. 5Mn were exposed to two different oxidizing pretreatment, while 20Mn-1Pt were reduced in H₂.

Table 5.3: Different pretreatments tested on 5Mn and 20Mn-1Pt.

Pretreatment	Pretreatment Gas	Temperature [°C]	Time [h]	Catalyst
1	10% O ₂	400	2	5Mn
2	15% H ₂ O	400	1	5Mn
3	8.7% H ₂	250	1	20Mn-1Pt

The gas-phase, empty reactor, and tubing contribution were measured by running blank tests without catalyst. When test running with silicon carbide, the reactor was charged with 3.25 g SiC. Both particle sizes of 50-90 μm and 30 mesh were performed to see the potential effect from pressure drop in the catalyst bed. One test run was performed additionally with 0.5 g of 53-90 μm and 2.75 g of 30 mesh (595 μm), named *SiC mix*, in order to potentially have more similar conditions as when the catalysts were tested. The different SiC test runs are displayed in Table 5.4.

Table 5.4: Amount of different particle sizes in the test runs with SiC in the reactor.

SiC	53-90 μm [g]	30 mesh [g]
<i>SiC 53-90 μm</i>	3.25	
<i>SiC 30 mesh</i>		3.25
<i>SiC mix</i>	0.5	2.75

NO conversion was used as a measure of catalytic activity in the calculations of conversion and demonstration of catalytic activity. Due to experimental challenges during the temperature scan measurements, the conversion data was modified to better compare the catalysts. The gas-phase contribution collected from SiC (30 mesh and mix) test runs was extrapolated to the starting point of all the catalyst conversion curves before the NO conversion contribution from SiC was subtracted from the total conversion. The modification is described in Appendix C.3. The data modification, and subtraction of SiC conversion were done for the temperature scan measurements, not the steady-state experiments. An overview is displayed in Table C.2 in Appendix C.3.

It was assumed that the nitrogen species in the system included NO and NO₂. From Equation 2.3 in Section 2.2, it is seen that for each NO molecule reacting one NO₂ molecule is produced. The steady state component molar balance over the reactor is shown in Equation 5.1.

$$\hat{n}_{NO_{in}} = \hat{n}_{NO_{2,out}} + \hat{n}_{NO_{in}} \quad (5.1)$$

The following equation was used to calculate the conversion, x_{NO_2} , of NO to NO₂:

$$NO_{\text{Conversion}} = x_{NO} = \lambda \cdot \frac{[NO_2]_{\text{outlet}}}{[NO]_{\text{inlet}}} \cdot 100 \quad (5.2)$$

where $[NO]_{\text{inlet}}$ and $[NO_2]_{\text{outlet}}$ are concentrations of NO at the inlet ($[NO]_{\text{in}} = [NO_2]_{\text{out}} + [NO]_{\text{in}}$), and NO₂ at the outlet of the reactor. The constant λ accounts for the volume change for different conditions, and nitric acid plant conditions are considered 0.99. The conversion presented after the gas-phase contribution is subtracted is presented as $x_{NO,c}$ where c refers to catalytic conversion.

The rate of reaction is based on the mass of the solid catalyst and was measured according to Equation 5.3 which is derived from the mole balance for a packed-bed reactor (PBR) at the differential form [74].

$$r_{NO_2} = \frac{x_{NO_2} \cdot \hat{F}_{NO_{in}}}{g_{cat.}} \quad (5.3)$$

$\hat{F}_{NO_{in}}$ is the molar flow of NO entering the reactor while x_{NO_2} is the conversion of NO₂. Equation 5.3 is used assuming PBR with no radial gradients in concentration, temperature or reaction rate. The calculated reaction rate will give a rough estimation and highlight the differences between the catalysts rather than treating the calculated values as a determined measure as radial gradients are difficult to avoid experimentally. The density of NO used in the rate calculations equals 1.249 g/l at normal temperature and pressure (20 °C and 1 bar) [75].

Salman *et al.* investigated catalytic oxidation of NO to NO₂ for nitric acid production over a Pt/Al₂O₃ catalyst and used the same rig and conditions used in this work [15]. They mixed the catalyst with SiC (53-90 μm), and the reactor looked as displayed in Figure 5.1 presented as b). They confirmed that that the system applied was free from internal diffusion limitations at the utilized conditions with the use of Weisz-Prater criterion [76]. Salman *et al.* also checked external mass and heat transfer limitations by calculating the Carberry number (Ca) and used appropriate criteria suggested by Mears [77]. The calculations indicated an absence of any external limitations when the Ca number was found to be in the order of 10⁻⁵ (<< 0,05) [15]. Due to the preliminary estimates, the same setup with a different catalyst and different particle size of SiC, were assumed to be free from internal diffusion limitations and external mass and heat transfer limitations.

5.4 Catalyst Characterization after Activity Testing

5.4.1 X-ray Diffraction

The same diffractometer, *Bruker D8 Advanced X-ray Diffractometer (D8 Davinci)*, utilized before the activity testing was used to study the catalyst after the activity testing. The settings were 40 kV and 40 mA with a wavelength of 1.54060 Å applying Cu K_α radiation. The samples were analyzed using a crystallinity program, measuring at 5-75 ° for 120 minutes with a slit opening of 0.1 degrees. Cavity sample holders with 10 mm in diameter were used under the analysis.

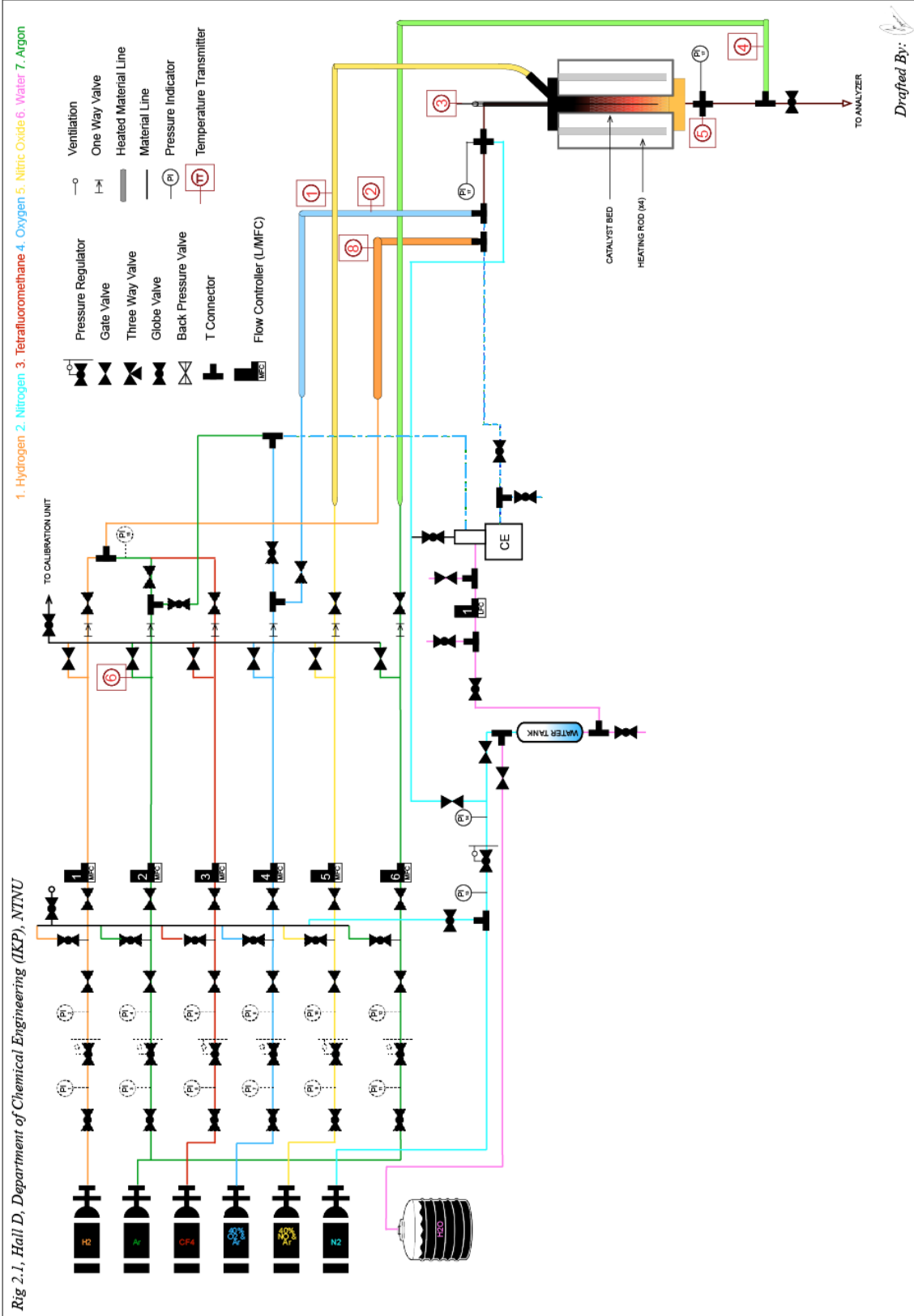


Figure 5.2: A simplified flow scheme of Rig 2.1 in Chemistry Hall D at NTNU in Trondheim, drafted by Jithin Gopakumar.

Chapter 6

Results and Discussion

6.1 Characterization Before Activity Testing

6.1.1 TGA

Before calcination, TGA was performed on the manganese catalysts to establish a temperature program for calcination and make sure manganese oxide remained in the desired γ -form. The manganese oxide appears to degrade and change phase above 450 °C [78]. It was desired to know that nitrates and water from the preparation of the catalyst decomposed at temperature below the phase change of manganese.

Figure 6.1 displays the TGA curves with the relative differential plots, including three parameters (temperature, mass, and DSC signal) analyzed as a function of time. The mass percent decreased with increasing temperature indicating the removal of species assumed to be mainly nitrates and water when manganese nitrate decomposes above 140 °C [64].

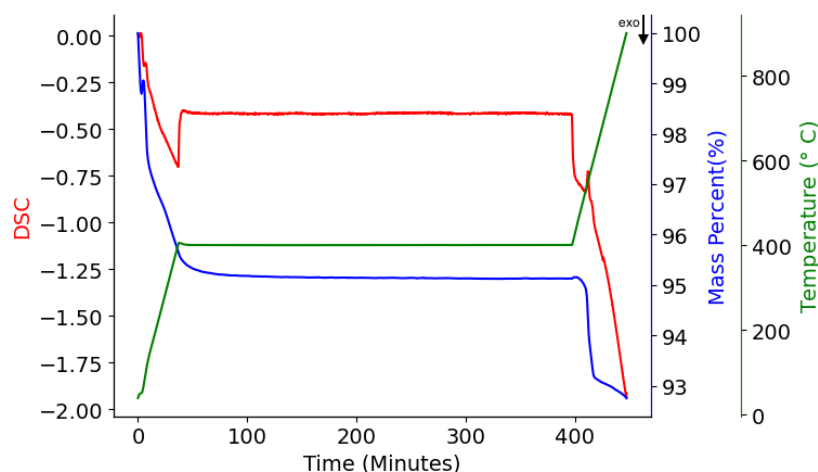


Figure 6.1: TGA curves for 20Mn with the relative differential plots, presenting the difference in DSC signal, mass percent and temperature as a function of time. The temperature was increased to 400 °C with a ramp rate of 10 °C/min and held for 6 hours before the temperature was increased to 900 °C with the same ramp rate.

During the isothermal period at 400 °C of six hours, neither weight loss nor DSC signal occurs, indicating no change in oxidation state for MnO₂ or other species going off from the catalyst. The results established that the temperature up to 400 °C is sufficient, and γ -MnO₂ was maintained. 400 °C was chosen as the maximum exposure temperature for the catalyst, and the calcination program was established accordingly.

During the last temperature interval, the mass percent decreases rapidly after 450 °C, and a DCS signal occurs. The manganese oxide forms to Mn₂O₃ [79]. Above 500 °C, oxygen is assumed liberated and could explain the decrease in mass percent after 450 °C [79].

6.1.2 Nitrogen Adsorption

The surface area, pore-volume, and pore size of the zirconia supported catalysts is given in table 6.1. The range of standard deviation, calculated between two parallel experiments, is given in the footnote, indicating uncertainty in the measurements. The internal surface area is calculated by measuring the number of N₂ molecules adsorbed at a monolayer coverage, but in practice, coverage beyond a monolayer occurs [55]. The approach utilized to find the surface area is the BET method showed in Equation 4.1 in Section 4.2.2. Several assumptions are behind this approach, as previously explained in Section 4.2.2, and the measurements should not be considered as a determined measure, and explains the lack of decimals in Table 6.1.

Table 6.1: Structural data from N₂ physisorption giving the BET surface area, the BJH desorption cumulative pore volume and BJH desorption average pore diameter for the catalysts.

Catalyst	Surface Area ^a [m ² /g]	Pore Volume ^b [cm ³ /g]	Average Pore Size ^c [nm]
ZrO ₂	72	0.24	9
5Mn	72	0.26	10
5Mn-1Pt	66	0.26	11
5Mn-1Ag	65	0.23	9
20Mn	49	0.17	10
20Mn-1Pt	45	0.16	10
20Mn-1Ag	44	0.15	8
5Ag	69	0.18	8

^a Average of two parallel experiments with the same material. The standard deviation was between 0.07 and 3.6 for the surface area.

^b Average of two parallel experiments with the same material. The standard deviation was between 0.0008 and 0.04 for the pore volume.

^c Average of two parallel experiments with the same material. The standard deviation was between 0.01 and 2.7 for the average pore size.

20Mn catalysts show a lower surface area than the 5Mn catalysts, and the promotion of platinum and silver results in minor differences. The surface area, pore-volume, and pore size decrease with increasing Mn loading according to Salman's studies [13]. The same trend is reported by Arena *et al.* which additionally explains the trend by the capability of manganese nitrate precursor to disperse on the surface of the support until a monolayer is reached [23]. The same trend in surface area is observed in this work. Regarding the pore volume, the

5Mn-catalysts remain approximately the same as ZrO_2 . The decreasing trend in pore volume, related to manganese loading, is more evident comparing ZrO_2 with the 20Mn catalysts.

The isotherm linear plot, BET surface area plot and average pore size distribution for the zirconia support is displayed in Appendix B.1. The zirconia-support and catalysts appears to follow a H3 hysteresis loop, and an isotherm of type II, explained and showed in Section 4.2.2. H3 hysteresis loops imply an irregular pore structure with flake grains or narrow slit-like shapes in the material [59, 80].

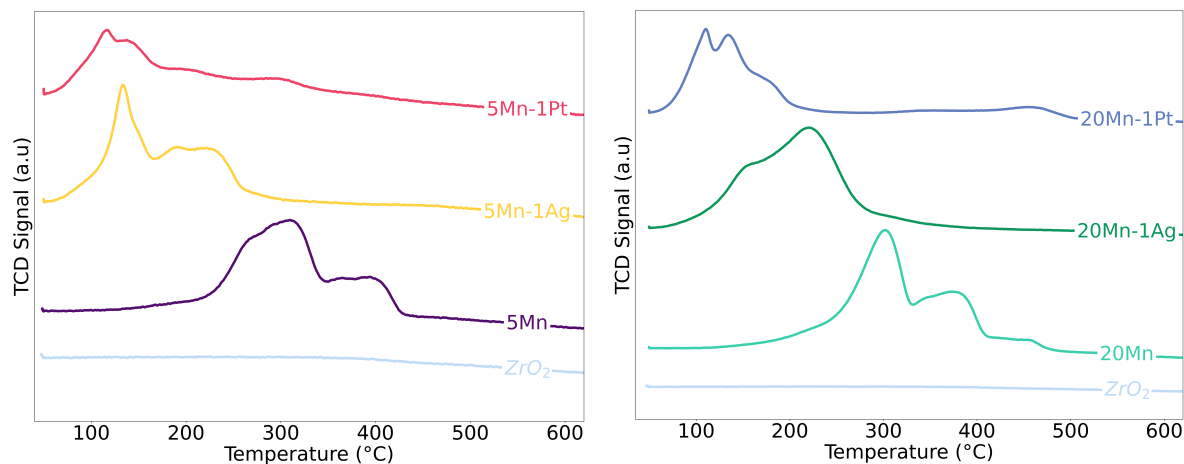
The procedure to find the average pore distribution size involves measuring the adsorbed or desorbed N_2 on the catalyst surface in the ascending or the descending branch of the BET plot at relative pressures (p/p_0) up to 1 [55]. It is important to highlight that mesopore size distribution cannot be assessed reliably from either branch of the loop as H3 loops does not have a plateau at high p/p_0 and no well defined mesopore volume is present in the material [59]. The Kelvin equation, displayed in Equation 4.2 in Section 4.2.2, describes the desorption isotherm, and is used to calculate the pore size distribution. The pore size distribution appears in one distribution, and the standard deviation is calculated between different samples of the same catalyst. It is believed that the average pore size remains approximately the same despite the loading of manganese on the support surface due to uncertainties related to the approach and the range in standard deviation.

The effect of the surface area, pore-volume, and pore size could be more evident in combination with the dispersion of manganese oxide on the catalyst surface in a possible explanation of the catalytic activity. *Chemisorption* is a characterization technique to find the metal dispersion on the catalyst surface and was attempted to find the dispersion. The most frequent gas in use during chemisorption analysis is H_2 [55]. Other gases such as CO and O_2 can be used but are not as consistent as H_2 . Because of CO's stoichiometry, the adsorption on metals is highly variable. The CO can adsorb either in the hollows of three or four-fold sites making CO chemisorption not a reliable method for determining the surface metal area [55]. Due to experimental challenges, and the fact that CO or H_2 should be used to find platinum dispersion and O_2 or CO could be used to find manganese and silver dispersion made it challenging to find a reasonable dispersion of the bi-metallic catalysts [55, 81, 82].

6.1.3 Temperature programmed reduction

The TPR profiles in Figure 6.2 show several peaks for each reduction pattern, indicating different reduction steps of manganese oxide during increased temperature. The H_2 consumption is described in Equation 4.3 in Section 4.2.3

It is expected that the first distinct peak is the transition Mn^{4+} to Mn^{3+} . Smaller crystallites at the surface of the catalyst can increase the difficulty of reduction [13]. According to calculations by Scherrer equation (4.5) presented in the next section, the 20Mn catalyst has smaller crystallite sizes than 5Mn. As observed in the TPR spectra, 5Mn and reduces at a slightly lower temperature, and could indicate a correlation between the crystallite size and reduction temperature.



(a) The TPR profile of 5Mn-1Pt, 5Mn-1Ag, 5Mn, and the zirconia support.

(b) The TPR profile of 20Mn-1Pt, 20Mn-1Ag, 20Mn, and the zirconia support.

Figure 6.2: The TPR curves for the zirconia-supported manganese catalysts.

A large band in the TPR spectra results from a thoroughly dispersed MnO_2 which is observed for the 5Mn catalyst, but is more apparent for 20Mn. A possible explanation could be that the reduction of Mn^{4+} appears to take place in close interaction with the support [23].

Silver and platinum were added as promoters to the manganese to initiate manganese reduction at a lower temperature. According to the TPR spectra in Figure 6.2, the promoted catalysts start reducing at a lower temperature than unpromoted catalysts, significantly affecting the reduction temperature. The first catalyst to be reduced is the platinum-promoted for both manganese oxide catalysts (5 and 20 wt%), indicating a better interaction between Pt and Mn in terms of common interface [34].

After the TPR analyses, the catalysts had partially turned from grey/brown to green, indicating the presence MnO in the sample. According to literature [32], the suggested reduction is $\text{MnO}_2 \rightarrow \text{Mn}_2\text{O}_3 \rightarrow \text{Mn}_3\text{O}_4 \rightarrow \text{MnO}$, which is in-line with the observations.

Comparing 5Mn-1Ag, 20Mn-1Ag, and 5Ag in Figure 6.3, 5Ag reduces at a lower temperature than the two other catalysts containing 1 wt% silver. The reduction of silver on zirconia support presented a signal at approximately 100 °C, and according to a study by Montana *et al.*, 5% silver on zirconia reduces at 90 °C [83].

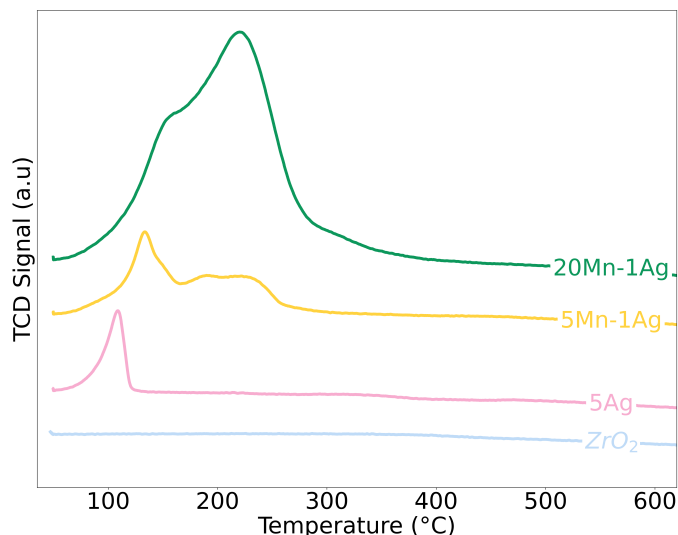


Figure 6.3: The H₂-TPR profile of two zirconia-supported manganese oxide catalysts with 5 and 20 wt% manganese loading with promotion of 1 wt% silver and one zirconia supported silver catalyst with 5wt% silver loading.

From the results, it is clear that the Mn-Ag catalysts reduce at a higher temperature than 5Ag and can be due to interaction between Mn and Ag, when manganese oxide reduces at a higher temperature than silver oxide. The first peak for 5Mn-1Ag could indicate more reduction of Ag in the first prominent peak. In contrast, for the 20Mn-1Ag, the prominent peak is shifted to a higher temperature indicating more enhanced interaction between Ag and Mn.

In Appendix B.2, Table B.1 displays the temperature of the different peaks in the TPR curves and Figure B.3 shows the TPR curves for the manganese oxide catalysts plotted in the same plot.

6.1.4 XRD

In Figure 6.4a, the XRD patterns are shown for the zirconia support and the two Mn/ZrO₂ catalysts. The zirconia is considerably crystalline and gives rise to numerous diffraction peaks. The zirconia support is in the monoclinic phase as desired due to the thermal stability.

Three diffraction peaks in the catalysts' XRD patterns differ from the zirconia pattern. The most prominent appears at 37.3° and two with lower intensity at 42.7° and 56.9°. In agreement with the results presented by Chen *et. al.*, the manganese phase obtained appeared to be γ -MnO₂ [11].

The broadened and weakened diffraction peaks of XRD prove that γ -MnO₂ is a highly disordered material. The structure of γ -MnO₂ is known to have defects in the crystalline structure as the γ -phase is a random combination between pyrolusite layers in a ramsdellite matrix preventing a perfect single crystal in the structure [84]. Materials with more vacancies and point defects may exhibit higher catalytic activity for oxidation reactions due to a higher amount of active sites in the material for reduction/oxidation [85]. The low intensity in the diffraction patterns for MnO₂ specific peaks can indicate high dispersion of MnO₂ and small crystallite size [13].

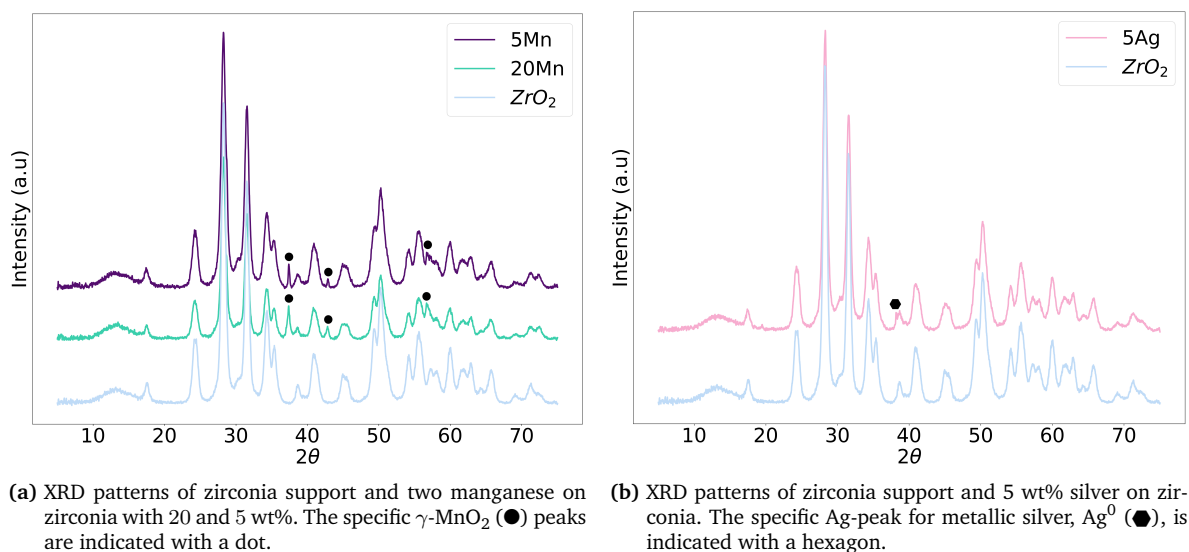


Figure 6.4: XRD patterns of ZrO₂, 5Mn, 20Mn and 5Ag in two separate plots. The settings were 40 kV and 40 mA with a wavelength of 1.54060 Å employing Cu K α radiation.

The XRD patterns for 5Ag compared with zirconia are shown in Figure 6.4b, and one specific peak is found for Ag at $2\theta = 38.1^\circ$. According to literature, the peak is Ag⁰ [86, 83].

Silver oxide appears to lose the oxygen at relative low temperatures even in excess of oxygen. Karski *et al.* studied the interaction between Pd and Ag on silica and observed the absence of hydrogen adsorption in H₂-TPR for the 5 wt% Ag/SiO₂ system. The results were as they expected as silver oxide loses oxygen quickly at a temperature higher than 250 °C, and their samples were calcined in air at 500 °C [87]. The silver catalyst in this work was calcined at 400 °C. Nevertheless, a peak in the TPR spectra was observed (Section 6.1.3), even though the presence of Ag₂O was not observed in the XRD profiles. It is important to note, that the present evidence relies on sufficient Ag₂O to be present in the catalyst bulk. XRD analysis gives information about crystallite planes in the catalyst bulk, and dispersed surface crystallites structures can be challenging to detect.

The results from XRD and TPR indicate that both metallic silver and silver oxide is present on the catalyst surface. The calcination temperature appeared to not be sufficient to reduce all the silver particles. The indication is in agreement with E. Aneggi *et al.* who studied soot combustion over silver-supported catalysts. They found that the silver particles were well-faceted on the zirconia support due to relatively weak interactions between silver and zirconia. They found that metallic Ag is dispersed on the surface of the zirconia together with Ag₂O particles from HRTEM images even though Ag₂O was not visible on the XRD pattern [88].

There is no distinct difference in XRD spectra when comparing the unpromoted and promoted manganese oxide catalysts other than a slight decrease in intensity for the specific MnO₂ peaks. The weaker intensity could be because of well dispersed MnO₂ species of small crystallite size and could indicate that the promotion of silver and platinum increased the dispersion of MnO₂. The XRD patterns for all the catalysts can be found in Appendix B.3.

Crystallite size calculations were based on the peak occurring at 37.3° . The line broadening was considered with an instrumental peak width equal to 0.05 Å. The shape of the particles are not investigated, but the constant K used were 0.9, assuming spherical particles. The results are displayed in Table 6.2. The crystallite size for 20Mn and 5Mn was 27 nm and 41

nm, respectively, resulting in a dispersion of 4% for 20Mn and 2% for 5Mn.

The results show a better dispersion and smaller crystallite size with a greater loading of manganese. The results show an unexpected trend, when a lower loading of active material was expected to give a better dispersion. The Scherrer equation, displayed in Equation 4.5 in Section 4.2.4 gives a rough estimation of crystalline size [67, 68]. The estimation is mainly used to compare within the different catalysts and should not be used for precise estimates of crystallite size [69]. As explained in Section 4.2.4, for crystallite sizes below 100 nm, the diffraction peak is broad enough for line broadening to occur due to incomplete destructive interference in scattering directions where the X-rays are out of phase. The peak used for crystallite size calculations, was weaker with lower loading of manganese, making it more challenging to obtain a somewhat reliable crystallite size. The silver peak was considered too weak, and too close to a zirconia-peak, so the crystallite was not calculated for the Ag⁰-peak.

Table 6.2: The Scherrer equation was used to calculate the crystallite size, $d_p = \frac{K\lambda}{B_p(2\theta)\cos(\theta)}$, where λ , $B_p(2\theta)$ and θ is given in radians. The specific peak for MnO₂ is where 2θ equals 37.3°, and for this peak the crystalline size of MnO₂ is calculated. θ is half of the diffraction angle, and the wavelength λ equals 1.54060 Å. The shape factor was chosen to be 0.9, and the dispersion was calculated from the crystalline size by the formula $D = \frac{1}{d_p}$.

Catalyst	2θ [°]	Crystallite size, d_p [nm]	MnO ₂ Dispersion [%]
5Mn	37.3	41	2%
5Mn-1Pt	37.3	41	2%
5Mn-1Ag	37.3	34	3%
20Mn	37.3	27	4%
20Mn-1Pt	37.3	20	5%
20Mn-1Ag	37.3	28	4%

6.2 Catalytic Activity

6.2.1 Blank Run

NO oxidation is favored by low temperature and high pressure, and the homogeneous gas-phase conversion was tested in the experimental setup without a catalyst present. The blank runs were performed with an empty reactor and 3,25 g SiC in the reactor. The blank run was performed to ensure that SiC was an inert diluent not making any contribution to the NO conversion and to create a baseline for identifying the onset temperature of catalytic activity.

Figure 6.5 illustrates the NO conversion as a function of temperature for the gas-phase reaction and SiC from 50 to 400 °C in dry conditions and 110 to 400 °C in wet conditions with a ramp rate of 5 °C/min at 1 bar.

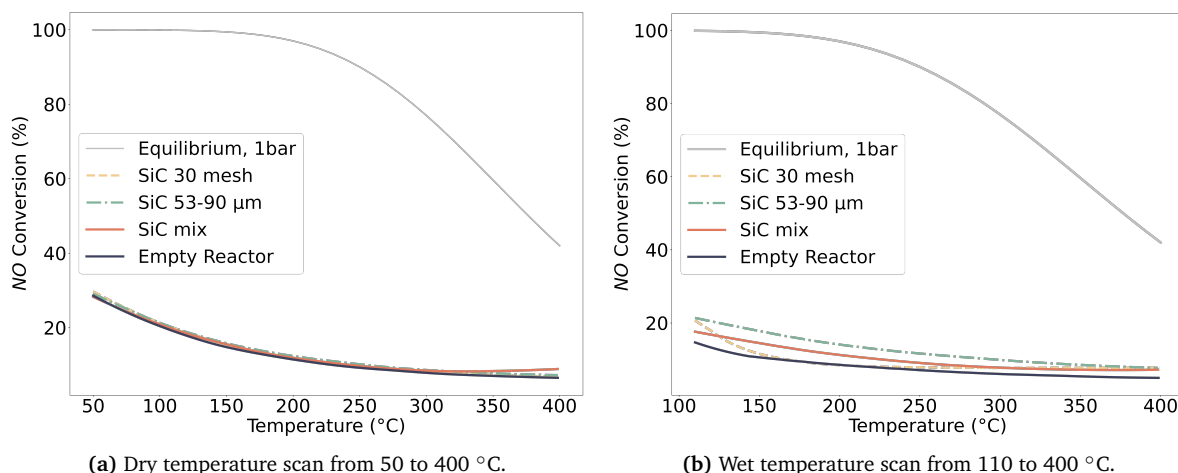


Figure 6.5: The NO conversion as a function of temperature for gas-phase reaction and SiC in two different particle fractions and a mix of the two particle sizes from 50-400 °C in dry conditions and 110-400 °C in wet conditions. The ramp rate was 5 °C/min and pressure at 1 bar with $WHSV = 24000 \text{ Nml/h} \cdot g_{cat}$. The NO_2 level considering the thermodynamic equilibrium of this reaction is represented as a grey line.

When temperature increases, the conversion decreases due to the negative rate constant for NO oxidation, as explained in Section 2.2. In agreement with Tsukahara *et al.* the rate constant decreases with a smaller gradient when temperature increases to 400 °C [89]. The trend is shown for the empty reactor experiment and the two different particle sizes of SiC (30 mesh and 53-90 μm). In addition, the SiC with mixed particle sizes are displayed.

In Figure 6.5a, the SiC 30 mesh and SiC 53-90 μm follows the same trend as the empty reactor test run in dry conditions. The gas-phase NO oxidation is highly pressure-sensitive, and the slightly higher conversion is assumed to be due to a slight pressure increase in the reactor when filled with SiC. Therefore, the SiC was assumed inert in the NO oxidation. Surprisingly, the SiC mixed showed some increase in NO conversion at high temperatures. When the particle sizes separately do not show any activity, it is assumed that an increase in NO conversion is due to experimental conditions and not that SiC is catalytically active.

During the wet conditions, displayed in Figure 6.5b, the differences between the test runs are more notable. The empty reactor experiment has the lowest NO conversion. A reasonable explanation is related to the sensitivity towards a pressure change. Some possible experimental challenges are explained in Section 6.2.3. The SiC tests runs increase the NO conversion but follow the same trend as the empty reactor experiment indicating an inert SiC. An exception is the SiC 30 mesh, which does not follow the same trend in the lower temperature regime. Anyway, the 30 mesh SiC was used in all the catalytic activity experiments making it was feasible to separate from the catalyst after the reaction.

6.2.2 Zirconia

A run with the zirconia support was conducted to investigate the reactivity in dry and wet conditions, shown in Figure B.1. The dry test run in Figure 6.6a follows the same trend as SiC until it reaches approximately 300 °C. In the temperature range 300-400 °C the NO conversion increases when the zirconia is present in the reactor. The results align with Zhao *et al.* who studied Mn/ZrO₂ catalysts for NO oxidation (500 ppm NO). They found that zirco-

nia showed catalytic activity over 300 °C for NO oxidation in diesel exhaust conditions, and demonstrated that ZrO₂ seemingly provided abundant adsorption sites for NO_x whether with or without MnO_x [44]. The weak basicity of ZrO₂ can form sufficient nitrogen-containing species in the surface/subsurface and could be a possible reason for the increased NO conversion [90, 91]. Compared with the dry run, the wet run does not show any catalytic activity in the same temperature range, displayed in Figure 6.6b.

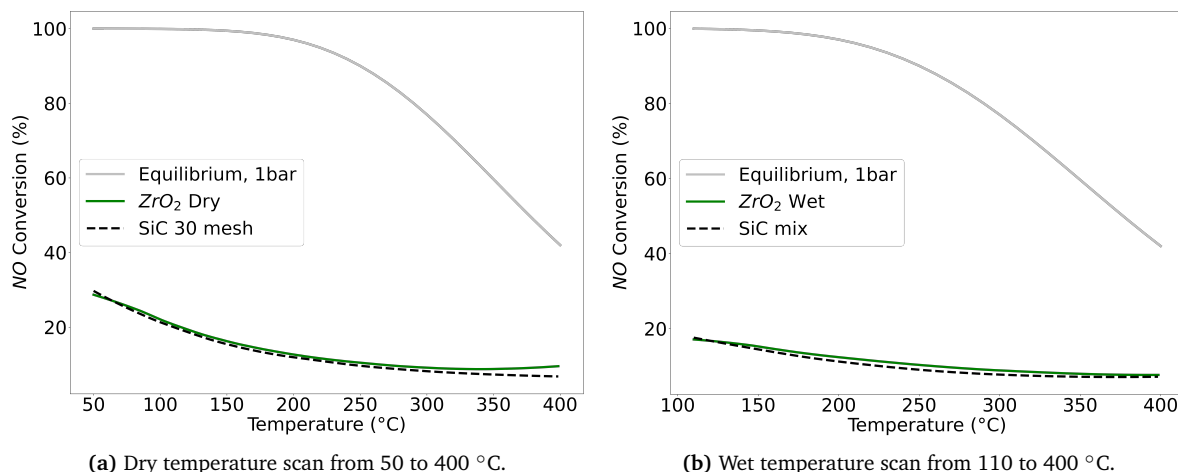


Figure 6.6: The NO conversion as a function of temperature for the zirconium oxide support, both dry and wet temperature ramp from 50 to 400 °C and 110 to 400 °C with a ramp rate of 5 °C/min at 1 bar with $WHSV = 24000 \text{ Nm}^3/\text{h} \cdot \text{g}_{cat}$. SiC in 30 mesh fraction is presented in both plots, and SiC in a mixed fraction in addition in the wet run.

6.2.3 Conversion and Experimental Challenges

The conversion of NO was used to measure the catalytic activity. All catalysts were packed the same way in the reactor, placed in the rig setup, treated with the same temperature program and equal amount of flow is fed in each experiment in resembling nitric acid plant conditions. However, during the temperature scan test runs, the NO conversion was significantly different for each catalyst initially at low temperatures where only the gas-phase conversion should be present. The observed results rise the possibility of both systematic and random errors during the activity measurements. This work assumes an equal systematic error for each test when comparing the catalysts, but this could be wrong, when the basis of comparison differ.

The most plausible reasons for the differences are pressure drop in the reactor and imprecise temperature measurements. Equation 5.3 in Section 2.2 in Chapter 2, show that the reaction rate is dependent on the oxygen content and the second power of the NO content. The reaction rate increases when the pressure of NO and O₂ increase and is sensitive to pressure drop when p_{NO} is squared. The catalyst particle was in size range of 53-90 μm, while the SiC was in 30 mesh (595 μm). Due to the apparent difference in particle size, it was challenging to mix the catalyst powder and SiC particles into a homogeneous mixture, and could have resulted in a different distribution of catalyst particles in the SiC for each catalyst when packing the reactor. The small particle size could lead to a pressure drop if the catalysts bed were packed compact, and experimentally this was challenging to control due to the reactor and experimental design. The packing of the catalyst bed could lead to differences in the conversion as a consequence of pressure drop and temperature differences.

There is most likely an error in the temperature measurements during the temperature scans. The thermocouple was placed inside the reactor and measured a point in the catalyst bed. The thermocouple was placed in the lower part of the catalyst bed, or the bed exit. As a result a part of the bed could be operated at a higher temperature than what was measured at low temperatures. The opposite effect will occur at high temperatures. The gas is heated when it enters the reactor before it hits the catalyst bed and will generate some non-uniformity in the temperature within the reactor. The dry test runs start when the reactor is 50 °C, but the gas-feed lines are heated to 200 °C, creating a significant temperature gradient inside the reactor during the experiment. When a catalyst is present in the reactor, and the feed entering is 200 °C, there is potentiality observed some catalytic activity. This likely resulted in a higher NO conversion even though the measured temperature in the reactor shows a value according to the set temperature program. The same significant temperature gradient will be present after the reactor temperature passes 200 °C, and the feed gas will cool the reactor. As a result, the measured NO conversion at the different temperatures could be lower in the higher temperature regime.

The NO oxidation is an exothermic reaction and will be an additional challenge regarding temperature control, correct temperature and NO conversion measurements. In general when diluting with the inert SiC, the reaction heat is diluted, and not the heating of the feed. Only a small part of the feed is reacting so it is most likely not making a significant temperature increase, and the heating takes place inside the reactor.

The gas-phase NO oxidation is spontaneous and will continue after the gases leave the reactor before entering the FTIR analyzer. The gases were diluted heavily at the reactor effluent with argon (argon/reactor effluent = 4) to minimize the gas-phase reaction. However, the exact % increase in NO conversion happening after the catalyst bed and downstream before it is measured in the FTIR analyzer is unknown. The argon dilution is in addition cooling the product stream to 191 °C, and could affect the NO conversion. The difference between the measured value and the actual value for catalytic activity results in an error in the measurements. However, the error is assumed approximately equal in each experiment to compare the catalysts.

As a result of the challenges regarding the NO conversion in the lower temperature regime in the temperature scan test run results, the gas-phase contribution was subtracted from the total NO conversion to compare the different catalysts. As shown in Figure 6.5, the SiC behaved differently in dry and wet conditions, so the background to subtract was chosen according to the best fit with the catalysts test runs. For the dry temperature scans (Dry 1 and Dry 2), SiC 30 mesh were used as a background. For the wet temperature scans (Wet 1 and Wet 2) SiC mixed fractions were used. The gas-phase contribution was subtracted in the presentation of temperature scan results, but not for the steady-state experiments. An overview of which background is used for subtraction is displayed in Table C.2 in the Appendix, section C.3.

6.2.4 Effect of Temperature

The differences in the NO conversion at low temperature highlight the experimental difficulties in the used experimental design. The conversion presentation has uncertainty factors due to the several influencing factors, discussed in the previous section, but will present the differences between the catalysts and their behavior in the different conditions. Regarding the limitations of temperature measurement and pressure drop in the reactor, it could be argued that the onset temperature and activation energy will not be reasonable to present from the

temperature scans and are not included in the following discussion.

Emphasis has been placed on the temperature dependence presented as catalytic NO conversion, $x_{NO,c}$ as a function of temperature. The data modification is described in Appendix C.3. Catalytic NO conversion at 250 and 350 °C is considered inaccurate in terms of uncertainties related to the experimental design, but is attached in Appendix C.3. The total NO conversion as a function of temperature without subtraction of the gas-phase contribution is presented in Figure C.1 and C.2 in Appendix C.2.

The amounts of catalyst sample and SiC used in activity measurements is displayed in Table C.1 in Appendix C.1.

This section illustrates experimental results from the first and second temperature scans in dry and wet conditions. The temperature program is described in Figure 5.3 in Section 5.3. In between the temperature scans, 16 hours (8h at 350 °C and 8h at 350 °C) on-stream experiments were conducted.

6.2.4.1 Silver Catalyst Compared with Manganese Oxide Catalyst

Figure 6.7 show the NO conversion of 5Mn Dry 1 and 2 is compared with 5Ag Dry 1 and 2 from 50-400 °C. The silver and manganese oxide catalysts show catalytic activity in both dry and wet conditions. The catalysts have the same wt% of metal oxide, but manganese shows significantly better catalytic activity after 200 °C.

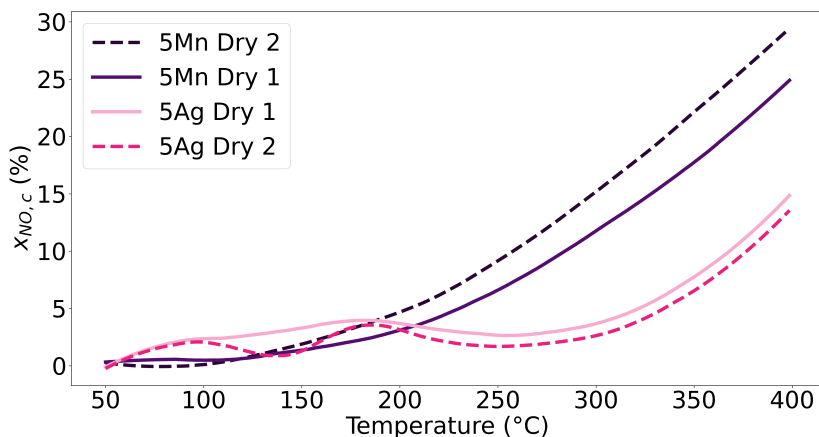


Figure 6.7: The catalytic NO conversion (%), $x_{NO,c}$, of 5Mn Dry 1 and 2 compared with 5Ag Dry 1 and 2 from 50-400 °C with a ramp rate of 5 °C/min. The WHSV = 24000 $Nml/h \cdot g_{cat}$, and pressure at 1 bar.

The silver catalyst is observed to increase the NO conversion to times shown as two peaks in the lower temperature regime before a more notable catalytic activity is shown at a higher temperature. The tendency in NO conversion is more prominent from the first to the second run, making the projections more explicit in Dry 2. The TPR profile of 5Ag exposes one specific peak at 100 °C, shown in Figure 6.3 in Section 6.1.3, which matches the first rise in catalytic activity for the 5Ag, indicating a possible change in oxidation state. How the silver oxidize interacts in the NO oxidation is unknown in resembling nitric acid plant conditions. However, a change in the oxidation state seems to increase NO conversion. The silver catalyst is observed to have minor differences between the first and the second temperature scan.

Männikkö *et al.* characterized the active species in the silver/alumina system for lean NO_x reduction with methanol by temperature-programmed desorption with 500 ppm NO (NO-TPD) in oxygen excess. The NO-TPD showed two or more peaks of NO₂ consumption for the alumina-supported silver catalysts as a function of temperature with a ramp rate of 10 °C/min [41]. The peaks occurring for the silver catalyst (5Ag) in this work could be linked to the NO₂ consumption on the silver catalyst. The silver catalyst should be further investigated by performing NO-TPD with a higher concentration of NO than Männikkö *et al.* in their research [41].

Figure 6.8 shows how the catalysts performed in dry and wet conditions. When water is present in the feed, the water will consume NO₂ and produce NO, moving the reaction in an undesired direction, and slowing down the NO oxidation [12]. In addition, water accelerates both the surface reconstruction and sintering process for the catalyst [13].

As expected, 5Mn Wet 1 shows less catalytic activity than Dry 1 in Figure 6.8b. The same trend is shown for the second temperature scans, and Wet 2 perform better than Wet 1 for 5Mn, indicating an activation of the catalyst during resembling nitric acid plant conditions. It is worth highlighting the observations that Dry 1 and Wet 2 follow the same catalytic activity. The results could demonstrate three things. First, the manganese oxide catalyst should have been oxidized to perform better in the NO oxidation. Second, the manganese oxide catalyst is activated due to the conditions involving nitrates, water and oxygen in temperatures up to 400 °C. Finally, the catalyst could have changed structure resulting in a higher catalytic activity. The possible reasons should be further investigated when there is insufficient knowledge about the system and reaction mechanism.

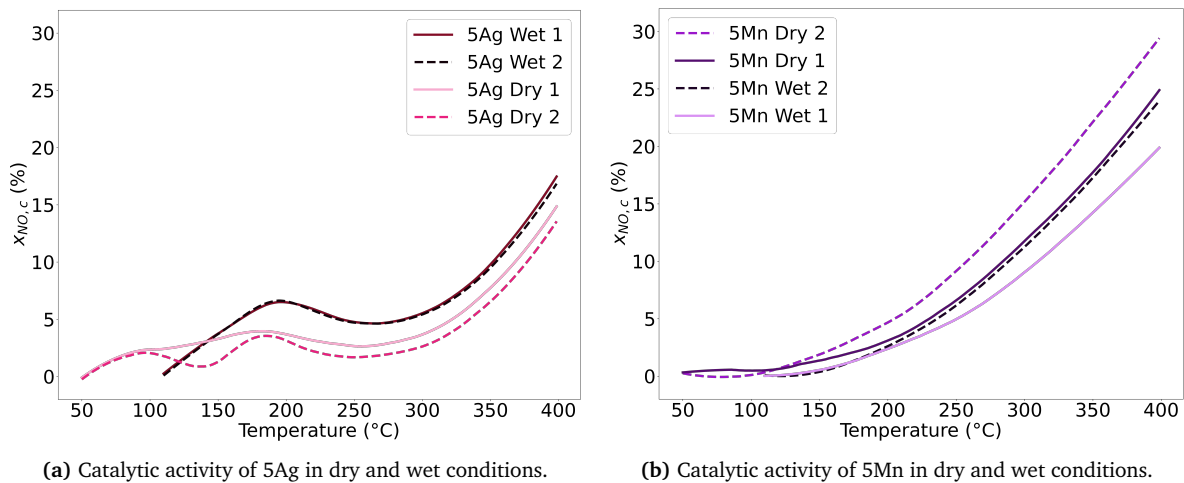


Figure 6.8: The catalytic NO conversion (%), $x_{NO,c}$, from 50-400 °C with a ramp rate of 5 °C/min. The WHSV = 24000 Nml/h · g_{cat} , and pressure is 1 bar.

In Figure 6.8a, the silver catalyst yield higher NO conversion in wet conditions. Water adsorption is inevitable in a given reaction on oxide surfaces but can also serve as a promoter/reactant, and not only an inhibitor [92]. For the silver catalyst, water is observed not to limit the NO conversion but enhances the catalytic activity and could mean that water serve as a promoter or reactant in the NO oxidation over the silver catalyst. As for the dry, there are neglectable differences between the first and second wet test runs.

The temperature dependency of the catalytic activity for 5Ag and 5Mn is presented as the slope of catalytic NO conversion $x_{NO,c}$ as a function of temperature in the range from 250 to

350 °C in Figure 6.9. The slope is calculated by regression, and the information regarding R^2 and p-value is given in Table C.3 in Appendix C.3.2.

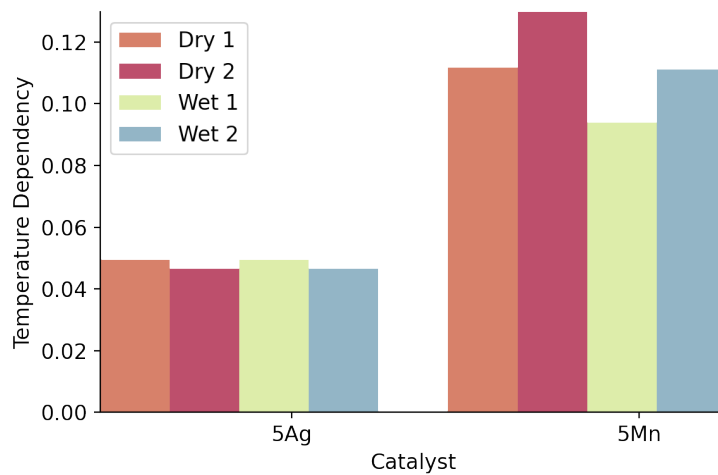


Figure 6.9: The temperature dependency of the catalytic activity for 5Ag and 5Mn presented as the slope of catalytic NO conversion $x_{NO,c}$ as a function of temperature in the range from 250 to 350°C.

From the results, it is clear that the 5Mn catalyst has an overall higher temperature dependency than the 5Ag catalyst. The manganese oxide catalyst is observed to enhance the temperature dependency in the second test runs while 5Ag has approximately the same temperature dependency in dry and wet conditions. The observed findings deduce the positive effect on the catalytic activity after hours on-stream in partially simulating nitric acid plant conditions for the zirconia-supported manganese oxide catalyst.

6.2.4.2 Promoted 5wt% Manganese Oxide on Zirconia

The zirconia-supported manganese oxide catalysts were promoted with 1 wt% platinum and silver, and the catalytic activity from Dry 1 and Wet 1 of the three catalysts with 5 wt% manganese is presented in Figure 6.15.

Salman *et al.* suggested that NO oxidation over a supported manganese oxide catalyst proceeded via a Mars-van Krevelen mechanism in resembling nitric acid plant conditions [13]. Their finding led to promoting the manganese oxide catalysts with metal oxides reducing at a lower temperature than manganese to possibly enhance the catalytic activity at a lower temperature. Promising results were observed from TPR results, in Section 6.1.3, as silver and platinum made manganese reduced at a lower temperature. Based on Salman's findings [13], it was expected that the promoted catalysts would exhibit catalytic performance earlier than unpromoted manganese.

It is important to highlight the uncertainties regarding the correct temperature measurement. The subtraction of the gas-phase contribution, make it difficult to determine which catalyst shows catalytic activity first. However, the three catalysts have the onset of catalytic activity close to 150 °C in Dry 1 in Figure 6.10a. As temperature increases, 5Mn-1Ag yields a significantly higher conversion than 5Mn and 5Mn-1Pt, which follows the same catalytic activity in the higher temperature regime.

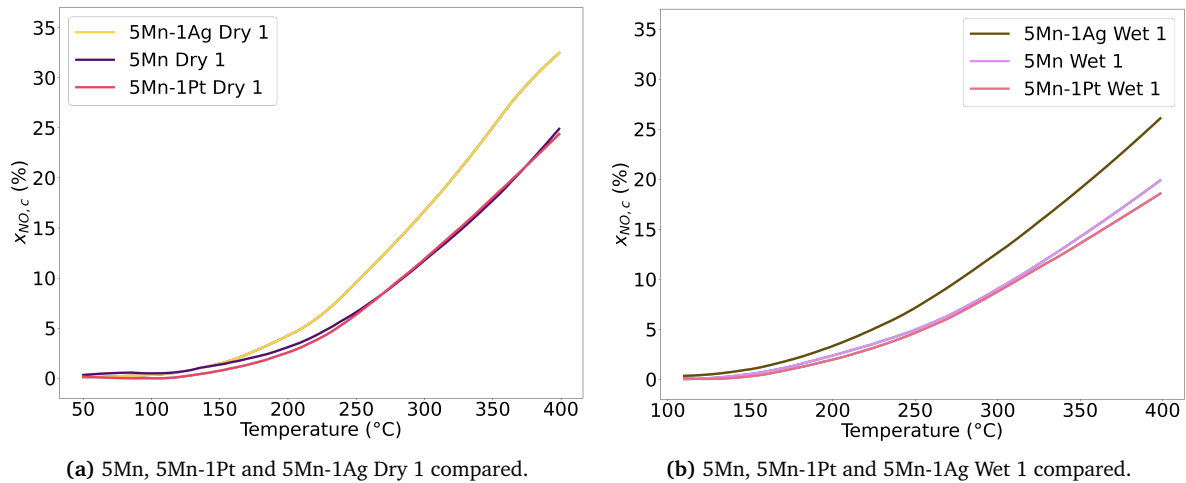


Figure 6.10: The NO conversion (%) of 5Mn, 5Mn-1Pt and 5Mn-1Ag in dry and wet conditions from 50-400 °C and 110-400 °C with a ramp rate of 5 °C/min. $WHSV = 24000 \text{ Nml/h} \cdot g_{cat}$ at 1 bar.

The platinum-promoted catalyst was not activated with H_2 to have the same basis of comparison for all the catalysts. According to research on manganese catalysts in diesel exhaust conditions, MnO_2 exhibits a higher NO conversion than Mn_2O_3 , so reducing the manganese was not desired [32]. Typically, platinum needs to be reduced in order to be catalytic active in an oxidation reaction and is exposed to H_2 before NO oxidation [15]. After calcination, platinum was assumed to be in oxide form, inhibiting the possible higher conversion expected from the platinum-promoted catalyst. 5Mn-1Pt resulted in having the same catalytic activity as the unpromoted catalyst, and no effect of the promotion was observed.

The first temperature scan under wet conditions is shown in Figure 6.10b. The same trend as the dry temperature scan is observed, but the water inhibits the catalytic activity, and the NO conversion is lower than in dry conditions. 5Mn-1Ag exhibits the best catalytic performance in wet conditions, while 5Mn and 5Mn-1Pt show roughly the same activity. The comparison between the first and second temperature scan test run for the promoted 5 wt% catalysts are displayed in Figure C.6 in Appendix C.3.1.

The temperature dependency of the catalytic activity for 5Mn, 5Mn-1Pt and 5Mn-1Ag is presented as the slope of catalytic NO conversion $x_{NO,c}$ as a function of temperature in the range from 250 to 350 °C in Figure 6.11. The slope is calculated by regression, and the information regarding R^2 and p-value is given in Table C.3 in Appendix C.3.2.

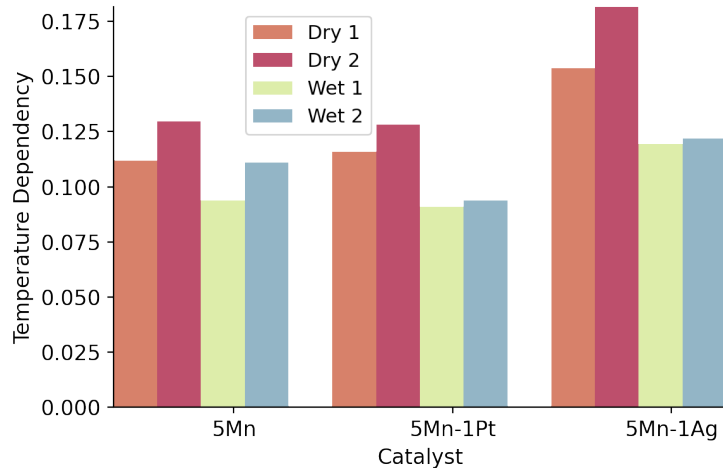


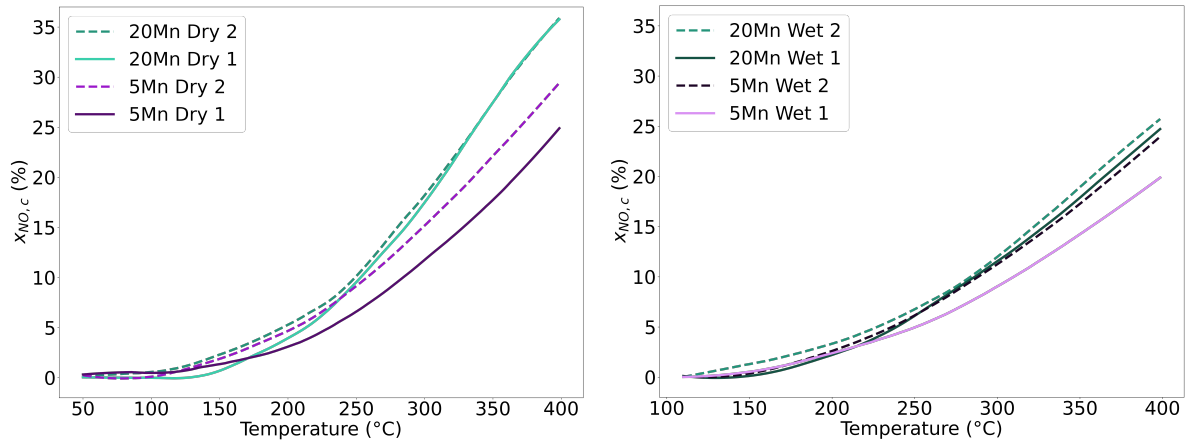
Figure 6.11: The temperature dependency of the catalytic activity for 5Mn, 5Mn-1Pt and 5Mn-1Ag presented as the slope of catalytic NO conversion $x_{NO,c}$ as a function of temperature in the range from 250 to 350 °C.

It is notable that 5Mn-1Ag has the highest temperature dependency compared to 5Mn and 5Mn-1Pt. The mechanism of the surface reactions is not studied in this work, but it is observed that silver in combination with manganese oxide supported on zirconia enhances NO oxidation at the studied conditions. If the oxidation of NO takes place via the MvK mechanism, the lattice oxygen in MnO_2 plays an essential role in catalytic oxidation. Based on other literature [26, 25, 37], one could assume that the lattice oxygen mobility of manganese oxides is improved, or the formation of abundant active lattice oxygen occurs by doping with silver, making the catalyst more efficient in the oxidation of NO.

The trend seen from the temperature dependency calculations reflects the conversion curve presented in Figure 6.15, and 5Mn and 5Mn-1Pt have the same temperature dependency in the dry conditions. In wet conditions, 5Mn-1Pt has the lowest temperature dependency. It is interesting to note that the 5Mn-catalysts has a slightly higher temperature dependency in the second dry temperature scan. The enhanced difference is more apparent in the dry test runs compared to the wet.

6.2.4.3 Effect of Manganese Loading on Zirconia

Figure 6.12 shows the catalytic activity of 5Mn compared with 20Mn in dry (Figure 6.12a) and wet (Figure 6.12b) conditions. The catalytic conversion is lower in the wet test runs compared to the dry. Salman found that the zirconia-supported catalysts were independent of manganese loading in resembling nitric acid plant conditions [13]. The results from the dry temperature scan test run demonstrate another trend regarding the manganese loading on zirconia, and the 20Mn catalyst exhibits a higher NO conversion than 5Mn. However, in the wet test runs, there is not much difference between the 20Mn and 5Mn in the second test run. As mentioned in Section 6.2.3, some of the main sources of uncertainty in this work are the baseline used for the presentation of the catalytic NO conversion and the temperature measurements. The small differences in catalytic activity shown in the temperature scans could be different if the catalyst got the time to stabilize with a slower temperature ramp rate.



(a) 20Mn Dry 1 and 2 compared with 5Mn Dry 1 and 2 from 50 – 400°C. (b) 20Mn Wet 1 and 2 compared with 5Mn Wet 1 and 2 from 110 – 400°C.

Figure 6.12: The NO conversion (%) of 5Mn and 20Mn in dry and wet conditions from 50-400 °C and 110-400 °C with a ramp rate of 5 °C/min respectively. $WHSV = 24000 \text{ Nm}l/h \cdot g_{cat}$ and pressure at 1 bar.

As 5Mn Dry 1 and Dry 2 show a notable difference, 20Mn is observed to perform the same catalytic activity from the first to the second temperature scan in the higher temperature regime. From this standpoint, the different trends between the catalysts can be considered as a deactivation happening for the 20 wt% manganese oxide catalyst. 20Mn has a higher dispersion than 5Mn based on the calculations using the Scherrer equation, presented in Table 6.2. In addition, 20Mn was observed to have a lower reduction temperature than 5Mn, presented in Section 6.1.3, which could indicate a better dispersion of the manganese on the zirconia support. This may improve aspects of a correlation between dispersion and catalytic activity, when 20Mn seems to have a higher deactivation rate than 5Mn, but should be further investigated when a higher dispersion is generally desired.

The slope of catalytic NO conversion $x_{NO,c}$ as a function of temperature in the range from 250 to 350 °C is displayed in Figure 6.13. The temperature dependency of the catalytic activity for 5Mn and 20Mn reflect the curves in Figure 6.12. The slope is calculated by regression, and the information regarding R^2 and p-value is given in Table C.3 in Appendix C.3.2. The temperature dependency reflect the trend in Figure 6.12

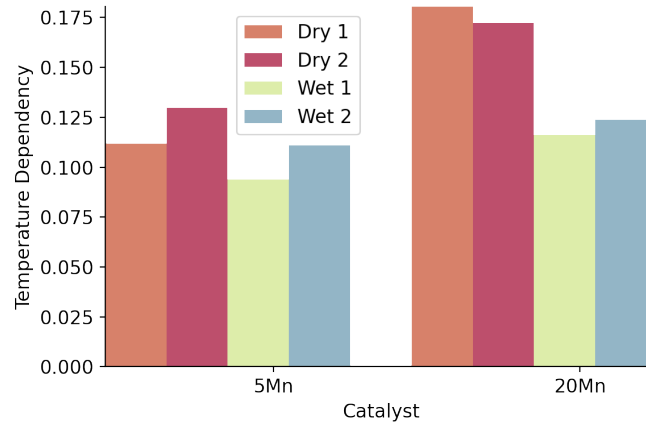


Figure 6.13: The temperature dependency of the catalytic activity for 5M and 20Mn presented as the slope of catalytic NO conversion $x_{NO,c}$ as a function of temperature in the range from 250 to 350 °C.

A correlation between the onset reduction temperature from TPR spectra and the onset temperature of the catalysts can indicate that the catalytic conversion of NO starts at the onset of surface manganese oxide reduction [13]. If the correlation is present, it implies that oxidation of NO over manganese oxides proceeds via the Mars-van Krevelen mechanism [93]. Figure 6.14 displays the total conversion of 20Mn and 5Mn in dry conditions (Figure 6.14a) and the TPR spectrum zoomed in on the initial reduction of 20Mn and 5Mn.

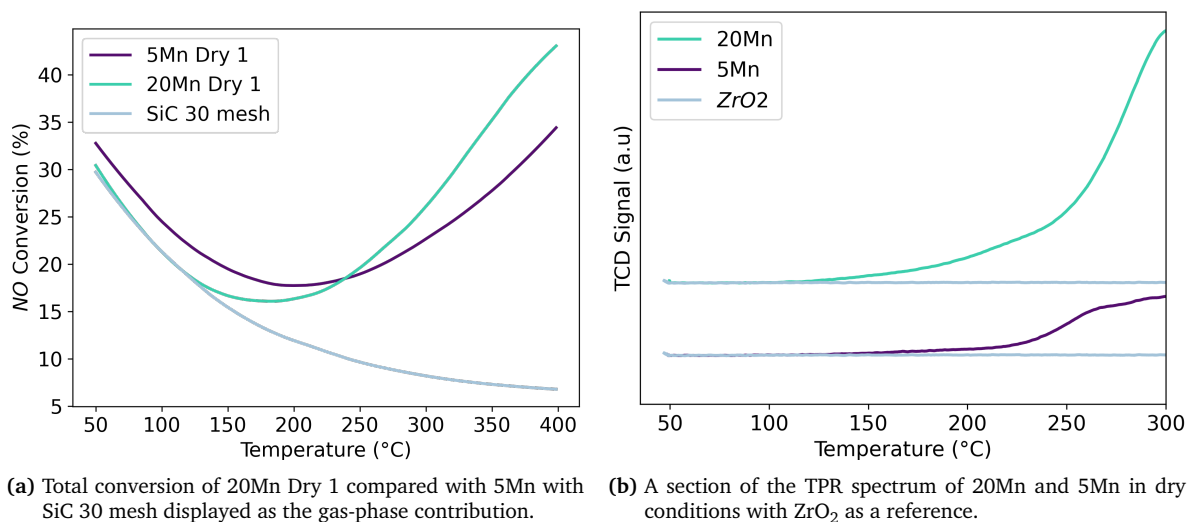


Figure 6.14: The total NO conversion of 5Mn and 20Mn as a function of temperature and the TPR spectrum of the same catalysts to see the correlation between the onset temperature of catalytic activity and reduction temperature.

As displayed in Figure 6.14b, 20Mn reduces at a lower temperature than 5Mn, and is reflected in the onset temperature of catalytic activity shown in Figure 6.14a where the 20Mn shows catalytic activity earlier than 5Mn.

It is worth highlighting the initial differences in the total conversion plot, where 5Mn starts at a higher NO conversion than 20Mn and SiC 30 mesh. Even though the catalysts were tested in the same conditions in the same setup, differences appeared in the low-temperature range,

resulting in uncertainties related to the catalytic activity from the temperature scans, as previously explained in Section 6.2.3. However, the onset temperature from the NO conversion plot and the reduction temperature from the TPR spectrum show correlation, which can indicate the oxidation of NO over zirconia-supported manganese oxides proceeds via a Mars van Krevelen mechanism. Further investigations should be performed to confirm the suggested mechanism. TPR in wet conditions would give a more reliable indication of a possible correlation between the catalytic conversion of NO and the reduction temperature of the catalyst in resembling nitric acid plant conditions where water is unavoidable. Overall these findings are in accordance with findings reported by Salman *et al.* studying supported manganese oxide catalysts in resembling nitric acid plant conditions [28].

Tang *et al.* studied the mechanism of NO oxidation at lean NO_x conditions (600 ppm NO, 4 vol% O₂) over Mn/TiO₂ catalyst through a systematic *in-situ* diffuse reflectance infrared Fourier transform spectroscopy (DRIFTS) investigation. The pathway of NO oxidation over MnO_x/TiO₂ was shown to proceed via a Mars-van Krevelen mechanism where the NO was first coordinated to Mn sites, forming nitrosyls, which were easily oxidized to nitrates by lattice oxygen before the nitrates were decomposed to NO₂ [94].

6.2.4.4 Promoted 20wt% Manganese Oxide on Zirconia

Figure 6.15 displays the results from the dry and wet temperature scans for 20Mn, 20Mn-1Pt, and 20Mn-1Ag. As the temperature increase in the dry test run, shown in Figure 6.15a, the catalytic activity increase, but different for each catalyst. At approximately 250 °C, 20Mn conversion crosses 20Mn-1Pt, which results in a higher NO conversion for 20Mn in the higher temperature regime. From these results it is clear that 20Mn-1Ag has a higher conversion than 20Mn and 20Mn-1Pt after 300°C in dry and wet condition. However, it is observed minor differences at lower temperatures. The comparison between the first and second temperature scan test run for the promoted 20 wt% catalysts are displayed in Figure C.7 in Appendix C.3.2.

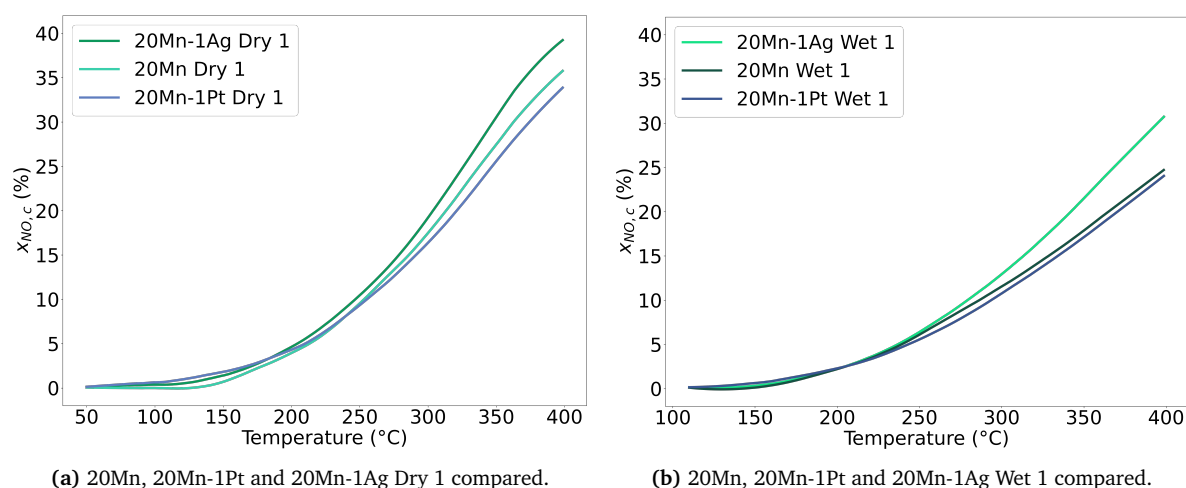


Figure 6.15: The NO conversion (%) of 20Mn, 20Mn-1Pt and 20Mn-1Ag in dry and wet conditions from 50-400 °C and 110-400 °C with a ramp rate of 5 °C/min. WHSV = 24 000 Nml/h · g_{cat} at 1 bar.

As previously explained for the 5Mn catalysts in Section 6.2.4.2, the platinum-promoted catalyst was not activated by reduction before the catalytic activity analysis. The platinum is

most likely in an oxide that is less active in the oxidation reaction. Even though manganese is highly dominant compared to the platinum related to loading in the 20Mn-1Pt catalyst, manganese was reduced at a lower temperature than unpromoted manganese according to TRP results, indicating a Pt-Mn bond between the species (Section 6.1.3). However, the catalytic NO conversion is not affected by this in the observed results from the temperature scan test runs.

The temperature dependency of the catalytic activity for 20Mn, 20Mn-1Pt and 20Mn-1Ag is presented as the slope of catalytic NO conversion $x_{NO,c}$ as a function of temperature in the range from 250 to 350°C as a bar plot in Figure 6.16. The slope is calculated by regression, and the information regarding R^2 and p-value is given in Table C.3 in Appendix C.3.2.

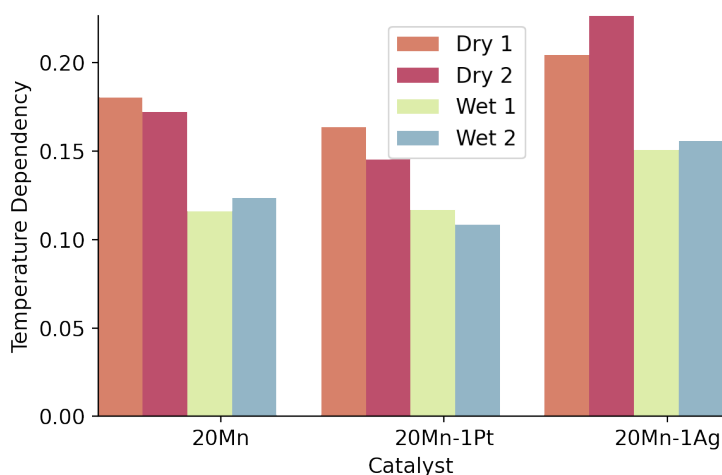


Figure 6.16: The temperature dependency of the catalytic activity for 20Mn, 20Mn-1Pt and 20Mn-1Ag presented as the slope of catalytic NO conversion $x_{NO,c}$ as a function of temperature in the range from 250 to 350°C.

The particle size of platinum particles are assumed to correlate with the catalytic activity in partially simulating nitric acid plant conditions [13]. Salman showed that platinum supported by zirconia and alumina catalyst exhibited higher catalytic activity after experimental runs in resembling nitric acid plant conditions. Due to the sintering of platinum nanoparticles, larger platinum particles were formed, resulting in a more active catalyst. The presence of water in the feed significantly accelerated both the surface reconstruction and sintering process [13]. In this work, platinum shared the support surface with manganese oxide. The 20Mn-1Pt is not showing a higher temperature dependency in the second run, indicating that the platinum particles are not aggregating in a structure with manganese. Further investigation for the platinum-promoted manganese catalysts should be performed regarding structure, for example, by transmission electron microscope (TEM) techniques.

In Section 6.2.4.3, it is suggested that oxidation of NO over unpromoted manganese oxides proceeded via a Mars-van Krevelen mechanism as a correlation between the onset temperature of catalytic activity and the initial reduction temperature from the TPR spectrum is observed. Researchers suggest that Mn-Ag catalysts proceed via an MvK mechanism in research regarding oxidation of volatile organic compounds (VOC) [25, 27]. In contrast, the correlation between catalytic conversion and reduction temperature is not observed for the promoted catalysts in this work. The initial reduction temperature is lower than the onset temperature of catalytic activity. A popular suggestion is that oxidation over platinum catalysts proceed via a

Langmuir-Hinselwood-Hougen-Watson (LHHW) mechanism or Langmuir-Hinselwood mechanism in NO oxidation [95, 15, 96], which is in contrast with the suggested mechanisms over manganese oxide and silver-manganese oxide catalysts. There is no evidence for a possible mechanism for the promoted catalysts in this work, and the mechanism of NO oxidation over the catalysts should be further investigated.

6.2.4.5 Comparison of all Catalysts

The temperature dependency for the catalysts is presented in Table 6.3 and Figure 6.17. 20Mn-1Ag displays the highest temperature dependency from the temperature scans, resulting in the highest catalytic activity in resembling nitric acid plant conditions.

Table 6.3: The temperature dependency, represented as the slope from the temperature interval between 250-350 °C of each catalyst during the temperature scans in dry and wet conditions.

Catalyst	Slope			
	Dry 1	Dry 2	Wet 1	Wet 2
5Ag	0.05	0.05	0.05	0.05
5Mn	0.11	0.13	0.09	0.11
5Mn-1Pt	0.12	0.13	0.09	0.09
5Mn-1Ag	0.15	0.18	0.12	0.12
20Mn	0.18	0.17	0.12	0.12
20Mn-1Pt	0.16	0.15	0.12	0.11
20Mn-1Ag	0.20	0.23	0.15	0.16

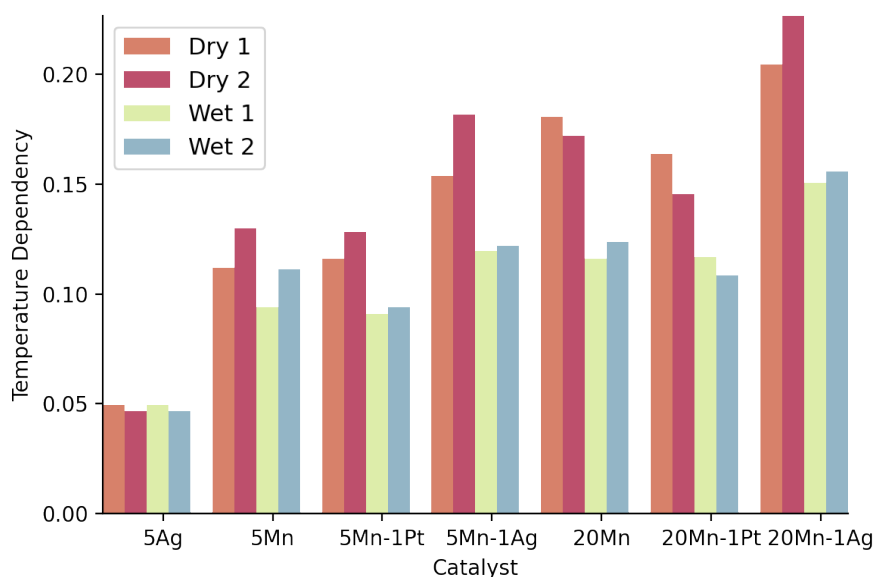


Figure 6.17: The temperature dependency of the catalytic activity for the catalysts presented as the slope of catalytic NO conversion $x_{NO,c}$ as a function of temperature in the range from 250 to 350 °C.

Considering the Wet 2 temperature scan test run, the catalysts were through approximately 18 hours on-stream in partially simulating nitric acid plant conditions, periodically in dry

and wet conditions. From these results, it is clear that 20Mn-1Ag shows the highest temperature dependency in the range between 250 and 350 °C. 20Mn and 5Mn-1Ag show the same temperature dependency, with minor differences to 5Mn and 20Mn-1Pt. 5Mn-1Pt showed the lowest temperature dependency compared to the other manganese oxide catalysts in wet conditions. The results can indicate that the loading of manganese does not scale with the catalytic activity. However, the molar ratio between Ag/Mn can be important when 20Mn-1Ag exhibits higher NO conversion than 5Mn-1Ag in the considered temperature range. The results indicate that the addition of platinum is not beneficial for catalytic activity in the studied conditions. Platinum catalysts are known to yield lower NO conversion when water is present in the system [15].

6.2.4.6 Activation of Manganese catalyst

5Mn was observed to enhance the catalytic activity from the initial to the final temperature scan. Based on the results, the manganese oxide catalyst were tested again in resembling nitric acid plant conditions after pretreatment. The pretreatment performed was 1) 10 vol% O₂ at 400 °C for 2 hours and 2) 15 vol% H₂O at 400 °C for 1 hour. The results are presented in Figure 6.18 where 5Mn with two different pretreatments, and the previous results with no pretreatment (Dry 1 and 2).

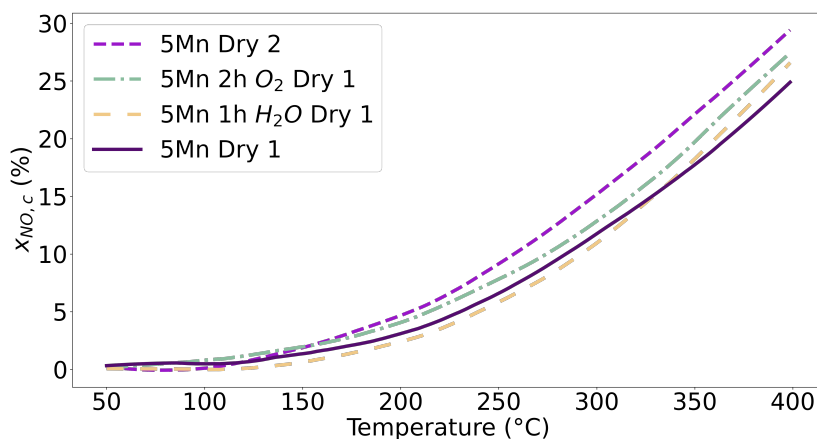


Figure 6.18: The NO conversion (%) of 5Mn Dry 1, water-pretreatment (5Mn 1h H₂O Dry 1), pre-oxidized (5Mn 2h O₂ Dry 1) and 5Mn Dry 2 from 50 to 400 °C with a ramp rate of 5 °C/min. WHSV = 24 000 Nml/h · g_{cat}, and pressure at 1 bar.

The first temperature scan without pretreatment performs better than the water-activated catalyst up to approximately 340°C, resulting in the lowest catalytic activity at a higher temperature. The oxidized 5Mn Dry 1 shows yields higher NO conversion than water-activated and no pretreatment (5Mn Dry 1). Based on the results, oxidation activates the manganese catalyst resulting in an overall higher NO conversion when looking at the first temperature scan. However, 5Mn Dry 2 performs better than all the Dry 1 with and without pretreatment. The results indicate that the conditions during the experimental run in resembling nitric acid plant conditions activate the catalyst to a greater extent than only oxidation of the catalyst. The results do not confirm that pretreatment a good choice for the unsupported manganese catalysts. However, they indicate that time in an atmosphere with excess oxygen is an essential factor in activating the catalyst.

6.2.4.7 Activation of Platinum-promoted Manganese Catalyst

The pretreatment of the platinum-promoted catalysts was challenging when it was desired to reduce the platinum meanwhile maintaining MnO_2 . A test run with pretreatment in H_2 was conducted to see the difference from catalytic activity after no pretreatment. The temperature for reduction chosen for 20Mn-1Pt was decided according to the TPR spectrum displayed in Section 6.1.3. The amount of hydrogen used in the feed was calculated from the TPR measurements, where 0.5 g catalyst required 17.5 ml/min H_2 (8.5 %).

Figure 6.19 displays the catalytic activity as a function of temperature for 20Mn-1Pt with and without pre-activation of the catalyst in dry and wet conditions. The catalyst going through the pretreatment is named *20Mn-1Pt Reduced*.

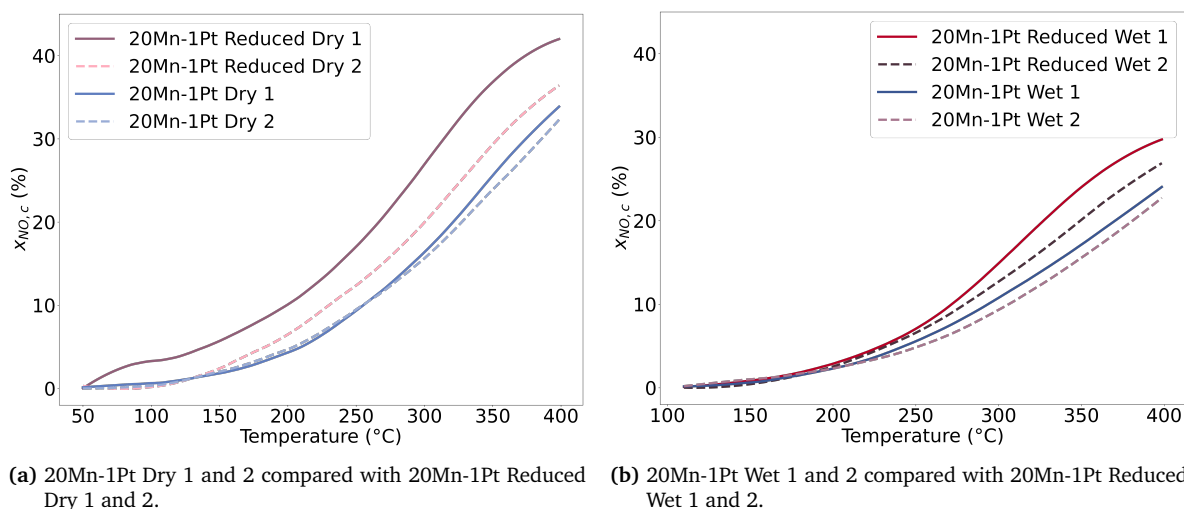


Figure 6.19: The NO conversion (%) of 20Mn-1Pt with and without pretreatment in H_2 (20Mn-1Pt vs 20Mn-1Pt Reduced) in dry and wet conditions from 50-400 °C and 110-400 °C with a ramp rate of 5 °C/min. $\text{WHSV} = 24\,000 \text{ Nml/h} \cdot g_{\text{cat}}$ at 1 bar.

The dry temperature scans, presented in Figure 6.19a, show a significant improvement in the catalytic activity as a consequence of the pretreatment. Initially, the 20Mn-1Pt Dry 1 Reduced had a lower NO conversion than the SiC resulting in a sudden catalytic activity after subtracting the gas-phase contribution. The total conversion as a function of temperature is shown in Figure C.3 in Appendix C.2.

The temperature dependency of the catalysts are presented in Figure 6.20, showing how the pretreated 20Mn-1Pt performs compared to the other 20Mn-catalysts. The slope of catalytic NO conversion $x_{\text{NO},c}$ as a function of temperature in the range from 250 to 350 °C displays the temperature dependency of the catalytic activity. The slope is calculated by regression, and the information regarding R^2 and p-value is given in Table C.3 in Appendix C.3.2. The temperature dependency reflect the trend in Figure 6.19.

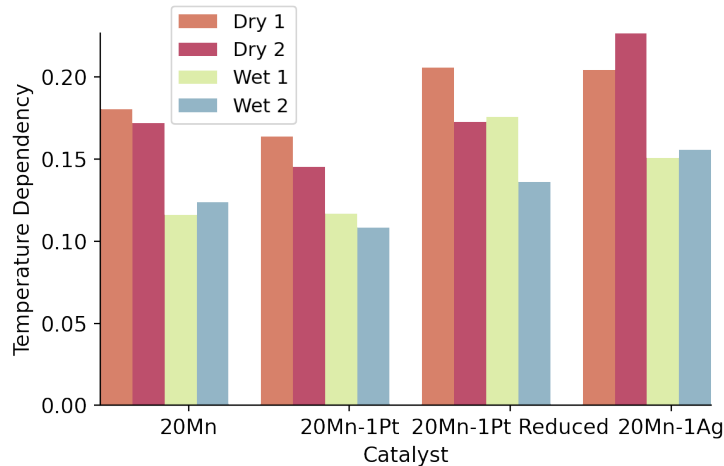


Figure 6.20: The temperature dependency of the catalytic activity for 20Mn, 20Mn-1Pt, 20Mn-1Pt Reduced and 20Mn-1Ag presented as the slope of catalytic NO conversion $x_{NO,c}$ as a function of temperature in the range from 250 to 350°C.

The results show a positive initial effect of the activation in hydrogen, and the temperature dependency for 20Mn-1Pt Reduced is more significant than both 20Mn and 20Mn-1Pt in dry and wet conditions. However, it is observed that the temperature dependency decreases in the second dry and wet test run. The results could demonstrate two things. First, a possible reason could be the oxidation of platinum inhibiting the catalytic activity. Second, the H₂ treatment also reduced manganese oxide, and the new phase of manganese oxide performs lower in the studied conditions. The phase change from Mn⁴⁺ to Mn³⁺ is, according to literature, less active in lean NOx catalytic oxidation [32]. The catalyst appears to deactivate in the time frame studied, indicating that the activation only enhances the catalyst's reactivity initially. A longer test run in steady-state conditions is necessary to examine the deactivation compared to the catalysts without pretreatment, and the effect on NO conversion when Mn₂O₃ is forming.

However, the reduced platinum-promoted manganese exhibits higher catalytic activity in the second temperature scan than 20Mn-1Pt even though it has been exposed to an oxidizing environment. One possible explanation could be that there is just enough oxygen for the NO oxidation over manganese oxide during the dry temperature scan to proceed, and not enough to oxidize platinum. There is an excess of oxygen during the water test runs, and the platinum will oxidize to some extent, and the catalyst deactivates as a consequence. The mechanism should be studied further as there is insufficient evidence to establish a mechanism at this research stage.

6.2.5 Steady-state Conditions

Between the temperature dependency investigation, the catalysts were tested for stability under steady-state conditions at 250 and 350 °C with sequential periods for two hours in dry-wet-dry-wet conditions. The temperature program is displayed in Figure 5.3 in Section 5.3. The NO conversion varied during the steady-state test runs, and calling it steady-state is not a correct term for the conditions. Neither is the use of *isothermal conditions*. Even though the temperature program was set to hold a temperature, the temperature inside the reactor would have a ΔT , and the temperature in the catalyst bed was most likely not isothermal

during the time interval. Therefore, the term *steady-state* will be used in order to discuss the observed experimental results.

According to the temperature scan test runs shown in the previous section, the SiC was largely inert, and the conversion measured with only SiC was subtracted. The SiC was investigated under the same steady-state conditions as the catalysts. The NO conversion initially, after one hour and two hours, is presented in Table C.4 in Appendix C.4. The results deduce a fluctuation during the test runs and are primarily prominent during the dry condition experiments. Because of the different parameters discussed in section 6.2.3, several reasons could lead to unstable NO conversion. As a result, the NO conversion extracted from the steady-state conditions is presented as total conversion where the gas-phase contribution is present.

6.2.5.1 Silver Catalyst compared to 5 wt% Manganese Oxide on Zirconia

The steady-state test runs at 250 and 350 °C for 5Ag and 5Mn are displayed in Figure 6.21. The gas-phase contribution is shown as SiC. The results confirm that the manganese oxide catalyst is a better choice for NO oxidation at the studied conditions than the silver catalyst. Furthermore, 5Mn exhibits higher conversion than 5Ag at both temperatures, and 5Mn additionally performs better at 250 °C in dry conditions than 5Ag at 350 °C.

The inhibition of water is significant for the manganese catalyst, while the silver catalyst yields approximately the same catalytic activity in dry and wet conditions. The silver catalyst performed better during wet conditions in the temperature scans, but the differences seem to minimize with increasing time-on-stream in partially simulating nitric acid plant conditions. Xu *et al.* studied alumina-supported silver catalyst with high water tolerance for H₂ assisted C₃H₆-SCR of NO_x. They found an enhancement in NO_x conversion after water vapor was introduced, particularly at low temperatures (200-300 °C), and confirmed with kinetic studies that H₂O addition did not change the apparent activation energy for NO_x reduction [97].

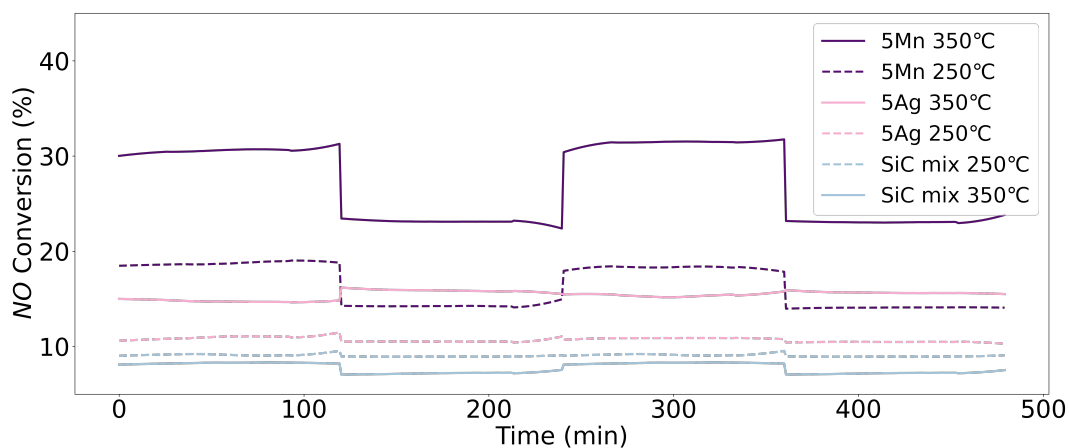


Figure 6.21: The steady-state runs at 250 °C (in dashed lines) and 350 °C for 5Ag and 5Mn, where the temperature program follows dry-wet-dry-wet conditions with two hours each test run. The gas-phase contribution is shown as SiC. $WHSV = 24\ 000\ N_{ml}/h \cdot g_{cat}$, and pressure at 1 bar.

Table 6.4 presents the first deactivation of 5Ag and 5Mn when water is added, the regenerability from Dry 1 to Dry 2, the second deactivation with water introduced, and the regenerability between the wet test runs at 350 and 250 °C. The changes reflect if the catalyst gets activated

or deactivated and the regenerability capacity in dry and wet conditions. The results show that the manganese oxide catalyst is significantly affected by water while the silver catalyst is not. However, the manganese oxide catalyst is observed to regain close to or more than the initial activity upon removal of water.

Table 6.4: The first deactivation for 5Ag and 5Mn when water is added, the regenerability from Dry 1 to Dry 2, the second deactivation with water introduced and the regenerability between the wet test runs at 350 and 250 °C.

Temperature	Catalyst	Deactivation 1	Regenerability Dry	Deactivation 2	Regenerability Wet
350 °C	5Ag	8%	104%	2%	99%
	5Mn	-25%	103%	-27%	100%
250 °C	5Ag	-5%	99%	-4%	100%
	5Mn	-25%	97%	-23%	99%

6.2.5.2 5 wt% Manganese Oxide catalyst on Zirconia

The performance of the 5 wt%-manganese catalysts is shown in Figure 6.22 during the steady-state test runs. 5Mn-1Ag yield the highest NO conversion, 5Mn second-highest, and 5Mn-1Pt the lowest at 250 °C and 350 °C. The same trend is evident in dry and wet conditions.

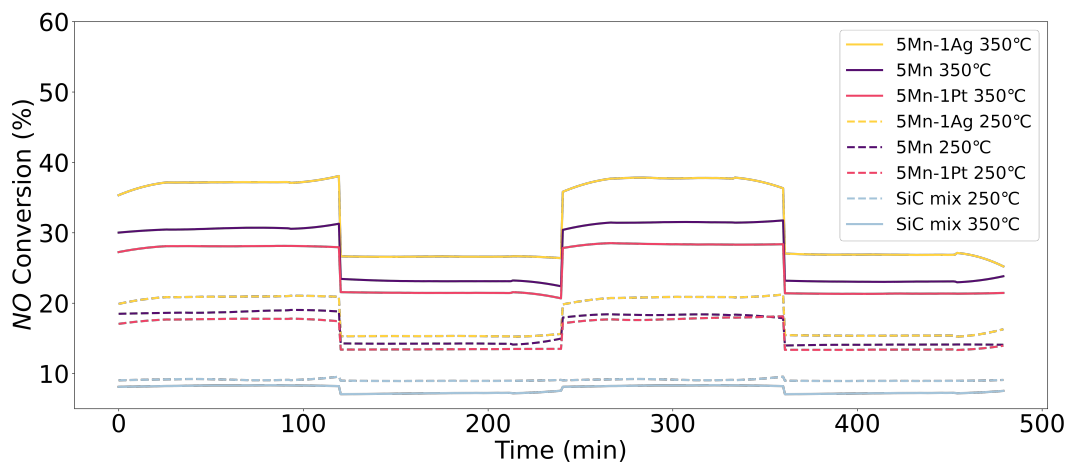


Figure 6.22: The steady-state runs at 250 °C (in dashed lines) and 350 °C for 5Mn, 5Mn-1Pt and 5Mn-1Ag, where the temperature program follows dry-wet-dry-wet conditions with two hours each test run. The gas-phase contribution is shown as SiC. $WHSV = 24000 \text{ Nm}^3/\text{h} \cdot g_{cat}$, and pressure at 1 bar.

Table 6.5 presents the first deactivation of 5Mn compared with 20Mn when water is added, the regenerability between the dry test runs, the second deactivation with water introduced, and the regenerability between the wet experiments. Minor differences are observed for the 5 wt% catalysts regarding regenerability and deactivation as a result of water.

Table 6.5: The first deactivation for 5Mn, 5Mn-1Pt and 5Mn-1Ag when water is added in the feed, the regenerability from Dry 1 to Dry 2, the second deactivation with water introduced and the regenerability between the wet test runs at 350 and 250 °C.

Temperature	Catalyst	Deactivation 1	Regenerability Dry	Deactivation 2	Regenerability Wet
350 °C	5Mn	-24%	101%	-25%	100%
	5Mn-1Pt	-24%	101%	-25%	100%
	5Mn-1Ag	-28%	101%	-29%	101%
250 °C	5Mn	-25%	97%	-23%	99%
	5Mn-1Pt	-24%	101%	-25%	100%
	5Mn-1Ag	-27%	99%	-26%	101%

6.2.5.3 Effect of Manganese loading

The effect of manganese loading in NO conversion is shown in Figure 6.23 where 20Mn is compared with 5Mn in approximately steady-state conditions for two hours. 5Mn performed better than 20Mn in dry conditions at both 250 °C and 350 °C. In contrast, the 20Mn has a higher resistance towards inhibition of water at 350 °C and yielded higher NO conversion than 5Mn. However, the catalytic performance remains the same for the two catalysts at 250 °C in wet conditions.

In the results observed from the dry temperature scan test runs, in Section 6.2.4, 20Mn performed better than 5Mn at both 250 and 350 °C, which is in contrast to the results conducted from the dry steady-state test runs. However, the 20Mn has a higher resistance towards inhibition of water at 350 °C, which is aligned with the temperature scan results. The results from steady-state are trusted to be more reliable when the catalyst had time to stabilize to a greater extent than for the temperature scan experiments.

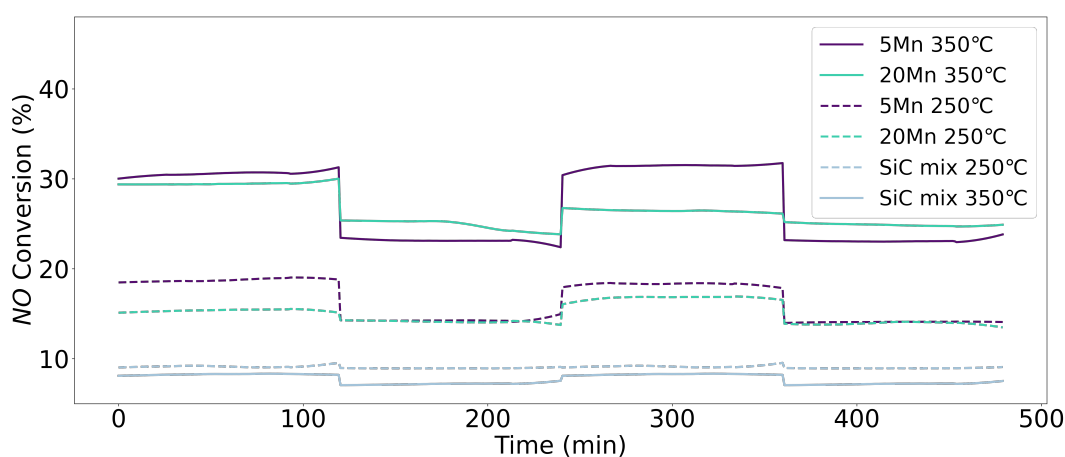


Figure 6.23: The steady-state runs at 250 °C (in dashed lines) and 350 °C for 5Mn and 20Mn, where the temperature program follows dry-wet-dry-wet conditions with two hours each test run. The gas-phase contribution is shown as SiC. $WHSV = 24\ 000\ Nm^3/h \cdot g_{cat}$, and pressure at 1 bar.

The effect of water and the regenerability of the 5Mn compared to 20Mn is presented in Table 6.6. At 350 °C, 20Mn is less deactivated than 5Mn with water present. However, the regen-

erability after the first wet test run is 89%, indicating a possible deactivation of the catalyst during the first wet steady-state experiment. 20Mn is still less deactivated at a low temperature than 5Mn caused by water. The results could indicate that the possible deactivation affect the catalytic performance mostly in dry conditions. 20 Mn is slightly activated during the following wet test run, resulting in a higher conversion from the first to the second dry experiment. The observed different catalytic activity performance of 20Mn is assumed to be because of deactivation during the high-temperature test runs.

Table 6.6: The first deactivation of 5Mn and 20Mn when water is added in the feed, the regenerability from Dry 1 to Dry 2, the second deactivation with water introduced and the regenerability between the wet test runs at 350 °C and 250 °C.

Temperature	Catalyst	Deactivation 1	Regenerability Dry	Deactivation 2	Regenerability Wet
350 °C	5Mn	-25%	103%	-27%	100%
	20Mn	-17%	89%	-6%	101%
250 °C	5Mn	-25%	97%	-23%	99%
	20Mn	-9%	109%	-17%	99%

On the timescale investigated, there is no evident benefit related to manganese loading. The wet test runs are more relevant for a nitric acid plant, and a higher loading seems to be less affected by the water. However, 20Mn seemed to deactivate during the time studied, but should be further investigated as this appear to be more prominent during the dry conditions.

Salman found hardly any change in activity between the 5, 10, and 20 wt% manganese in partially simulating nitric acid plant conditions for zirconia-supported manganese catalysts. In his results, 5Mn exhibited slightly higher NO conversion in all activity measurement tests [13]. When the catalysts perform close to the same with minor differences, it appears to be sufficient active sites available for the NO oxidation with lower loading of manganese with zirconia as support [14]. The results in this work tend to follow the same trend and are possibly due to the zirconia support. Zhao et al. indicated that ZrO₂ could provide abundant adsorption sites for NO_x whenever with or without MnO_x which could accelerate the catalytic oxidation of NO [44]. Their findings could explain why the catalytic activity does not scale with the loading of manganese oxide investigated.

6.2.5.4 Promoted 20 wt% Manganese Oxide on Zirconia

The 20wt%-manganese catalysts are shown in Figure 6.24, where the effect of promotion with platinum and silver is compared with the unpromoted 20Mn. At 250 and 350 °C in dry conditions, the catalysts perform in the order 20Mn-1Ag > 20Mn-1Pt > 20Mn. The trend is different than for the 5wt%-manganese catalysts and strengthens the assumption of deactivation of 20Mn. The results show that 20Mn-1Ag exhibits higher NO conversion at 250 °C than 20Mn at 350 °C. In contrast, 20Mn performs better than 20Mn-1Pt during wet conditions at 350 °C.

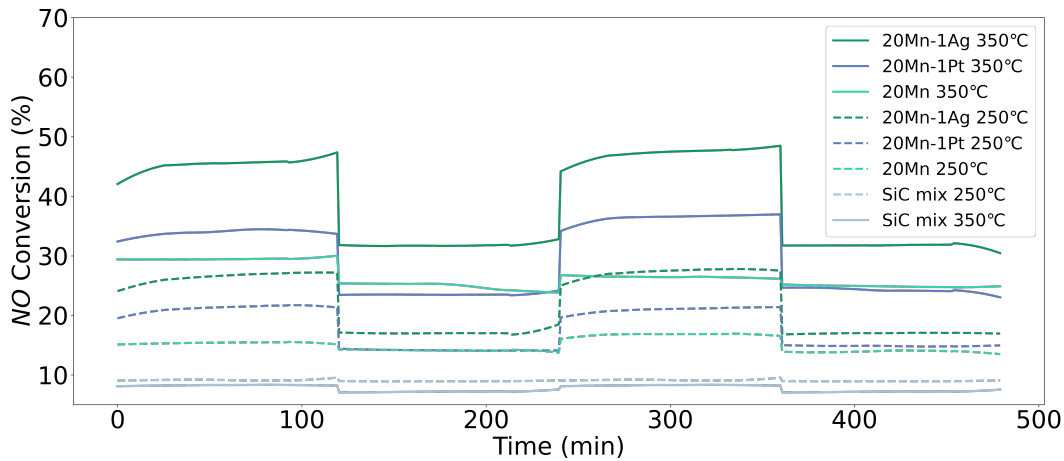


Figure 6.24: The steady-state runs at 250 °C (in dashed lines) and 350 °C for 20Mn, 20Mn-1Pt and 20Mn-1Ag, where the temperature program follows dry-wet-dry-wet conditions with two hours each test run. The gas-phase contribution is shown as SiC. $WHSV = 24\ 000\ Nml/h \cdot g_{cat}$, and pressure at 1 bar.

Table 6.7 displays the % change of the first deactivation of the 20 wt% manganese oxide catalysts when water is added, the regenerability between the dry test runs, the second deactivation with water introduced, and the regenerability between the wet experiments. Minor differences are observed between the promoted 20 wt% catalysts regarding regenerability and deactivation as a result of water, while unpromoted 20Mn shows a different trend. As discussed, a possible deactivation is assumed for 20Mn, but the possible phase change of manganese oxide appears to affect the conversion during wet conditions to a lower extent compared to the dry conditions.

Table 6.7: The first deactivation of the catalyst when water is added, the regenerability from Dry 1 to Dry 2, the second deactivation with water introduced and the regenerability between the wet test runs for 20Mn, 20Mn-1Pt and 20Mn-1Ag at 350 and 250 °C.

Temperature	Catalyst	Deactivation 1	Regenerability Dry	Deactivation 2	Regenerability Wet
350 °C	20Mn	-17%	89%	-6%	101%
	20Mn-1Pt	-32%	107%	-34%	103%
	20Mn-1Ag	-31%	104%	-33%	100%
250 °C	20Mn	-9%	109%	-17%	99%
	20Mn-1Pt	-35%	98%	-30%	105%
	20Mn-1Ag	-37%	102%	-38%	100%

6.2.5.5 Comparison of all Catalysts

Figure 6.25a and 6.25b displays the average total conversion in each steady-state test run at 250 and 350 °C respectively. The average NO conversion is calculated from the last hour in the two-hour test run, so the catalyst had time to stabilize to some extent.

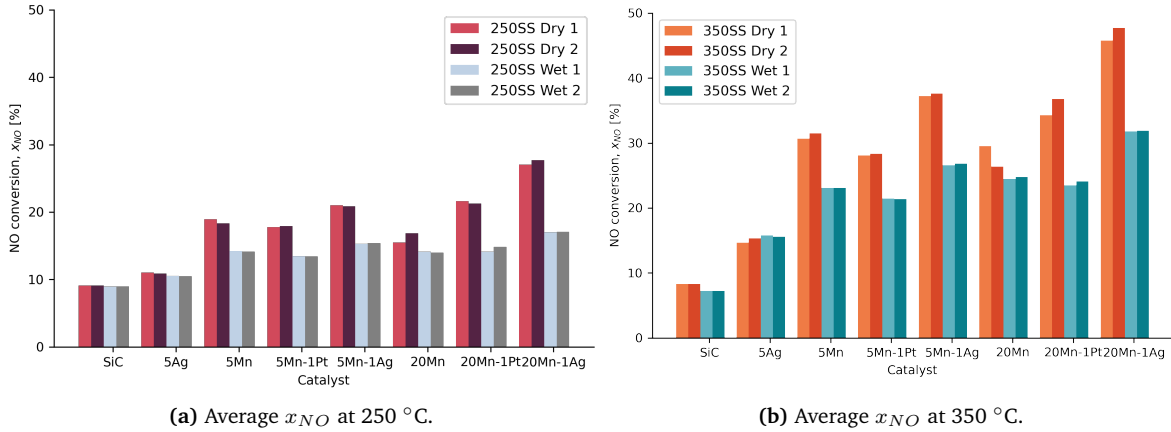


Figure 6.25: The total conversion, x_{NO} , is presented at 250 and 350 °C for each catalyst. SiC is displayed, presenting the gas-phase reaction conversion. The conversion is an average calculated from the last hour within each steady-state experiment.

From the steady-state test run results, it is clear that 20Mn-1Ag exhibits the highest NO conversion in dry and wet conditions at both 250 and 350 °C. Manganese oxide loading does not seem to make much difference related to NO conversion. However, the 20Mn-1Ag yields significantly higher NO conversion than 5Mn-1Ag, indicating the Ag/Mn molar ratio is related to the reactivity of the catalysts. Qu et al. reported related results, stating that the reactivity of catalyst is closely correlated to the Ag/Mn molar ratio related to oxidation of toluene [26]. The TPR analysis results, shown in Section 6.1.3, indicate a more enhanced interaction between Ag and Mn in 20Mn-1Ag than 5Mn-1Ag, which appears beneficial in the NO oxidation in resembling nitric acid plant conditions.

The catalytic activity for the manganese oxide catalysts is observed to be significantly inhibited in the presence of water. The adsorption of water on the manganese oxide hinders the reduction of surface MnO_x and slows the acceleration of NO oxidation [13]. It is impossible to predict the long-term effect of water inhibition based on the short time-on-stream studied in this work. Still, the results demonstrate, in general, a largely reversible inhibition effect.

The reaction rate, calculated from total conversion, is displayed in Table 6.8 for the catalysts at 250 and 350 °C. Equation 5.3 in Section 5.3. The same trend in the conversion is reflected in the reaction rate, where 20Mn-1Ag has the highest reaction rate.

Table 6.8: The reaction rate, r_{NO} [$\mu\text{mol} \cdot \text{g}_{\text{cat}}^{-1} \cdot \text{s}^{-1}$] for the different catalysts at 250 °C and 350 °C.

Catalyst	r_{NO} [$\mu\text{mol} \cdot \text{g}_{\text{cat}}^{-1} \cdot \text{s}^{-1}$] at 250 °C				r_{NO} [$\mu\text{mol} \cdot \text{g}_{\text{cat}}^{-1} \cdot \text{s}^{-1}$] at 350 °C			
	Dry 1	Dry 2	Wet 1	Wet 2	Dry 1	Dry 2	Wet 1	Wet 2
5Ag	3.1	3.0	2.9	2.9	4.1	4.3	4.4	4.3
5Mn	5.3	5.1	4.0	3.9	8.5	8.7	6.4	6.4
5Mn-1Pt	5.3	5.1	4.0	3.9	7.8	7.9	6.0	5.9
5Mn-1Ag	5.8	5.8	4.2	4.3	10.3	10.4	7.4	7.5
20Mn	4.3	4.7	3.9	3.9	8.2	7.3	6.8	6.9
20Mn-1Pt	4.9	5.9	3.9	4.1	9.5	7.9	6.5	6.7
20Mn-1Ag	7.5	7.7	4.7	4.7	12.7	13.2	8.8	8.8

Figure 6.26 displays the reaction rate for the zirconia-supported manganese catalysts at 250

and 350 °C during the second wet temperature scan. During the considered test run, the catalysts have been on-stream for approximately 16 hours, including the temperature scan test runs. The timescale is not sufficient to say if the catalysts are fully activated, but it indicates the performance after several hours in resembling nitric acid plant conditions.

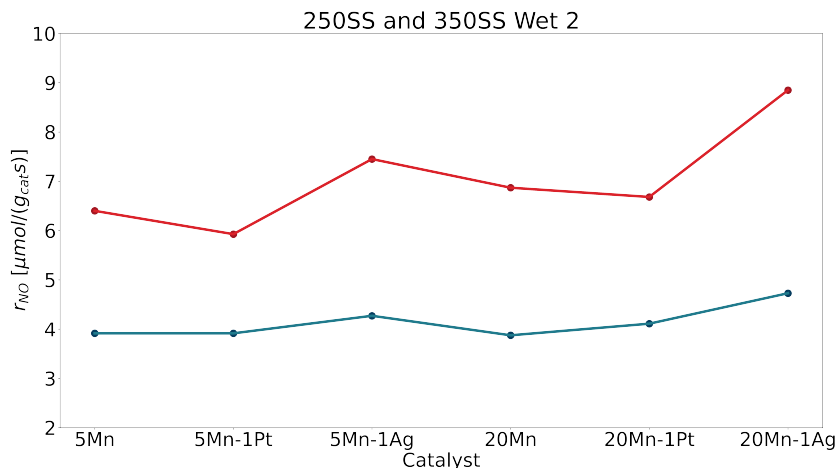
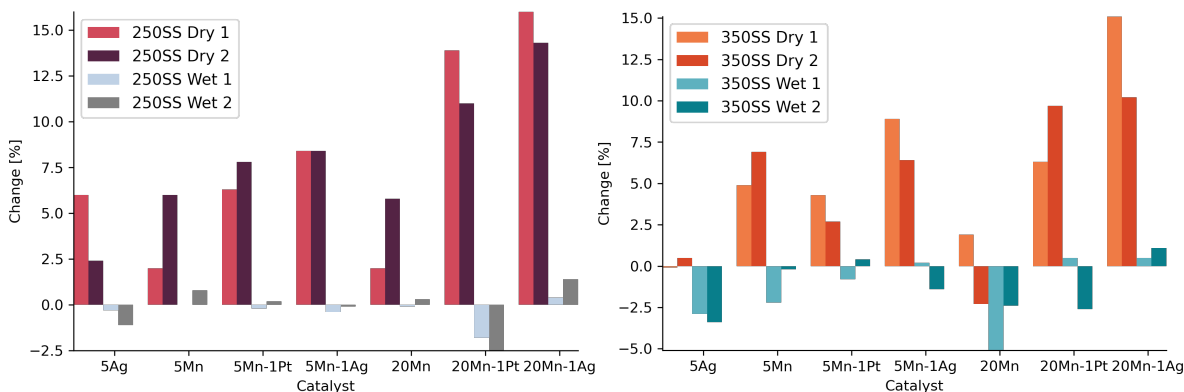


Figure 6.26: The reaction rate, r_{NO} [$\mu\text{mol}/(\text{g}_{\text{cat}}\text{s})$], calculated from total NO conversion of the zirconia-supported manganese catalysts during the second wet temperature scan at 250 °C (blue line) and 350 °C (red line).

The trend is different at the two temperatures. At 250 °C, there is no difference between 5Mn and 20Mn, and the rate seems to be independent of manganese loading at this temperature in wet conditions. The platinum-promoted catalysts perform slightly better than the unpromoted catalysts at 250 °C, and the higher loading of manganese seems beneficial with 1 wt% platinum. The reaction rate increases when silver is added to the manganese catalysts, and 20Mn-1Ag has the highest reaction rate of the catalysts at 250 °C. At 350 °C, the loading of manganese appears more compelling, and 20Mn has a higher reaction rate than 5Mn. The promotion of platinum on the manganese catalysts decreases the reaction rate at a higher temperature. The same trend is observed for the silver-promoted manganese catalysts at 350 °C, and 20Mn-1Ag has the highest reaction rate.

During each steady-state experiment, an internal change was observed. The percentage change within each time interval is displayed in Figure 6.27a and 6.27b at 250 and 350 °C respectively. The difference is calculated as the %-change between the initial NO conversion and the NO conversion after 120 minutes. During the dry steady-state test runs, there is a clear trend that the catalytic activity increase and indicate an activation of the catalysts with time on-stream. When water is present, the NO conversion is nearly stable or slightly decreasing. The %-change within the test runs for 20Mn indicates a catalytic deactivation. Table C.5 and C.6 in Appendix C.4 displays the %-change in numbers where the NO conversion is presented at the start and end of each steady-state experiment.



(a) %-change within each steady-state tests run for two hours at 250 °C. (b) %-change within each steady-state tests run for two hours at 350 °C.

Figure 6.27: The %-change within each steady-state experiment is displayed in [6.27a](#) and [6.27b](#) at 250 and 350 °C for each catalyst.

A none-steady state on the surface of the catalyst is observed in the time intervals. However, there is a trend in the change within dry and wet conditions. The silver-promoted catalysts show the most significant internal activation and perform a better catalytic activity in NO oxidation. One limitation is the short temperature program. It is important to note that the present evidence on catalytic performance relies on two hours time-on-stream in nitric-acid conditions. The differences seen during the steady-state test runs could be initial differences due to the early activation stage of the catalysts. Even with attempted steady-state conditions, the activation of the catalysts can change without being deactivated. Some catalysts need several hours to activate and stabilize. In order to say which catalyst is better, a deactivation curve is necessary, and therefore longer test runs should be performed. The catalysts will not necessarily deactivate at the same rate. A lower initial activation combined with a lower deactivation rate could be better in the long run than a catalyst with high initial activation and high deactivation rate.

After eight steady-state test runs (16 hours), the manganese catalysts, except for 20Mn, were observed to show sufficient stability with no significant deactivation. Within the time scale considered, it is assumed that the high oxygen content in the feed regenerates the preferred oxidized state of the active MnO_2 phase resulting in good catalytic stability [\[13\]](#).

6.3 Characterization After Activity Testing

The catalysts were sieved after the activity measurements to separate them from the SiC particles. Quartz wool particles were still in the sample, impossible to sieve from the catalyst particles, and could explain some of the additional noise in the XRD measurements after activity measurements. The catalysts were analyzed in XRD with the same program as before the activity testing.

5Ag show a significant difference in the XRD pattern after the test runs and is presented in [Figure C.11b](#) in [Appendix C.5](#). Before the activity testing, analysis from XRD indicated metallic silver in the catalyst sample with a peak at $2\theta = 38.1^\circ$. After the test runs, the specific peak for Ag^0 was more prominent, and additional peaks at $2\theta = 44.4^\circ$ and 64.4° agreeing with the identification card of Ag (PDF: 00-004-0783). Silver got reduced to a greater extent during

the test runs, still in an oxidizing atmosphere.

20Mn and 20Mn-1Ag showed differences in the XRD pattern for the manganese catalysts when comparing the sample before and after the catalytic activity measurements, shown in Figure 6.28. For both the catalysts it is observed one new peak at 32.9° which is not observed in the XRD patterns before the activity measurements. In addition, 20Mn USED is observed to have a peak at 23.1° . The peak at 32.9° and 23.1° is assumed to be the specific peaks for Mn_2O_3 which is reported at 32.9° by Chen *et al.* [80] and is agreeing with the identification card of Mn_2O_3 (PDF: 04-007-0856). It appears like manganese changed oxidation state from MnO_2 to Mn_2O_3 to some extent during the activity measurements, resulting in a mix of both MnO_2 and Mn_2O_3 in the catalyst sample.

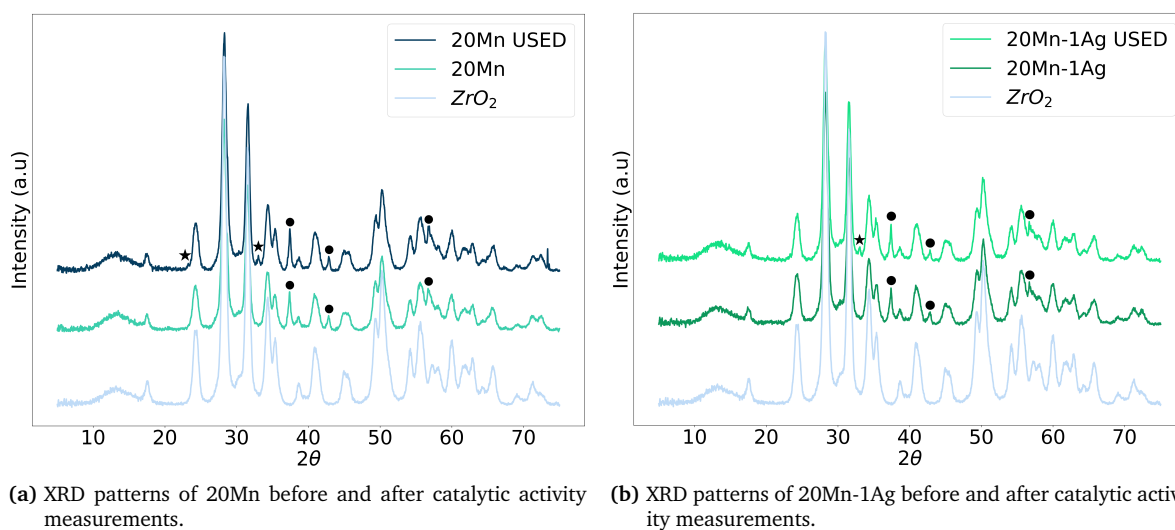


Figure 6.28: The settings were 40 kV and 40 mA with a wavelength of 1.54060 \AA employing $\text{Cu K}\alpha$ radiation. $\gamma\text{-MnO}_2$ (●) is indicated with a dot and Mn_2O_3 (★) is indicated with a star.

A possible deactivation for the 20Mn catalyst can be the phase transition from MnO_2 to Mn_2O_3 . The reduction of manganese to Mn_2O_3 may indicate insufficient oxygen in the system, not constantly keeping manganese oxidized, and could be a possible reason for a less efficient catalyst behavior in nitric acid plant conditions. According to Wang *et al.*, the catalytic activity increased in the order of $\text{MnO}_2 > \text{Mn}_2\text{O}_3 > \text{Mn}_3\text{O}_4$ when they investigated the catalytic activity for unsupported manganese oxide in NO oxidation (500 ppm NO, 5 vol% O_2 , 200 ppm SO_2 (when used) and 15 vol% H_2O (when used)) [32]. 20Mn appeared to deactivate during the steady-state experiments as discussed in Section 6.2.5.3.

However, 20Mn-1Ag does not seem to deactivate due to the phase change of manganese oxide and exhibits the highest catalytic activity compared to all other catalysts in this work. Qu *et al.* reported, in their research on oxidation of toluene, that coexistence of MnO_2 , Mn_2O_3 and $\text{Ag}_{1.8}\text{Mn}_8\text{O}_{16}$ and the strong interaction between Ag and Mn species shows good synergetic interaction. This promotes the reducibility of the catalyst and the formation of plentiful active lattice oxygen, consequently enhancing the catalytic activity of toluene oxidation [26]. In addition, they found that Ag leads to parts of MnO_2 being transformed into Mn_2O_3 . If the same phenomena described by Qu *et al.* appears in the NO oxidation at the studied conditions, the silver could be the reason for some of the MnO_2 is reduced to Mn_2O_3 , and not insufficient oxygen. Thus, while the phase-change seemed to deactivate the unpromoted manganese catalyst, the silver promoted enhanced the catalytic activity.

$\text{Ag}_{1.8}\text{Mn}_8\text{O}_{16}$ could be present in 20Mn-1Ag in this work but is not marked in the XRD pattern in Figure C.12, as the specific peaks for $\text{Ag}_{1.8}\text{Mn}_8\text{O}_{16}$ (PDF: 01-077-1987) appears at the same 2θ as $\gamma\text{-MnO}_2$. Further characterization, like X-ray photoelectron spectroscopy (XPS), could be performed to indicate if $\text{Ag}_{1.8}\text{Mn}_8\text{O}_{16}$ is present.

The bulk average crystallite size of manganese was investigated in catalyst samples before and after catalytic activity experiments. Approximate bulk crystallite sizes calculations were calculated from the peak occurring at 37.3° . The line broadening was regarded with an instrumental peak width equal to 0.05 \AA . The constant K was assumed to be 0.9 assuming spherical particles. The Scherrer equation and dispersion calculations, presented in Section 4.2.4 are rough estimations and are primarily used to differentiate the different catalysts. The results are displayed in Table 6.9 and show an increase in crystallite size in the catalysts samples after activity testing.

Table 6.9: The Scherrer equation was used to calculate the crystallite size, $d_p = \frac{K\lambda}{B_p(2\theta)\cos(\theta)}$, where λ , $B_p(2\theta)$ and θ is given in radians. The specific peak for MnO_2 is where 2θ equals 37.3° , and for this peak the crystalline size of MnO_2 is calculated. θ is half of the diffraction angle, and the wavelength λ equals 1.54060 \AA . The shape factor was chosen to be 0.9, and instrumental line broadening is 0.05. *Before* is crystallite size before catalytic activity testing, and *After* is the crystallite size after approximately 20 hours on stream.

Catalyst	Crystallite size [nm]		%-change
	Before	After	
5Mn	41	56	37%
5Mn-1Pt	41	46	11%
5Mn-1Ag	34	63	85%
20Mn	27	39	42%
20Mn-1Pt	20	25	20%
20Mn-1Ag	28	39	38%

An increase in crystallite size can indicate sintering occurring during the catalytic experiments and that the structure of the catalysts has changed. There are reasons to doubt this explanation when XRD is a bulk technique and will not give specific information about the catalyst's surface. Even though these are metal oxides on a support, the changes on the surface might not reflect particularly well in XRD. This is important to keep in mind to interpret the results correctly.

However, the increase in approximate bulk crystallite sizes does not appear to affect the catalytic activity negatively. 20Mn-1Ag exhibited the highest catalytic activity in all activity test runs and has a significant %-change in crystallite size. The lower manganese loaded catalyst with 1wt% silver is observed to have the most significant change from before and after activity measurements. 5Mn-1Ag show enhanced catalytic activity in the temperature scans conducted last (Dry 2 and Wet 2) than initial temperature scans. An overview of the catalytic performance in the temperature scan is shown in Figure C.2b in Appendix C.2, where 5Mn-1Ag exhibits next best after 20Mn-1Ag at higher temperature in the second wet temperature scan.

The 20 wt% manganese oxide catalyst with 1 wt% platinum was reduced before the catalytic activity experiment in order to activate the platinum. Concerns were highlighted regarding manganese also reducing in addition to platinum. Even though the activation improved the NO conversion, the catalyst deactivated after being exposed to an oxidizing atmosphere (Sec-

tion 6.2.4.7). XRD analysis was conducted after the catalytic activity measurements, and the X-ray diffraction pattern is displayed in Figure 6.29.

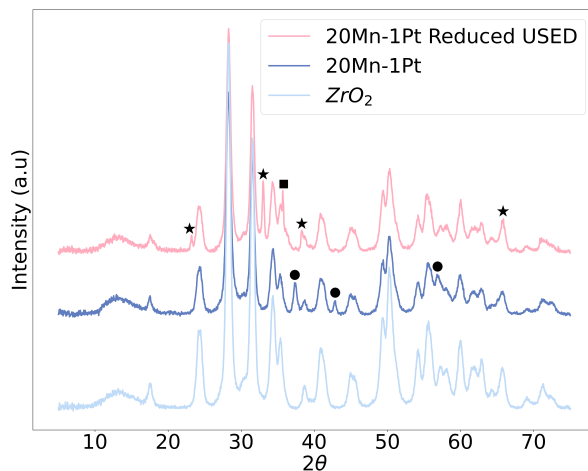


Figure 6.29: XRD patterns of 20Mn-1Pt (with pretreatment in H_2) before and after catalytic activity measurements. The settings were 40 kV and 40 mA with a wavelength of 1.54060 Å employing Cu α radiation. γ - MnO_2 (●) is indicated with a dot and Mn_2O_3 (★) is indicated with a star. The peak indicated with a square is assumed to be $Mn_{0.5}Pt_{0.5}O_2$ (■).

The results show a phase-change for the manganese oxide, and all the MnO_2 peaks disappeared, and Mn_2O_3 peaks occurred at $2\theta = 23.1^\circ$, 32.9° , 38.2° and 65.8° agreeing well with the identification card of Mn_2O_3 (PDF: 04-007-0856). This could be an important finding in the understanding of the deactivation of the catalyst. The rapid deactivation of the pretreated 20Mn-1Pt catalysts was assumed to be due to the oxidation of metallic platinum. However, it could also be due to manganese oxide reducing and appearing in a different phase. Even though the experimental conditions have an excess of oxygen, it appeared insufficient to oxidize the manganese oxide when a phase change of manganese oxide occurred in the bulk of the catalyst.

The peak indicated with a square is assumed to be $Mn_{0.5}Pt_{0.5}O_2$ (PDF 04-021-9826), but this should be further investigated by running a more extended scan in the XRD, so the peaks obtain a higher resolution. The peak is only visible in the 20Mn-1Pt Reduced catalyst, not in the platinum promoted catalysts without pretreatment.

The comparison of all catalysts before and after catalytic activity measurements can be found in Appendix C.5.1.

Chapter 7

Conclusion and future work

7.1 Conclusions

A series of zirconia-supported manganese oxide catalysts with two manganese loadings (5 and 20 wt%) with the promotion of silver and platinum were prepared by incipient wetness impregnation. In addition, one 5 wt% silver/ZrO₂ catalyst was prepared by the same method. The characterization results confirmed the presence of γ -MnO₂ for all manganese oxide catalysts and metallic silver in addition to silver oxide for the silver catalyst. The effect of manganese loading, as well as the effect of promotion with silver and platinum, was investigated for the oxidation of NO to NO₂ in a feed holding 10 vol% NO, 6 vol% O₂ and 15 vol% H₂O (when present) at atmospheric pressure partially reproducing nitric acid plant conditions. The catalytic activity was considered as a function of temperature and time, and catalytic performance at 250 and 350 °C was highlighted due to preferred working conditions at a nitric acid plant.

The steady-state experiments demonstrated minor differences between 5Mn and 20Mn. The NO conversion does not seem to scale with the amount of manganese loaded on the catalyst during the time scale considered in this work. However, 20Mn-1Ag exhibits higher NO conversion than 5Mn-1Ag, indicating a correlation between the catalysts' reactivity and the molar ratio of Ag/Mn. 20Mn-1Ag yielded the highest catalytic activity in all the catalytic activity experiments, both in dry and wet feed.

The inhibition effect of water appeared for all the manganese oxide catalysts. However, the inhibition effect is reversible, and the activity was recovered upon elimination of water. The zirconia-supported silver catalyst shows catalytic activity in the oxidation of NO but performed poorly compared to the manganese oxide catalysts. However, the silver catalyst achieved the same or higher catalytic activity in a wet feed.

Within the time scale considered, it is assumed that the high oxygen content in the feed regenerates the preferred oxidized state of the active MnO₂ phase resulting in good catalytic stability. However, a partial phase transition was observed for 20Mn and 20Mn-1Ag after the catalytic activity experiments, detected in XRD. As a result, the 20Mn was assumed to deactivate due to the phase change of manganese from MnO₂ to Mn₂O₃, but the deactivation was more prominent during dry conditions. In contrast, the reduction of manganese appeared to yield higher NO conversion for 20Mn-1Ag.

Changes in catalytic activity were observed after a short time on-stream. The silver-promoted catalysts got activated during the test runs in an oxidizing atmosphere with nitrates. The same was observed for 5Mn, but possibly due to a phase change of manganese, not for 20Mn. The platinum-promoted catalysts did not tend to get activated in oxidizing atmosphere assumingly due to platinum being oxidized. However, it is challenging to say whether fundamental changes are observed that will have a long time effect or whether this is just a steady-state indication that the catalyst is still undergoing activation and stabilization.

20Mn-1Pt was exposed to H₂ for one hour at 250°C before the activity testing, and the catalyst exhibited higher NO conversion initially. However, the catalyst deactivated relatively fast, and XRD performed on the sample after the test runs revealed that manganese oxide was present as Mn₂O₃.

A correlation between the reducibility and catalytic activity was observed for the unpromoted manganese catalysts (5Mn and 20Mn). The results indicated that the oxidation of NO over zirconia-supported manganese oxide catalysts proceeds through a Mars-van Krevelen mechanism.

7.2 Future Work

It is advised to gain better temperature control and axial temperature measurement inside the reactor. In the current setup, the temperature is measured at one point inside the reactor, and there is no information about the temperature profile. One possible way is to have a movable thermocouple in a cap inside the reactor. It will then be possible to get more details about the actual temperature throughout the bed when the temperature most likely will not be uniform inside the reactor.

The activation energy was not calculated because of the relatively high heating rate and the several issues with the correct temperature measurements and pressure gradients. A better situation would be to stabilize the conversion at a specific temperature before ramping to the following temperature and then measure the activation energy. The ramp rate in the temperature program in this work was 5 °C, and it was possibly not slow enough for the conversion to stabilize. A slower ramp rate is recommended in future temperature scan experiments.

The reactor could be optimized to minimize dead volume and mix the gases as close to the catalyst bed as possible. The diameter of the reactor should be decided along with the particle size of catalyst and dilutant material, so pressure drop in the reactor is minimized. The particle size used in this work (53-90 μm) appeared too small when the pressure gradient was most likely developed during the activity tests.

Different particle sizes of the catalysts should be investigated, and different gas hourly space velocities (GHSV) during the activity measurements. With the pressure building up, the particles might be too small regarding the reactor diameter. The SiC particles used in the catalytic activity were more significant than the particles to separate them after the test runs. With a prominent difference, a uniform mixture of the catalyst and the dilutant is hard to obtain.

The FTIR analyzer has a minimum and maximum limit regarding the amount of gas entering the analyzer. The lower limit is 1 l/h, equivalent to the amount used in this work. In future work, it is advised to go above this lower limit recommended by the supplier of the FTIR analyzer [73].

In the conversion calculations, NO and NO₂ are assumed to be the only nitrogen species included in the mass balance. There is a need to investigate if other nitrogen species are involved in NO oxidation. The error in the mass balance should be found better to understand the uncertainties in the NO conversion measurements.

Salman *et al.* confirmed that the system applied was free from internal diffusion limitations and external mass and heat transfer limitations. This was while they investigated catalytic oxidation of NO to NO₂ for nitric acid production over a Pt/Al₂O₃ catalyst and used the same rig and conditions used in this work. However, they mixed the catalyst with SiC (53-90 μm), and the reactor was slightly different. The calculations regarding internal diffusion limitations and external mass and heat transfer limitations should be done after the experimental modifications.

Some of the catalysts yielded higher catalytic activity in the second temperature scan test run, indicating that the catalysts needed time to activate. The catalyst may not be fully activated. More extended experiments need to be conducted to investigate this and the rate of deactivation.

Activation of the catalyst with different pretreatments should be further investigated. The results showed that the silver-promoted catalysts are activated during the test runs, which are in oxidizing conditions with nitrate species. The reaction mechanism over the manganese catalyst should be investigated to understand a suitable activation better.

It would be interesting to understand the structure of the catalyst and how the structure changes during the experiment. The XRD gave some indication, but the crystallite size is calculated from the Scherrer, which gives a rough estimation [67, 68]. The silver-promoted catalysts exhibited higher NO conversion during the test runs, and sintering possibly occurred during the activity measurements. TEM images could give a better indication of how the structure changed during the catalytic activity testing.

The spent catalyst will contain quartz wool if the same method used in this work is continued. The impurities could affect the results when further characterizing is conducted. Ex-situ analysis might be inaccurate with impurities inside the spent catalyst sample, and more in-situ techniques like in situ powder XRD experiments should be performed on the catalyst.

As platinum particles on the surface could provide a better catalytic activity after sintering, the preparation methods of the catalyst and how the platinum is dispersed on the surface should be considered.

The XRD patterns for some catalysts showed a change when comparing catalyst samples before and after activity measurements. However, the peaks are measured with an insufficient number of measured points. The XRD program should be run for a longer time, up to six hours, to resolve the peaks better.

The calcination temperature was determined based on keeping the manganese in γ-MnO₂, but the promotion metals were not considered. Silver oxide loses oxygen quickly at a temperature higher than 250 °C. Further examination should be conducted to understand and design an ideal calcination temperature for the catalyst to perform better in NO oxidation.

H₂-TPR analysis in wet conditions and NO-TPD can indicate the correlation between the catalysts reduction temperature and the onset temperature in catalytic activity measurements and the reaction mechanism. These analyses should be conducted in further studies of the man-

ganesse oxide and silver catalysts. Temperature-Programmed Desorption (TPD) gives quantitative information regarding adsorbate coverage and the adsorption energy, which equals the desorption's activation energy. Additionally, TPD provides information about the lateral interactions between the adsorbates through the adsorption energy coverage dependence [63].

An acid-treatment of the manganese oxide catalyst with H_2SO_4 could enhance the catalytic activity in NO conversion. Quiroz *et al.* published a paper concerning the effect of acid treatment in the total oxidation of formaldehyde over MnO_x - CeO_2 . They found that the pore volume and specific surface area could be significantly increased owing to the dissolution of Mn^{2+} species present between the particles. This can enable access to the primary porosity and oxidize the manganese species to a higher oxidation state via an Mn dismutation reaction and possibly enhance the oxidation [98].

Gunnarson *et al.* studied the effect of silver loading and low-level platinum doping on the distribution of silver species, the hydrocarbon activation, and the low-temperature activity for lean NO_x reduction over silver-alumina catalysts. The study points that as the samples doped with trace-amounts of platinum, enhanced the activity for lean NO_x reduction at low temperatures [99]. In this work, platinum did not appear to enhance the NO conversion compared to the unpromoted. It could be an idea to add both platinum and silver to the zirconia-supported manganese oxide catalyst in future work.

Silver supported by zirconia exhibited low performance in NO oxidation compared to manganese oxide catalysts. However, the silver promotion to manganese catalysts revealed promising results. Männikkö *et al.* found that silver species, within the size range of small silver clusters to small nanoparticles, were essential for the lean NO_x reduction with methanol for low temperatures over Ag/Al_2O_3 [100]. Suppose the particles need to be in a specific size. In that case, one possible future work could be to try different preparation methods to obtain a well-dispersed silver on the manganese catalyst and try different particle sizes dispersed on the surface.

Bibliography

- [1] United Nations The 17 Goals. <https://sdgs.un.org/goals>. Accessed: 2021-04-12.
- [2] Eileen Crist, Camilo Mora, and Robert Engelman. The interaction of human population, food production, and biodiversity protection. *Science* 365, pages 260–264, 2017.
- [3] Jonathan A Foley, Ruth DeFries, Gregory P Asner, Carol Barford, Gordon Bonan, Stephen R Carpenter, F Stuart Chapin, Michael T Coe, Gretchen C Daily, Holly K Gibbs, et al. Global consequences of land use. *science*, 309(5734):570–574, 2005.
- [4] U.N. Food and Agricultural Organization. How to Feed the World: Global Agriculture Towards 2050. Technical report, Rome, 2009.
- [5] Yara International ASA. Mission, vision and values. <https://www.yara.com/this-is-yara/mission-vision-and-values/>. Accessed: 2020-11-20.
- [6] Yara International ASA. Why is fertilizer important for feeding the world? <https://www.yara.com/crop-nutrition/why-fertilizer/feeding-the-world/>. Accessed: 2020-11-10.
- [7] Øystein Nirisen, David Waller, and David M. Brackenbury. The Development of a N₂O Abatement Catalyst: from Laboratory Scale to Plant Testing. *Topics in Catalysis*, 62(17-20), 11 2019.
- [8] IHS Markit. Chemical Economics Handbook, Nitric Acid. <https://ihsmarkit.com/products/nitric-acid-chemical-economics-handbook.html>, 2020. Accessed: 2021-02-30.
- [9] Britannica, The Editors of Encyclopaedia. Nitric acid. <https://www.britannica.com/science/nitric-acid>, 2007. Accessed: 2021-02-30.
- [10] Jacob A Moulijn, Michiel Makkee, and Annelies E Van Diepen. *Chemical process technology*. John Wiley & Sons, 2013.
- [11] Hu Chen, Ying Wang, and Yong Kang Lv. Catalytic oxidation of NO over MnO₂ with different crystal structures. *RSC Advances*, 6(59):54032–54040, 2016.
- [12] G. D. Honti. *The Nitrogen Industry*. Akademia Kiado, 1976.
- [13] Ata ul Rauf Salman. *Catalytic oxidation of NO to NO₂ for nitric acid production*. PhD thesis, 2019.
- [14] Beate Meisland Østrådt. Supported Manganese Oxide Catalysts for NO Oxidation in Nitric Acid Production, 2018. Master thesis.

- [15] Ata ul Rauf Salman, Bjørn Christian Enger, Xavier Auvray, Rune Lødeng, Mohan Menon, David Waller, and Magnus Rønning. Catalytic oxidation of NO to NO₂ for nitric acid production over a Pt/Al₂O₃ catalyst. *Applied Catalysis A: General*, 564:142–146, 8 2018.
- [16] Sardui S Pannu. Nitric Acid. *Journal of Chemical Education*, pages 174–176, 1984.
- [17] Michael Thiemann, Erich Scheibler, and Karl Wilhelm Wiegand. Nitric Acid, Nitrous Acid, and Nitrogen Oxides. In *Ullmann's Encyclopedia of Industrial Chemistry*. Wiley-VCH Verlag GmbH & Co. KGaA, Weinheim, Germany, 6 2000.
- [18] Xi Xia and Zaiping Guo. Studies on a novel secondary battery: MH/MnO₂ rechargeable battery: II. characteristics of the cathode. *Journal of the Electrochemical Society*, 144(8):L213, 1997.
- [19] Safia Hamoudi, Al Larachi, Graciela Cerrella, and Myrian Cassanello. Wet Oxidation of Phenol Catalyzed by Unpromoted and Platinum-Promoted Manganese/Cerium Oxide. pages 3561–3566, 1998.
- [20] S Hamoudi, A Sayari, K Belkacemi, L Bonneviot, and F Larachi. Catalytic wet oxidation of phenol over Pt_xAg_{1-x}MnO₂/CeO₂ catalysts. *Catalysis today*, 62(4):379–388, 2000.
- [21] Freek Kapteijn, A Dick Vanlangeveld, Jacob A Moulijn, Amedeo Andreini, Michael A Vuurman, Andrzej M Turek, Jih-Mirn Jehng, and Israel E Wachs. Alumina-supported manganese oxide catalysts: I. characterization: effect of precursor and loading. *Journal of Catalysis*, 150(1):94–104, 1994.
- [22] Annemarieke Maltha, Thomas LF Favre, Heleen F Kist, Adrianus P Zuur, and Vladimir Ponec. Manganese oxides as catalysts for the selective reduction of nitrobenzene to nitrosobenzene. *Journal of Catalysis*, 149(2):364–374, 1994.
- [23] Francesco Arena, Teresa Torre, Carmelo Raimondo, and Adolfo Parmaliana. Structure and redox properties of bulk and supported manganese oxide catalysts. *Physical Chemistry Chemical Physics*, 3(10):1911–1917, 2001.
- [24] Frédéric Wyrwalski, Jean-Marc Giraudon, and Jean-François Lamonier. Synergistic Coupling of the Redox Properties of Supports and Cobalt Oxide Co₃O₄ for the Complete Oxidation of Volatile Organic Compounds. *Catalysis Letters*, 137(3-4), 7 2010.
- [25] V.P. Santos, M.F.R. Pereira, J.J.M. Órfão, and J.L. Figueiredo. The role of lattice oxygen on the activity of manganese oxides towards the oxidation of volatile organic compounds. *Applied Catalysis B: Environmental*, 99(1-2), 8 2010.
- [26] Zhenping Qu, Yibin Bu, Yuan Qin, Yi Wang, and Qiang Fu. The improved reactivity of manganese catalysts by Ag in catalytic oxidation of toluene. *Applied Catalysis B: Environmental*, 132-133, 3 2013.
- [27] Sang Chai Kim and Wang Geun Shim. Catalytic combustion of VOCs over a series of manganese oxide catalysts. *Applied Catalysis B: Environmental*, 98(3-4), 8 2010.
- [28] Ata ul Rauf Salman, Beate Meisand Østrådt, Bjørn Christian Enger, Rune Løberg, David Waller, and Magnus Rønning. Effect of loading, support material and water on the catalytic oxidation of no over supported manganese oxide catalysts for nitric acid production. Manuscript in preparation, 2019.

- [29] Shuhui Liang, Fei Teng, G Bulgan, Ruilong Zong, and Yongfa Zhu. Effect of phase structure of MnO_2 nanorod catalyst on the activity for CO oxidation. *Journal of Physical Chemistry C*, 112(14):5307–5315, 2008.
- [30] Fangyi Cheng, Jianzhi Zhao, Wene Song, Chunsheng Li, Hua Ma, Jun Chen, and Panwen Shen. Facile controlled synthesis of MnO_2 nanostructures of novel shapes and their application in batteries. *Inorganic Chemistry*, 45(5):2038–2044, 2006.
- [31] C Lahousse, A Bernier, P Grange, B Delmon, P Papaefthimiou, T Ioannides, and X Verykios. Evaluation of $\gamma\text{-MnO}_2$ as a voc removal catalyst: comparison with a noble metal catalyst. *Journal of Catalysis*, 178(1):214–225, 1998.
- [32] Hui Wang, Hu Chen, Ying Wang, and Yong Kang Lyu. Performance and mechanism comparison of manganese oxides at different valence states for catalytic oxidation of NO. *Chemical Engineering Journal*, 361:1161–1172, 2019.
- [33] Jiahao Chen, Meiqing Shen, Xinquan Wang, Gongshin Qi, Jun Wang, and Wei Li. The influence of nonstoichiometry on LaMnO_3 perovskite for catalytic NO oxidation. *Applied Catalysis B: Environmental*, 134-135, 5 2013.
- [34] JL Ayastuy, MP Gonzalez-Marcos, JR Gonzalez-Velasco, and MA Gutiérrez-Ortiz. $\text{MnO}_x/\text{Pt}/\text{Al}_2\text{O}_3$ catalysts for co oxidation in H_2 -rich streams. *Applied Catalysis B: Environmental*, 70(1-4):532–541, 2007.
- [35] Dimitrios Delimaris and Theophilos Ioannides. VOC oxidation over $\text{MnO}_x\text{-CeO}_2$ catalysts prepared by a combustion method. *Applied Catalysis B: Environmental*, 84(1-2), 10 2008.
- [36] María Roxana Morales, Bibiana P Barbero, and Luis E Cadús. Evaluation and characterization of Mn-Cu mixed oxide catalysts for ethanol total oxidation: influence of copper content. *Fuel*, 87(7):1177–1186, 2008.
- [37] Andrzej Machocki, Theophilos Ioannides, Beata Stasinska, Wojciech Gac, George Avgouropoulos, Dimitris Delimaris, Wieslaw Grzegorzczak, and Sylwia Pasieczna. Manganese-lanthanum oxides modified with silver for the catalytic combustion of methane. *Journal of Catalysis*, 227(2):282–296, 2004.
- [38] Wojciech Gac, Grzegorz Giecko, Sylwia Pasieczna-Patkowska, Tadeusz Borowiecki, and Leszek Kępiński. The influence of silver on the properties of cryptomelane type manganese oxides in N_2O decomposition reaction. *Catalysis Today*, 137(2-4), 9 2008.
- [39] Meng-fei Luo, Xian-xin Yuan, and Xiao-ming Zheng. Catalyst characterization and activity of Ag-Mn, Ag-Co and Ag-Ce composite oxides for oxidation of volatile organic compounds. *Applied Catalysis A: General*, 175(1-2), 12 1998.
- [40] Marika Männikkö, Magnus Skoglundh, and Hanna Härelind Ingelsten. Selective catalytic reduction of NO_x with methanol over supported silver catalysts. *Applied Catalysis B: Environmental*, 119:256–266, 2012.
- [41] Marika Männikkö, Xueting Wang, Magnus Skoglundh, and Hanna Härelind. Characterization of the active species in the silver/alumina system for lean NO_x reduction with methanol. *Catalysis Today*, 267:76–81, 2016.
- [42] Koichi Eguchi, Mitsunori Watabe, Shigeki Ogata, and Hiromichi Arai. Reversible Sorption of Nitrogen Oxides in Mn-Zr Oxide. *Journal of Catalysis*, 158(2), 2 1996.

- [43] Izumi Matsukuma, Suzue Kikuyama, Ryuji Kikuchi, Kazunari Sasaki, and Koichi Eguchi. Development of zirconia-based oxide sorbents for removal of NO and NO₂. *Applied Catalysis B: Environmental*, 37(2), 4 2002.
- [44] Baohuai Zhao, Rui Ran, Xiaodong Wu, Duan Weng, Xueyuan Wu, and Chunyi Huang. Comparative study of Mn/TiO₂ and Mn/ZrO₂ catalysts for NO oxidation. *Catalysis Communications*, 56:36–40, 2014.
- [45] PDL Mercera, JG Van Ommen, EBM Doesburg, AJ Burggraaf, and JRH Ross. Zirconia as a support for catalysts influence of additives on the thermal stability of the porous texture of monoclinic zirconia. *Applied catalysis*, 71(2):363–391, 1991.
- [46] Ib Chorkendorff and Johannes W Niemantsverdriet. *Concepts of modern catalysis and kinetics*. John Wiley & Sons, 2017.
- [47] K.P. de Jong. *Synthesis of Solid Catalysts*. Wiley-VCH, 2009.
- [48] NM Deraz. The comparative jurisprudence of catalysts preparation methods: I. precipitation and impregnation methods. *J. Ind. Environ. Chem*, 2(1):19–21, 2018.
- [49] Jerzy Haber, Jochen H Block, and Bernard Delmon. Methods and Procedures for Catalyst Characterization. In *UPAC Recommendations*, volume 67, pages 1257–1306. IUPAC, 1995.
- [50] Eric Marceau, Xavier Carrier, and Michel Che. Impregnation and Drying. In *Synthesis of Solid Catalysts*. Wiley-VCH Verlag GmbH & Co. KGaA, Weinheim, Germany.
- [51] John Regalbuto. *Catalyst preparation: science and engineering*. CRC press, 2016.
- [52] AW Coats and JP Redfern. Thermogravimetric analysis. a review. *Analyst*, 88(1053):906–924, 1963.
- [53] NETZSCH-Gerätebau GmbH. Reaction Temperature and Reaction Enthalpy. <https://www.netzsch-thermal-analysis.com/en/contract-testing/glossary/reaction-temperature-and-reaction-enthalpy/>. Accessed: 2021-02-30.
- [54] Oxford English Dictionary. Sinter. <https://www.oed.com/view/Entry/180272?rskey=MkgLmY&result=2&isAdvanced=false#eid>. Accessed: 2021-03-30.
- [55] Calvin H Bartholomew and Robert J Farrauto. *Fundamentals of industrial catalytic processes*. John Wiley & Sons, 2011.
- [56] Stephen Brunauer and Paul H Emmett. The use of low temperature van der waals adsorption isotherms in determining the surface areas of various adsorbents. *Journal of the American Chemical Society*, 59(12):2682–2689, 1937.
- [57] Elliott P. Barrett, Leslie G. Joyner, and Paul P. Halenda. The Determination of Pore Volume and Area Distributions in Porous Substances. I. Computations from Nitrogen Isotherms. *Journal of the American Chemical Society*, 73(1), 1 1951.
- [58] Kenneth SW Sing. Reporting physisorption data for gas/solid systems with special reference to the determination of surface area and porosity (recommendations 1984). *Pure and applied chemistry*, 57(4):603–619, 1985.
- [59] Kenneth SW Sing and Ruth T Williams. Physisorption hysteresis loops and the characterization of nanoporous materials. *Adsorption Science & Technology*, 22(10):773–782, 2004.

- [60] Kenneth SW Sing. Reporting physisorption data for gas/solid systems with special reference to the determination of surface area and porosity (recommendations 1984). *Pure and applied chemistry*, 57(4):603–619, 1985.
- [61] Nicholas W Hurst, Stephen J Gentry, and Alan Jones. Temperature Programmed Reduction. *Catalysis Reviews*, 24(2):233–309, 1982.
- [62] John L. Falconer and James A. Schwarz. Temperature-Programmed Desorption and Reaction: Applications to Supported Catalysts. *Catalysis Reviews*, 25(2), 6 1983.
- [63] Johannes W Niemantsverdriet. *Spectroscopy in catalysis*. Wiley Online Library, 2007.
- [64] MA Reiche, M Maciejewski, and A Baiker. Characterization by temperature programmed reduction. *Catalysis today*, 56(4):347–355, 2000.
- [65] C. Suryanarayana and M. Grant Norton. *X-Ray Diffraction*. Springer US, Boston, MA, 1998.
- [66] Ahmad Monshi, Mohammad Reza Foroughi, and Mohammad Reza Monshi. Modified Scherrer Equation to Estimate More Accurately Nano-Crystallite Size Using XRD. *World Journal of Nano Science and Engineering*, 02(03), 2012.
- [67] H Topsøe. *An examination of keystroke dynamics for continuous user authentication*. PhD thesis, Stanford University, 1972.
- [68] Harold P Klug and Leroy E Alexander. *X-ray Diffraction Procedures for Polycrystalline and Amorphous Materials*. Wiley, 2 edition, 1974.
- [69] SR Sashital, JB Cohen, RL Burwell Jr, and JB Butt. PtSiO₂: *ii*. characterization of the gel and the platinum particles by x-ray diffraction. *Journal of Catalysis*, 50(3):479–493, 1977.
- [70] C.G. Zhou and Q.H. Yu. Nanostructured thermal barrier coatings. In *Thermal Barrier Coatings*. Elsevier, 2011.
- [71] C Prado-Burguete, A Linares-Solano, F Rodriguez-Reinoso, and C Salinas-Martinez De Lecea. Effect of carbon support and mean pt particle size on hydrogen chemisorption by carbon-supported Pt catalysts. *Journal of Catalysis*, 128(2):397–404, 1991.
- [72] Peter R. Griffiths and James A. de Haseth. *Fourier Transform Infrared Spectrometry*. John Wiley & Sons, Inc., Hoboken, NJ, USA, 4 2007.
- [73] MKS Instruments. Hardware Instructions Manual, MKS Type Multigas Analyzer. Models 2030,2031 and 2032. 2011.
- [74] H. Scott Folger. *Elements of Chemical Reaction Engineering*. Pearson Education, fifth edition, 2016.
- [75] Engineering Toolbox. Nitric Oxide Density. https://www.engineeringtoolbox.com/gas-density-d_158.html. Accessed: 2021-04-02.
- [76] PB Weisz and CD Prater. Interpretation of measurements in experimental catalysis. In *Advances in Catalysis*, volume 6, pages 143–196. Elsevier, 1954.
- [77] David E Mears. Diagnostic criteria for heat transport limitations in fixed bed reactors. *Journal of Catalysis*, 20(2):127–131, 1971.

- [78] Wesley M Dose, Neeraj Sharma, Nathan A S Webster, Vanessa K Peterson, and Scott W Donne. Kinetics of the thermally-induced structural rearrangement of γ - MnO_2 . *Journal of Physical Chemistry C*, 118(42):24257–24265, 2014.
- [79] Arno H. Reidies. Manganese Compounds. In *Ullmann's Encyclopedia of Industrial Chemistry*. Wiley-VCH Verlag GmbH & Co. KGaA, Weinheim, Germany, 6 2000.
- [80] Hu Chen, Ying Wang, and Yong Kang Lyu. High catalytic activity of Mn-based catalyst in NO oxidation at low temperature and over a wide temperature span. *Molecular Catalysis*, 454:21–29, 7 2018.
- [81] Margarita Kantcheva, Mustafa U Kucukkal, and Sefik Suzer. Spectroscopic investigation of species arising from co chemisorption on titania-supported manganese. *Journal of Catalysis*, 190(1):144–156, 2000.
- [82] NE Bogdanchikova, GK Boreskov, NE Buyanova, OV Kovrizhina, and AV Khasin. Oxygen chemisorption on silver catalysts. *Reaction Kinetics and Catalysis Letters*, 12(3):201–205, 1979.
- [83] Maia Montaña, María Leguizamón Aparicio, Marco Ocsachoque, Marisa Navas, Ivoneide de C. L. Barros, Enrique Rodríguez-Castellón, Mónica Casella, and Ileana Lick. Zirconia-Supported Silver Nanoparticles for the Catalytic Combustion of Pollutants Originating from Mobile Sources. *Catalysts*, 9(3), 3 2019.
- [84] PM De Wolff. Interpretation of some γ - MnO_2 diffraction patterns. *Acta Crystallographica*, 12(4):341–345, 1959.
- [85] Xiongfei Shen, Yunshuang Ding, Jia Liu, Kate Laubernds, Richard P Zerger, Mihai Polverejan, Young-Chan Son, Mark Aindow, and Steven L Suib. Synthesis, characterization, and catalytic applications of manganese oxide octahedral molecular sieve (oms) nanowires with a 2×3 tunnel structure. *Chemistry of materials*, 16(25):5327–5335, 2004.
- [86] K.A. Bethke and H.H. Kung. Supported Ag Catalysts for the Lean Reduction of NO with C_3H_6 . *Journal of Catalysis*, 172(1), 11 1997.
- [87] S Karski, I Witońska, J Rogowski, and J Gołuchowska. Interaction between Pd and Ag on the surface of silica. *Journal of Molecular Catalysis A: Chemical*, 240(1-2):155–163, 2005.
- [88] Eleonora Aneggi, Jordi Llorca, Carla de Leitenburg, Giuliano Dolcetti, and Alessandro Trovarelli. Soot combustion over silver-supported catalysts. *Applied Catalysis B: Environmental*, 91(1-2):489–498, 2009.
- [89] Hirokazu Tsukahara, Takanobu Ishida, and Mitsufumi Mayumi. Gas-Phase Oxidation of Nitric Oxide: Chemical Kinetics and Rate Constant. *Nitric Oxide*, 3(3), 6 1999.
- [90] Qiang Zhao. *The Thermal Stability and Catalytic Application of MnO_x - ZrO_2 Oxide Powders*. PhD thesis, Drexel University, 4 2004.
- [91] Bruno Azambre, Idriss Atribak, Agustín Bueno-López, and Avelina García-García. Probing the Surface of CeriaZirconia Catalysts Using NO Adsorption/Desorption: A First Step Toward the Investigation of Crystallite Heterogeneity. *The Journal of Physical Chemistry C*, 114(31), 8 2010.

- [92] Weichao Wang, Geoffrey McCool, Neeti Kapur, Guang Yuan, Bin Shan, Matt Nguyen, Uschi M Graham, Burtron H Davis, Gary Jacobs, Kyeongjae Cho, et al. Mixed-phase oxide catalyst based on mn-mullite (sm, gd) Mn_2O_5 for no oxidation in diesel exhaust. *Science*, 337(6096):832–835, 2012.
- [93] Mahnaz Ghiasi, Mario Ulises Delgado-Jaime, Azim Malekzadeh, Ru-Pan Wang, Piter S. Miedema, Martin Beye, and Frank M. F. de Groot. Mn and Co Charge and Spin Evolutions in $LaMn_{1-x}/Co_x/O_3$ Nanoparticles. *The Journal of Physical Chemistry C*, 120(15), 4 2016.
- [94] Nian Tang, Yue Liu, Haiqiang Wang, and Zhongbiao Wu. Mechanism Study of NO Catalytic Oxidation over MnO_x/TiO_2 Catalysts. *The Journal of Physical Chemistry C*, 115(16), 4 2011.
- [95] S.S. Mulla, N. Chen, W.N. Delgass, W.S. Epling, and F.H. Ribeiro. NO_2 inhibits the catalytic reaction of NO and O_2 over Pt. *Catalysis Letters*, 100(3-4), 4 2005.
- [96] Louise Olsson, Hans Persson, Erik Fridell, Magnus Skoglundh, and Bengt Andersson. A kinetic study of NO oxidation and NO_x storage on Pt/ Al_2O_3 and Pt/ BaO/Al_2O_3 . *The Journal of Physical Chemistry B*, 105(29):6895–6906, 2001.
- [97] Guangyan Xu, Jinzhu Ma, Guangzhi He, Yunbo Yu, and Hong He. An alumina-supported silver catalyst with high water tolerance for H_2 assisted C_3H_6 -SCR of NO_x . *Applied Catalysis B: Environmental*, 207, 6 2017.
- [98] Jhon Quiroz, Jean-Marc Giraudon, Antonella Gervasini, Christophe Dujardin, Christine Lancelot, Martine Trentesaux, and Jean-François Lamonier. Total Oxidation of Formaldehyde over MnO_x-CeO_2 Catalysts: The Effect of Acid Treatment. *ACS Catalysis*, 5(4), 4 2015.
- [99] Fredrik Gunnarsson, Hannes Kannisto, Magnus Skoglundh, and Hanna Härelind. Improved low-temperature activity of silver–alumina for lean nox reduction—effects of ag loading and low-level pt doping. *Applied Catalysis B: Environmental*, 152:218–225, 2014.
- [100] Marika Männikkö, Xueting Wang, Magnus Skoglundh, and Hanna Härelind. Silver/alumina for methanol-assisted lean NO_x reduction — on the influence of silver species and hydrogen formation. *Applied Catalysis B: Environmental*, 180:291–300, 2016.

Appendix A

Catalyst Preparation

A.1 Preparation Calculations

The manganese precursor used was $\text{Mn}(\text{NO}_3)_2 \cdot 4\text{H}_2\text{O}$, provided by Merck, with CAS-no: 20694-39-7. The zirconia support was provided Alfa Aesar GmbH (1/8" pellets) with CAS nr: 1314 – 23 – 4.

The Platinum Nitrate Solution (15%w/w solution) from Alfa Aesar with CAS nr:10102 – 09 – 7 were used. Finally, the silver used, AgNO_3 , were from the same provider (99 + % purity) with CAS nr: 7761 – 88 – 8.

Table A.1: Total weight of prepared catalyst and incipient wetness point for the used zirconia.

Total weight of catalyst	10 g
H_2O incipient for ZrO_2	0.5 g/g _{cat}

Table A.2: Molar mass of chemicals used in the preparation of the catalysts.

Chemical	Molar Mass [g/mol]
ZrO_2	123.22
Manganese(II) Nitrate Tetrahydrate	251.01
Mn	54.94
Platinum(IV) nitrate, solution, Pt 15% w/w	443.10
Pt	195.08
Silver Nitrate	169.87
Ag	107.87
H_2O	18.02

Table A.3: An overview of the catalysts, the wt% of active material and promoter, and the support as % of the total weight.

Catalyst	Active metal	Active metal [wt%]	Promoter	Promoter [wt%]	Support	Support [%]
5Mn	Mn	5%	-	0%	ZrO ₂	95%
20Mn	Mn	20%	-	0%	ZrO ₂	80%
5Mn-1Pt	Mn	5%	Pt	1%	ZrO ₂	94%
20Mn-1Pt	Mn	20%	Pt	1%	ZrO ₂	79%
5Mn-1Ag	Mn	5%	Ag	1%	ZrO ₂	94%
20Mn-1Ag	Mn	20%	Ag	1%	ZrO ₂	79%
5Ag	Ag	5%	-	0%	ZrO ₂	95%

The catalysts were prepared by incipient wetness impregnation. An example of the calculations done for preparing 20Mn is as follows:

$$\text{Zirconia}(g) = 0.8 \cdot 10 g = 8 g \quad (\text{A.1})$$

$$\text{Mn}(g) = 0.2 \cdot 10 g = 2 g \quad (\text{A.2})$$

$$\text{Mn}(mol) = \frac{2 g}{54.94 g/mol} = 0.0364 mol \quad (\text{A.3})$$

$$\text{Mn}(\text{NO}_3)_2 \cdot 4\text{H}_2\text{O}(g) = 0.0364 mol \cdot 251.01 g/mol = 9.1379 g \quad (\text{A.4})$$

$$\text{H}_2\text{O}_{\text{in Mn}(\text{NO}_3)_2 \cdot 4\text{H}_2\text{O}}(g) = 4 \cdot 0.0364 mol \cdot 18.01 g = 2.6211 g \quad (\text{A.5})$$

$$\text{H}_2\text{O}_{\text{incipient wetness}}(g) = 8 g \cdot 0.5 g = 4 g \quad (\text{A.6})$$

$$\text{H}_2\text{O}_{\text{added, deionized}} = 4 g - 2.6211 g = 1.3789 g \quad (\text{A.7})$$

The bi-metallic catalysts were prepared by co-impregnation of manganese and platinum, and manganese and silver. Below is the calculation for preparation of 20Mn-1Ag as an example.

$$\text{Zirconia}(g) = 0.8 \cdot 10 g = 7.9 g \quad (\text{A.8})$$

$$\text{Mn}(g) = 0.2 \cdot 10 g = 2 g \quad (\text{A.9})$$

$$\text{Mn}(\text{NO}_3)_2 \cdot 4\text{H}_2\text{O}(g) = 0.0364 mol \cdot 251.01 g/mol = 9.1379 g \quad (\text{A.10})$$

$$\text{H}_2\text{O}_{\text{in Mn(NO}_3)_2 \cdot 4\text{H}_2\text{O}}(g) = 4 \cdot 0.0364 \text{ mol} \cdot 18.01 \text{ g} = 2.621 \text{ g} \quad (\text{A.11})$$

$$\text{Ag}(g) = 0.01 \cdot 10 \text{ g} = 0.1 \text{ g} \quad (\text{A.12})$$

$$\text{Ag}(\text{mol}) = \frac{0.1}{107.87} = 0.001 \text{ mol} \quad (\text{A.13})$$

$$\text{AgNO}_3(g) = 0.001 \text{ mol} \cdot 169.87 \text{ g/mol} = 0.157 \text{ g} \quad (\text{A.14})$$

$$\text{H}_2\text{O}_{\text{incipient wetness}}(g) = 7.9 \cdot 0.5 \text{ g} = 3.950 \text{ g} \quad (\text{A.15})$$

$$\text{H}_2\text{O}_{\text{added, deionized}} = 3.950 \text{ g} - 2.621 \text{ g} = 1.329 \text{ g} \quad (\text{A.16})$$

A.2 Used Measurements

Table A.4: Amounts of zirconia, metal precursor and deionized water used in catalyst preparation for 5Mn catalysts.

Catalyst	5Mn	5Mn-1Pt	5Mn-1Ag
ZrO ₂	9.5001 g	9.4091 g	9.4011 g
Mn(NO ₃) ₂ ·4H ₂ O	2.2856 g	2.2865 g	2.2836 g
Pt(NO ₃) ₄	-	0.6738 g	-
AgNO ₃	-	-	0.1575 g
Deionized water	4.0985 g	3.4884 g	4.0454 g

Table A.5: Amounts of zirconia, metal precursor and deionized water used in catalyst preparation for 20Mn catalysts.

Catalyst	20Mn	20Mn-1Pt	20Mn-1Ag
ZrO ₂	8.003 g	7.9026 g	7.9062 g
Mn(NO ₃) ₂ ·4H ₂ O	9.1414 g	9.1366 g	9.1370 g
Pt(NO ₃) ₄	-	0.6640 g	-
AgNO ₃	-	-	0.1570 g
Deionized water	1.3808 g	0.7615 g	1.3365 g

Table A.6: Amounts of zirconia, metal precursor and deionized water used in catalyst preparation for 5Ag.

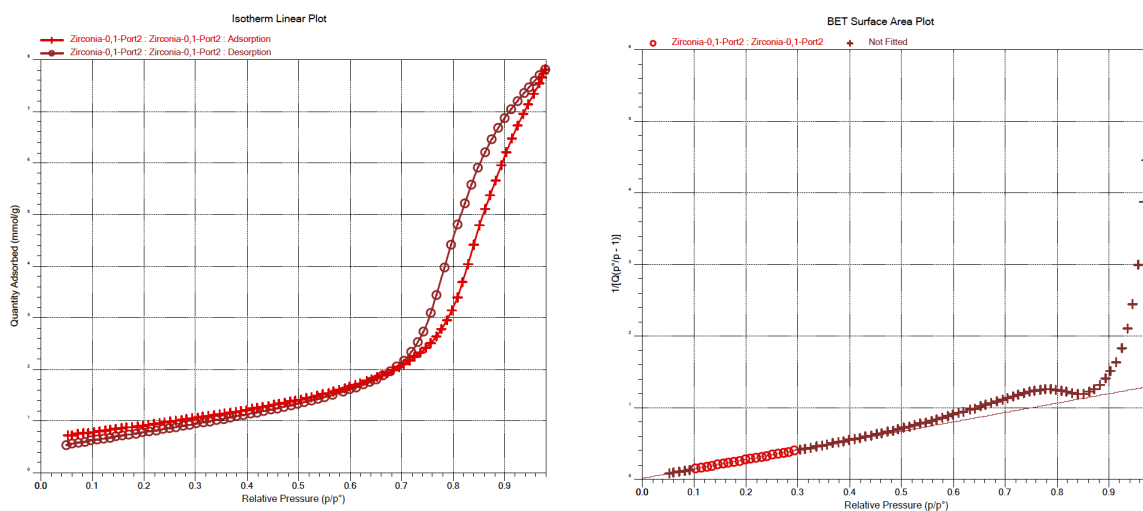
Catalyst	5Ag
ZrO ₂	9.5044 g
AgNO ₃	0.7887 g
Deionized water	4.7491 g

Appendix B

Characterization Results

B.1 Nitrogen Adsorption

Figure B.1a and B.1b in B.1 show the the isotherm linear plot and BET surface area plot for the zirconia support. Figure B.2 shows the BJH desorption pore size distribution for the zirconia support.



(a) The isotherm linear plot for zirconia.

(b) The BET surface area plot for zirconia.

Figure B.1: The isotherm linear plot and BET surface area plot for the zirconia support.

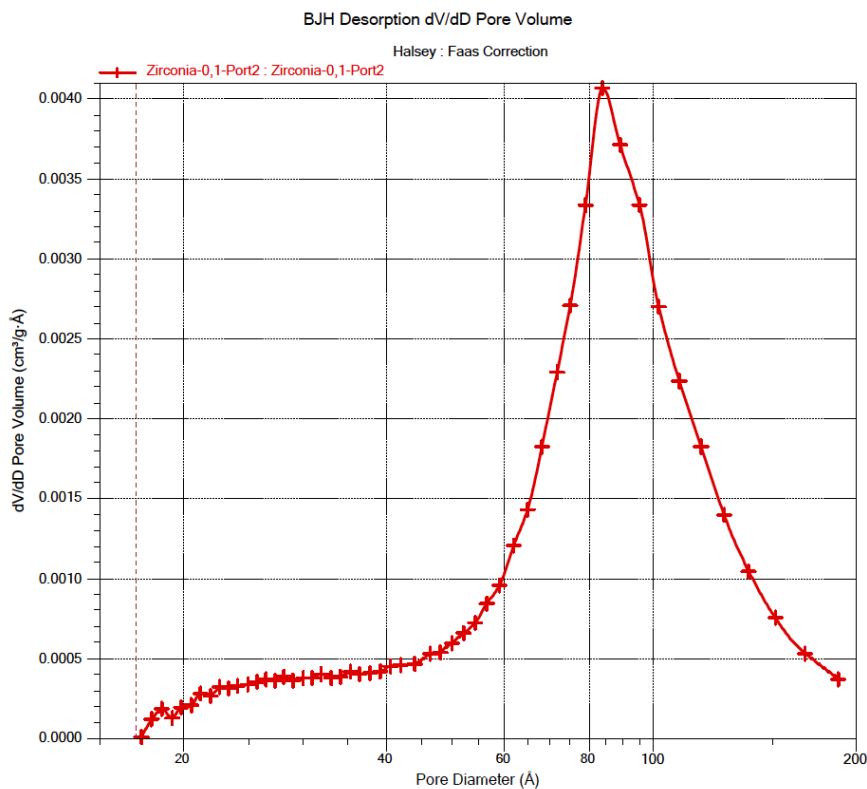


Figure B.2: The BJH desorption average pore size distribution for zirconia.

B.2 TPR

Figure B.3 display the TRP spectra for the zirconia-supported manganese oxide catalysts.

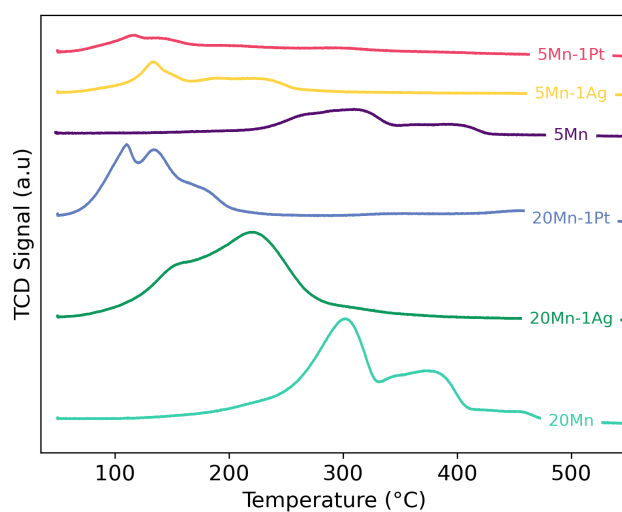


Figure B.3: The H₂-TPR profile of the zirconia-supported manganese oxide catalysts.

The results of the different manganese oxide catalysts from TPR is presented in Table B.1. The

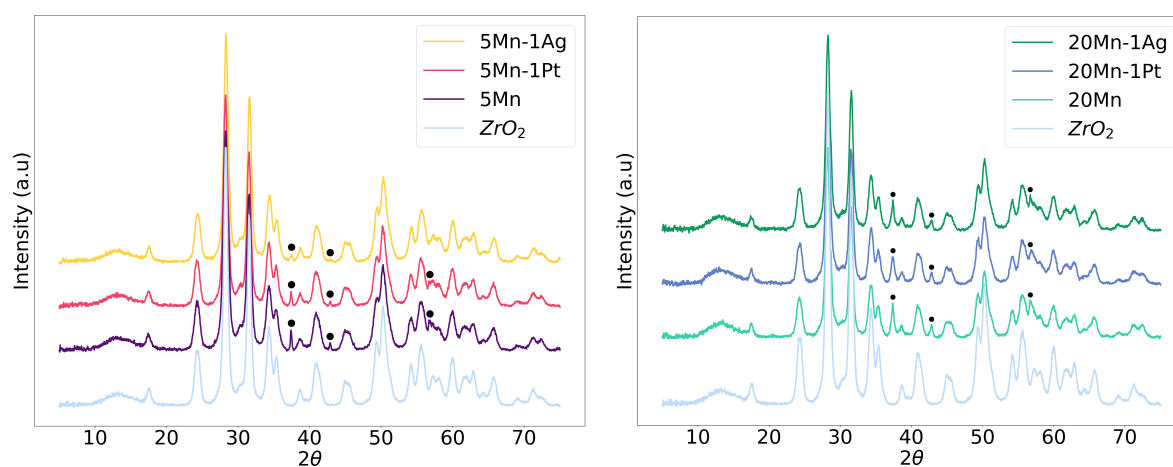
Table displays the temperatures where reduction peaks occurs in Figure B.3. $T_{o,red}$ indicates the onset temperature of reduction.

Table B.1: The results of the different manganese oxide catalysts from TPR show the temperatures where reduction peaks occurs in Figure B.3. $T_{o,red}$ indicates the onset temperature, where the catalyst starts the consumption of H_2 . T_{M0} gives information about the first reduction appearing before the highest peak. T_{M1} indicates the temperature occurring at the highest peak, while the remaining T_{M2} , T_{M3} and T_{M4} indicate high temperature peaks.

Catalyst	$T_{o,red}$ [°C]	T_{M0} [°C]	T_{M1} [°C]	T_{M2} [°C]	T_{M3} [°C]	T_{M4} [°C]
5Mn-1Pt	75	-	119	145	207	-
5Mn-1Ag	85	-	138	196	224	-
5Mn	170	275	313	375	398	-
20Mn-1Pt	60	-	114	139	180	459
20Mn-1Ag	73	150	225	-	-	-
20Mn	145	-	306	350	377	458

B.3 XRD

In the following section the diffraction patterns from XRD is shown. Figure B.4a, and Figure B.4b in B.4 shows the diffraction pattern with promotion of 1wt% platinum and silver with 5 and 20 wt% manganese oxide on zirconia support.



(a) XRD patterns of zirconia support and two manganese on zirconia with 5 wt%. (b) XRD patterns of zirconia support and two manganese on zirconia with 20 wt%.

Figure B.4: XRD patterns of zirconia support and two manganese on zirconia with 20 and 5 wt%. The specific MnO₂ peaks are indicated with a dot.

Appendix C

Catalytic Activity Measurements

C.1 Amounts used in Activity Measurements

The exact amount used of SiC, catalysts and zirconia in activity measurements is given in Table [C.1](#). The catalysts were weighted after activity measurements, and is additionally displayed before and after sieving.

Table C.1: Mass of catalyst, zirconia and SiC used in activity measurements, and weight after the activity experiments.

Sample	<i>Before Experiment</i>		<i>After Experiment</i>	
	Catalyst sample [g]	SiC ^a [g]	Catalyst sample and SiC [g]	Catalyst after sieving [g]
<i>SiC 30mesh</i>		3.2534		
<i>SiC 53-90 μm</i>		3.2556		
<i>SiC mix</i>	0.5045 ^b	2.7539		
<i>ZrO₂</i>	0.5013	2.7530	3.2235	0.4585
<i>20Mn</i>	0.5091	2.7531	3.3500	0.4401
<i>20Mn-1Pt</i>	0.5015	2.7524	3.2640	0.4402
<i>20Mn-1Pt Reduced</i>	0.5056	2.7556	3.1214	0.3797
<i>20Mn-1Ag</i>	0.5058	2.7526	3.2010	0.4313
<i>5Mn</i>	0.5041	2.7526	3.2263	0.4676
<i>5Mn-1Pt</i>	0.5069	2.7549	3.1995	0.4537
<i>5Mn-1Ag</i>	0.5049	2.7563	3.2397	0.4646
<i>5Ag</i>	0.5530	2.7535	3.2448	0.4701

^a 30 mesh particle size.

^b 53-90 microns particle size of SiC.

C.2 Total NO conversion

The total NO conversion for the manganese catalysts during the temperature scan experiments are displayed in Figure [C.1](#) and [C.2](#).

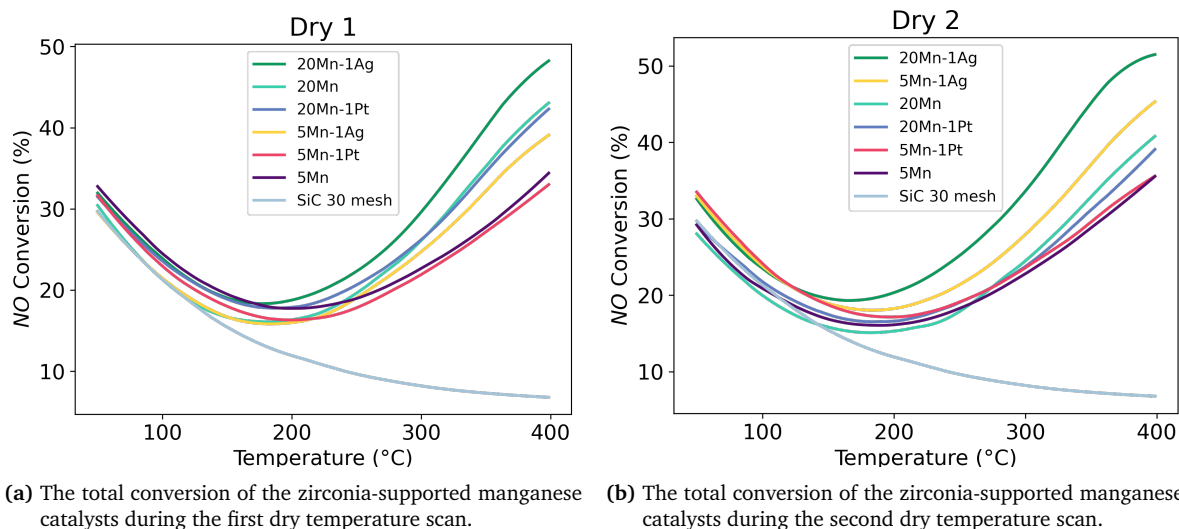


Figure C.1: The total NO conversion (%) of the manganese catalysts from 110 – 400°C with a ramp rate of 5 °C/min. $WHSV = 24\ 000\ Nml/h \cdot g_{cat}$ and pressure at 1 bar.

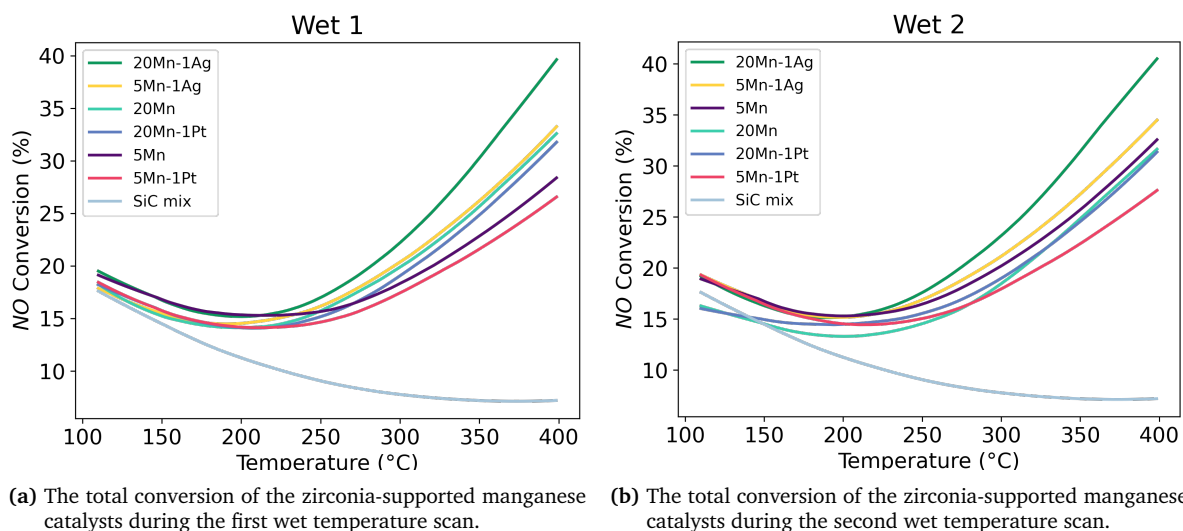


Figure C.2: The total NO conversion (%) of the manganese catalysts from 110 – 400°C with a ramp rate of 5 °C/min. $WHSV = 24000\ Nml/h \cdot g_{cat}$ and pressure at 1 bar.

The total NO conversion (%) of 20Mn-1Pt with and without pretreatment in the first and second temperature scan in dry conditions is shown in Figure [C.3](#).

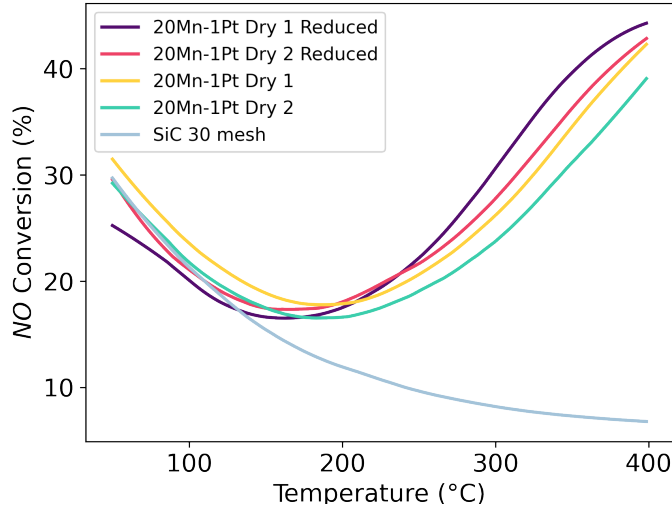


Figure C.3: The total NO conversion (%) of 20Mn-1Pt with and without pretreatment in the first and second temperature scan in dry conditions from 50 – 400°C with a ramp rate of 5 °C/min. $WHSV = 24000 \text{ Nm}^3/\text{h} \cdot g_{cat}$ and pressure at 1 bar.

C.3 Catalytic Conversion

Due to the experimental design and parameters like temperature and pressure, the catalysts exhibited differences in the lower temperature regime where only the gas-phase contribution should be present. To compare the catalysts and present catalytic activity, the SiC was subtracted from the conversion curves. Before the subtraction, the SiC was extrapolated to the conversion line for the catalysts. The equation used for the extrapolation is presented in Equation C.1. The subtraction is shown in Equation C.2.

$$x_{SiC,new} = x_{SiC} + (x_{NO}[0] - x_{SiC}[0]) \quad (\text{C.1})$$

$$x_{NO,c} = x_{NO} - x_{SiC,new} \quad (\text{C.2})$$

The x_{SiC} is the gas-phase contribution from the run with only SiC in the reactor, [0] indicates is the first measured NO conversion in the test run. x_{NO} is the total catalytic conversion, with gas-phase contribution included, and $x_{NO,c}$ is only catalytic NO conversion after subtracting the gas-phase contribution.

The subtraction was only performed for the temperature scans when the gas-phase contribution with SiC was not stable during the steady-state conditions. Table C.2 displays which SiC was used as subtraction in the different temperature programs.

Table C.2: An overview of which background used to subtract NO conversion from the total NO conversion. SiC mix contained 2.75 g of 30 mesh particle size and 0.5 g 53-90 μm article fraction.

Temperature Program	Background used for subtraction
Dry 1	SiC 30 mesh
Dry 2	SiC 30 mesh
Wet 1	SiC mix
Wet 2	SiC mix
250SS Dry	-
250SS Wet	-
350SS Dry	-
350SSWet	-

C.3.1 Effect of Temperature

The catalytic NO conversion is presented in a bar plot for all the catalysts at 250°C in Figure C.4 and at 350°C in Figure C.5. The conversion is calculated from results conducted during the temperature scan test runs, and the NO conversion contribution from the gas-phase reaction is subtracted.

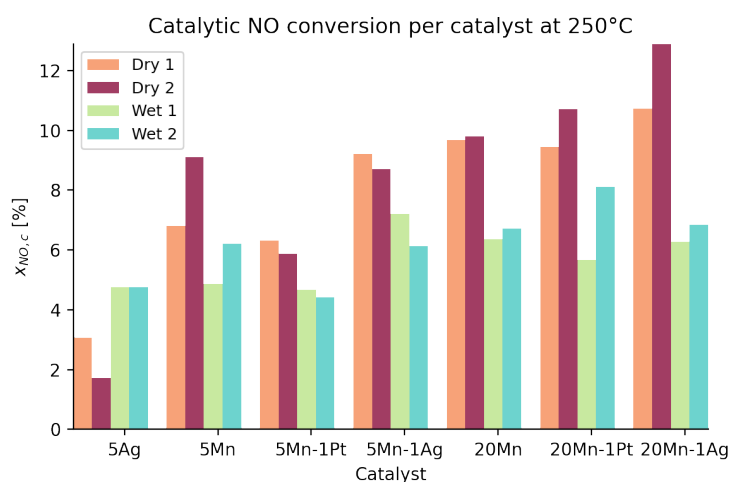


Figure C.4: The catalytic NO conversion of the catalysts at 250°C extracted from the temperature dependency experiments.

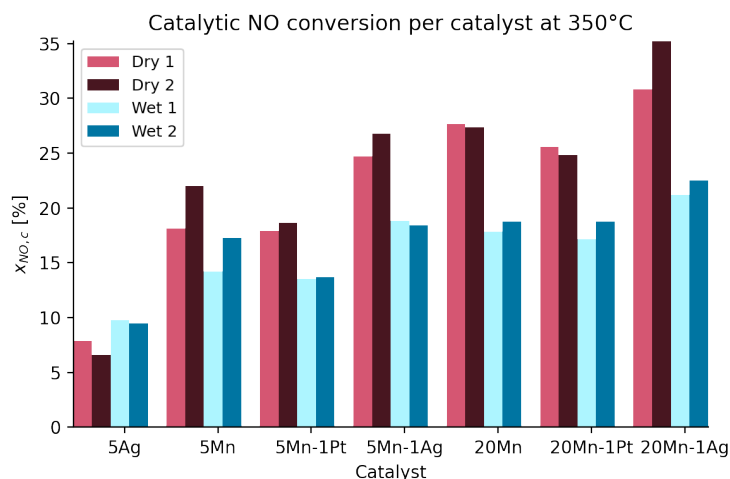
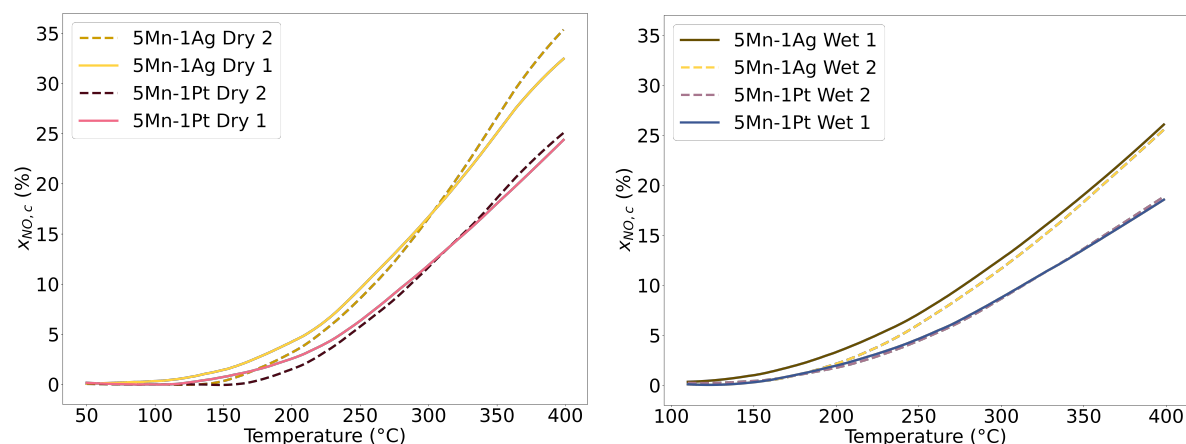


Figure C.5: The catalytic NO conversion of the catalysts at 350°C extracted from the temperature dependency experiments.

C.3.1.1 Promoted 5 wt% Manganese Oxide Catalysts

Figure C.6a and C.6b in C.6 displays how the promoted 5 wt% manganese oxide catalysts perform in the temperature scan test runs in dry and wet conditions.



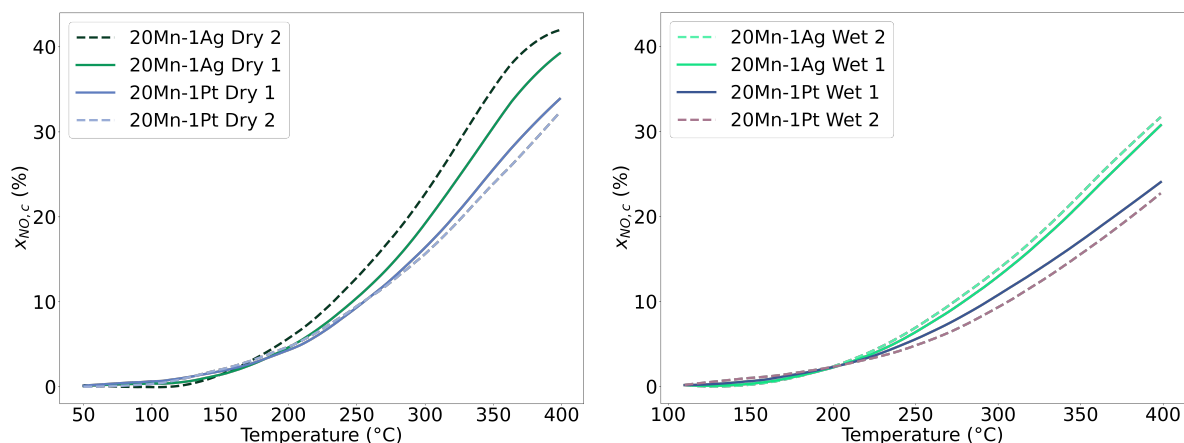
(a) The catalytic conversion of the zirconia-supported promoted 5 wt% manganese oxide catalysts during the first and second dry temperature scan.

(b) The catalytic conversion of the zirconia-supported promoted 5 wt% manganese oxide catalysts during the first and second wet temperature scan.

Figure C.6: The total NO conversion (%) of the 5 wt% manganese oxide catalysts from 110 – 400°C with a ramp rate of 5 °C/min. $WHSV = 24000 \text{ Nml/h} \cdot g_{cat}$ and pressure at 1 bar.

C.3.1.2 Promoted 20 wt% Manganese Oxide Catalysts

Figure C.7a and C.7b in C.7 shows how the promoted 20 wt% manganese oxide catalysts perform in the temperature scan test runs in dry and wet conditions.



(a) The catalytic conversion of the zirconia-supported promoted 20 wt% manganese oxide catalysts during the first and second dry temperature scan.

(b) The catalytic conversion of the zirconia-supported promoted 20 wt% manganese oxide catalysts during the first and second wet temperature scan.

Figure C.7: The catalytic NO conversion (%) of the 20 wt% manganese oxide catalysts from 110 – 400°C with a ramp rate of $5\text{ }^{\circ}\text{C}/\text{min}$. $WHSV = 24000\text{ Nm}l/h \cdot g_{cat}$ and pressure at 1 bar.

C.3.1.3 Platinum-promoted Catalysts

The catalytic activity exhibited from the platinum-promoted catalysts are displayed in Figure [C.8](#), and the differences between the initial and final temperature scans are shown.

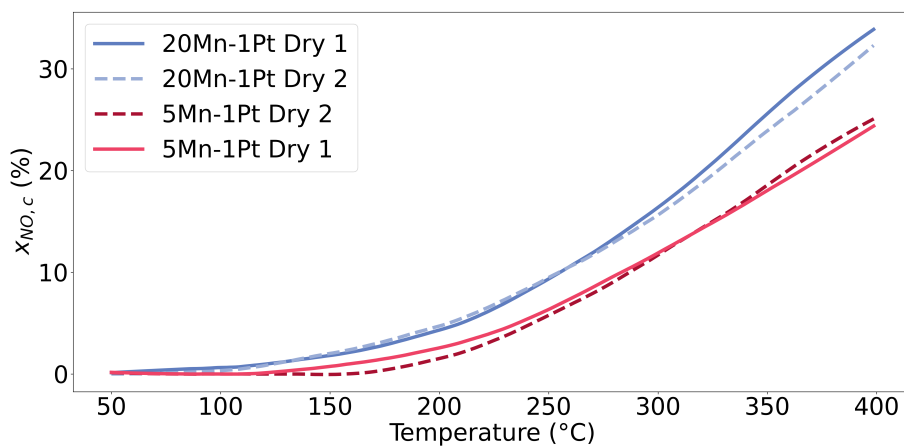


Figure C.8: The NO conversion (%) of 20Mn-1Pt Dry 1 and 2 compared with 5Mn-1Pt Dry 1 and 2 from 50 – 400°C with a ramp rate of $5\text{ }^{\circ}\text{C}/\text{min}$ in dry conditions at 1 bar. $WHSV = 24000\text{ Nm}l/h \cdot g_{cat}$

C.3.1.4 Silver-promoted Catalysts

The catalytic activity exhibited from the silver-promoted catalysts are displayed in Figure [C.9](#), and the differences between the initial and final temperature scans are shown.

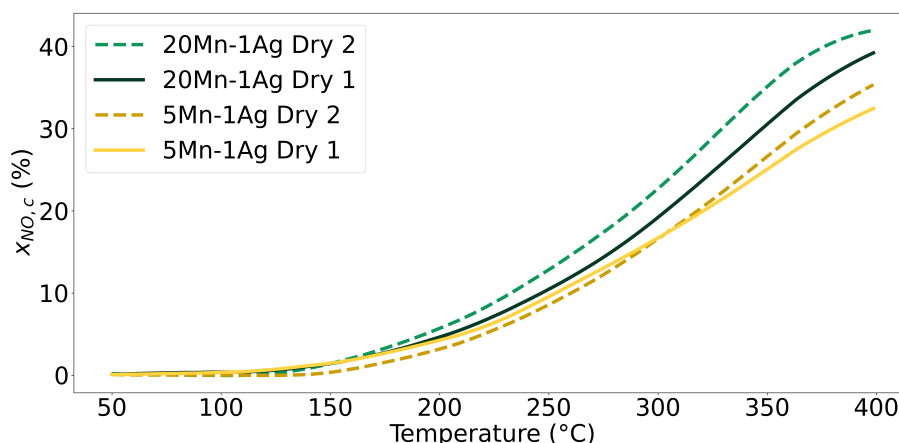
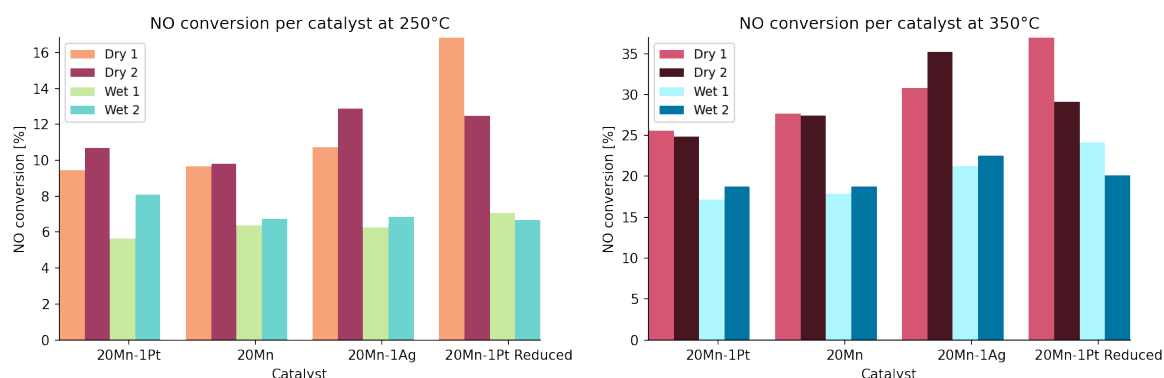


Figure C.9: The NO conversion (%) of 20Mn-1Ag Dry 1 and 2 compared with 5Mn-1Ag Dry 1 and 2 from 50 – 400°C with a ramp rate of 5°C/min in dry conditions at 1 bar. WHSV = 24000 $Nml/h \cdot g_{cat}$

C.3.1.5 Activated Pt-promoted manganese catalyst

The catalytic NO conversion is presented in a bar plot the 20 wt% manganese oxide catalysts at 250°C in Figure C.4 and at 350°C in Figure C.5 where the pretreated 20Mn-1Pt is included. The conversion is calculated from results conducted during the temperature scan test runs, and the NO conversion contribution from the gas-phase reaction is subtracted.



(a) The catalytic NO conversion for the 20wt% manganese catalysts at 250°C. **(b)** The catalytic NO conversion for the 20wt% manganese catalysts at 350°C.

Figure C.10: The catalytic NO conversion is extracted from the temperature scan test runs at 250°C and 350°C.

C.3.2 Temperature Dependency

The temperature dependency for each catalyst is calculated by regression on measured NO conversion in the temperature interval between 250 and 350 °C. The slope is found from the linear equation $y = mx + c$, where m is displayed as *Slope* in Table C.3. P-value is used to assess whether the effect of temperature on NO conversion is statistically significant.

Table C.3: The temperature dependency for each catalyst in the four temperature programs in dry and wet conditions presented as the slope of catalytic conversion as a function of temperature, the R^2 and p-value of each regression calculation.

Catalyst	Temperature Program	Slope	R^2	P-value
5Ag	Dry 1	0.0495	0.9506	4.31E-52
	Dry 2	0.0467	0.9441	1.60E-49
	Wet 1	0.0495	0.9390	1.14E-47
	Wet 2	0.0467	0.9342	4.23E-46
5Mn	Dry 1	0.1118	0.9993	9.49E-143
	Dry 2	0.1298	0.9993	5.61E-144
	Wet 1	0.0940	0.9980	4.77E-121
	Wet 2	0.1111	0.9992	1.92E-139
5Mn-1Pt	Dry 1	0.1165	0.9997	4.91E-163
	Dry 2	0.1283	0.9993	1.69E-143
	Wet 1	0.0910	0.9992	2.68E-139
	Wet 2	0.1111	0.9992	1.92E-139
5Mn-1Ag	Dry 1	0.1538	0.9991	4.25E-138
	Dry 2	0.1816	0.9983	2.17E-124
	Wet 1	0.1195	0.9992	4.72E-141
	Wet 2	0.1219	0.9990	1.88E-134
20Mn	Dry 1	0.1805	0.9978	3.56E-118
	Dry 2	0.1721	0.9994	1.46E-145
	Wet 1	0.1162	0.9991	1.98E-137
	Wet 2	0.1237	0.9972	3.09E-113
20Mn-1Pt	Dry 1	0.1637	0.9973	6.95E-114
	Dry 2	0.1455	0.9970	3.76E-112
	Wet 1	0.0910	0.9992	2.68E-139
	Wet 2	0.1085	0.9964	6.83E-108
20Mn-1Ag	Dry 1	0.2044	0.9977	2.71E-117
	Dry 2	0.2266	0.9979	8.88E-120
	Wet 1	0.1507	0.9975	1.02E-115
	Wet 2	0.1559	0.9977	9.35E-118

C.4 Steady-state conditions

The SiC were investigated under steady-state conditions, and the NO conversion initially, after one hour and two hours, is presented in Table [C.4](#).

Table C.4: NO conversion during two hours at 250°C and 350°C at 1 bar with $WHSV = 24000 Nmn \cdot h^{-1} \cdot g_{cat}^{-1}$ where $t_0 = 0$ min, $t_1 = 60$ min and $t_2 = 120$ min. The %-change between the time increments are presented together with the overall %-change from t_0 to t_2 .

SiC test run	t_0	t_1	t_2	Overall change
NO conversion 250SS Dry	9.03	9.12	9.27	
% change	-	1.1%	1.7%	2.8%
NO conversion 250SS Wet	9.09	8.98	9.03	
% change	-	-1.2%	0.6%	-0.7%
NO conversion 350SS Dry	8.02	8.36	8.19	
% change	-	4.2%	-2.1%	2.0%
NO conversion 350SS Wet	7.09	6.93	7.26	
% change	-	-2.2%	4.7%	2.4%

Table C.5: The %-change within each steady-state experiment at 350° where t_0 represent the start time and t_1 is the final time at 120 minutes. The NO conversion is total conversion, and the gas-phase contribution is included in the conversion.

Catalyst	Change within each test run at 250SS			
	Temperature Program	x_{NO} at t_0	x_{NO} at t_1	% Change
5Ag	Dry 1	10.4	11.0	6.0%
	Dry 2	10.6	10.8	2.4%
	Wet 1	10.6	10.5	-0.3%
	Wet 2	10.5	10.4	-1.1%
5Mn	Dry 1	18.5	18.9	2.0%
	Dry 2	17.4	18.4	6.0%
	Wet 1	14.3	14.3	0.0%
	Wet 2	14.0	14.1	0.8%
5Mn-1Pt	Dry 1	16.7	17.7	6.3%
	Dry 2	16.6	17.9	7.8%
	Wet 1	13.5	13.4	-0.2%
	Wet 2	13.5	13.5	0.2%
5Mn-1Ag	Dry 1	19.4	21.0	8.4%
	Dry 2	19.3	20.9	8.4%
	Wet 1	15.4	15.4	-0.4%
	Wet 2	15.3	15.3	-0.1%
20Mn	Dry 1	15.1	15.4	2.0%
	Dry 2	15.9	16.8	5.8%
	Wet 1	14.3	14.3	-0.1%
	Wet 2	13.8	13.8	0.3%
20Mn-1Pt	Dry 1	19.1	21.8	13.9%
	Dry 2	19.3	21.4	11.0%
	Wet 1	14.3	14.1	-1.8%
	Wet 2	15.1	14.7	-2.5%
20Mn-1Pt Reduced	Dry 1	19.6	21.2	8.1%
	Wet 1	15.0	14.8	-1.0%
20Mn-1Ag	Dry 1	23.4	27.4	16.8%
	Dry 2	24.3	27.8	14.3%
	Wet 1	17.2	17.2	0.4%
	Wet 2	16.8	17.0	1.4%

Table C.6: The %-change within each steady-state experiment at 350° where t_0 represent the start time and t_1 is the final time at 120 minutes. The NO conversion is total conversion, and the gas-phase contribution is included in the conversion.

Catalyst	Change within each test run at 350SS			
	Temperature Program	x_{NO} at t_0	x_{NO} at t_1	% Change
5Ag	Dry 1	14.7	14.7	-0.1%
	Dry 2	15.2	15.3	0.5%
	Wet 1	16.3	15.8	-2.9%
	Wet 2	16.0	15.5	-3.4%
5Mn	Dry 1	29.4	30.9	4.9%
	Dry 2	29.6	31.6	6.9%
	Wet 1	23.5	23.0	-2.2%
	Wet 2	23.3	23.2	-0.2%
5Mn-1Pt	Dry 1	26.8	27.9	4.3%
	Dry 2	27.4	28.2	2.7%
	Wet 1	21.6	21.4	-0.8%
	Wet 2	21.3	21.4	0.4%
5Mn-1Ag	Dry 1	34.3	37.4	8.9%
	Dry 2	35.1	37.4	6.4%
	Wet 1	26.6	26.6	0.2%
	Wet 2	27.0	26.7	-1.4%
20Mn	Dry 1	29.2	29.7	1.9%
	Dry 2	26.8	26.2	-2.3%
	Wet 1	25.3	24.0	-5.1%
	Wet 2	25.2	24.6	-2.4%
20Mn-1Pt	Dry 1	32.1	34.2	6.3%
	Dry 2	33.7	37.0	9.7%
	Wet 1	23.4	23.5	0.5%
	Wet 2	24.7	24.1	-2.6%
20Mn-1Pt Reduced	Dry 1	35.0	36.2	3.6%
	Wet 1	27.6	26.6	-3.7%
20Mn-1Ag	Dry 1	40.4	46.4	15.1%
	Dry 2	43.4	47.8	10.2%
	Wet 1	31.9	32.1	0.5%
	Wet 2	31.8	32.1	1.1%

C.5 Characterization after Activity Measurements

C.5.1 XRD

The XRD patterns after analyzing the catalysts before and after the catalytic activity experiments are presented in Figure [C.12](#), [C.13](#) and [C.14](#) for unpromoted manganese catalysts, silver-promoted manganese catalysts and platinum-promoted catalysts respectively.

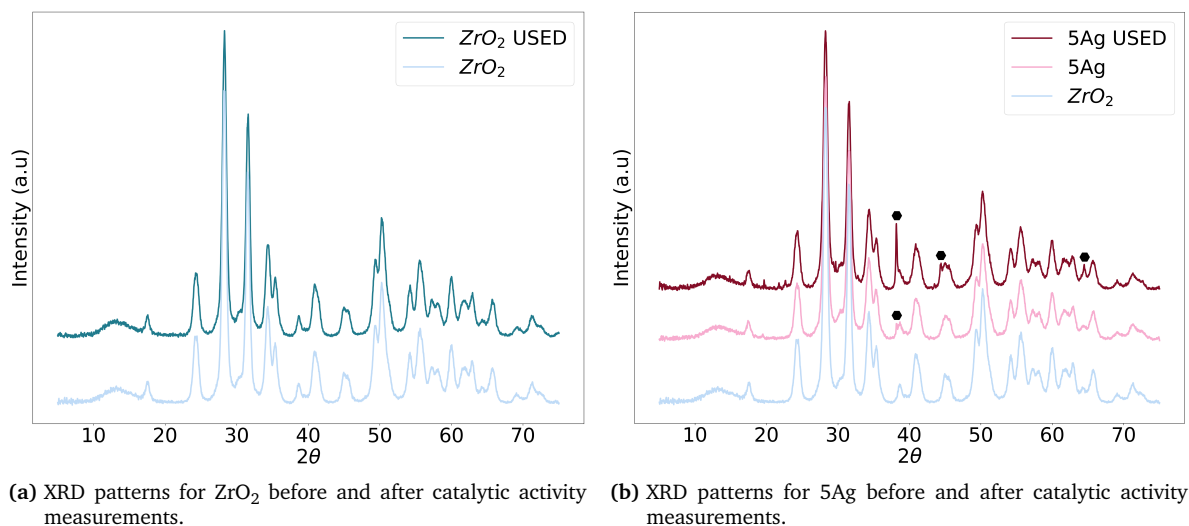


Figure C.11: XRD patterns of ZrO_2 and 5Ag before and after catalytic activity measurements. The settings were 40 kV and 40 mA with a wavelength of 1.54060 \AA employing $Cu \alpha$ radiation. Ag^0 (●) is indicated with a hexagon.

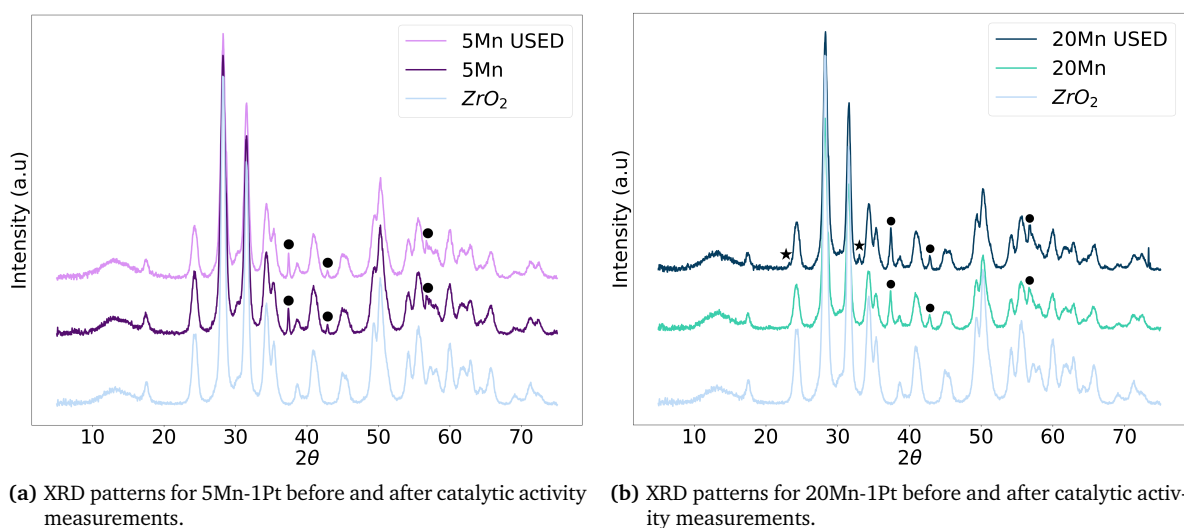


Figure C.12: XRD patterns of 5Mn and 20Mn before and after catalytic activity measurements. The settings were 40 kV and 40 mA with a wavelength of 1.54060 \AA employing $Cu \alpha$ radiation. $\gamma\text{-MnO}_2$ (●) is indicated with a dot and Mn_2O_3 (★) is indicated with a star.

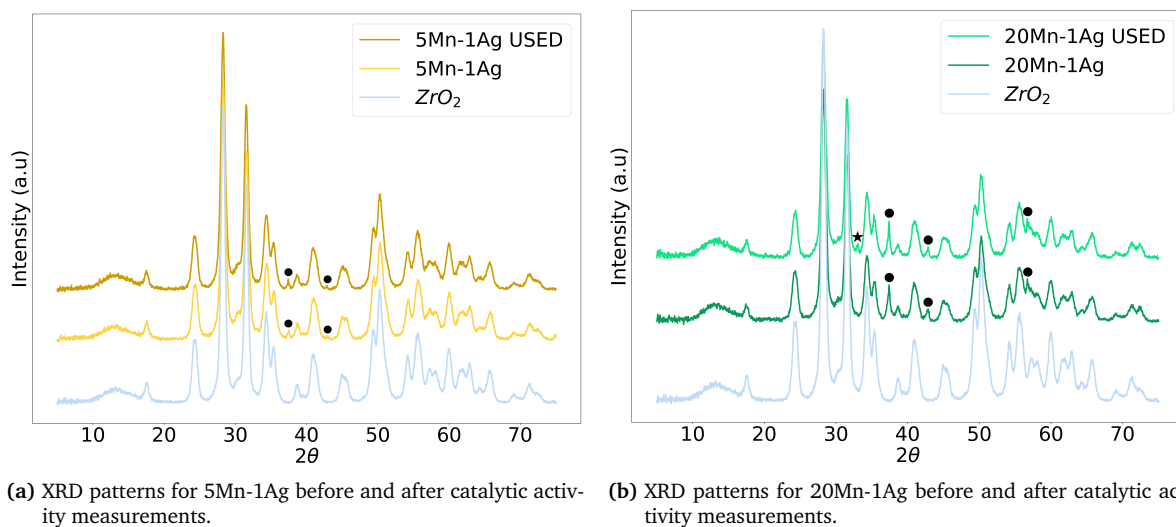


Figure C.13: XRD patterns of 5Mn-1Ag and 20Mn-1Ag before and after catalytic activity measurements. The settings were 40 kV and 40 mA with a wavelength of 1.54060 Å employing Cu α radiation. γ -MnO₂ (●) is indicated with a dot and Mn₂O₃ (★) is indicated with a star.

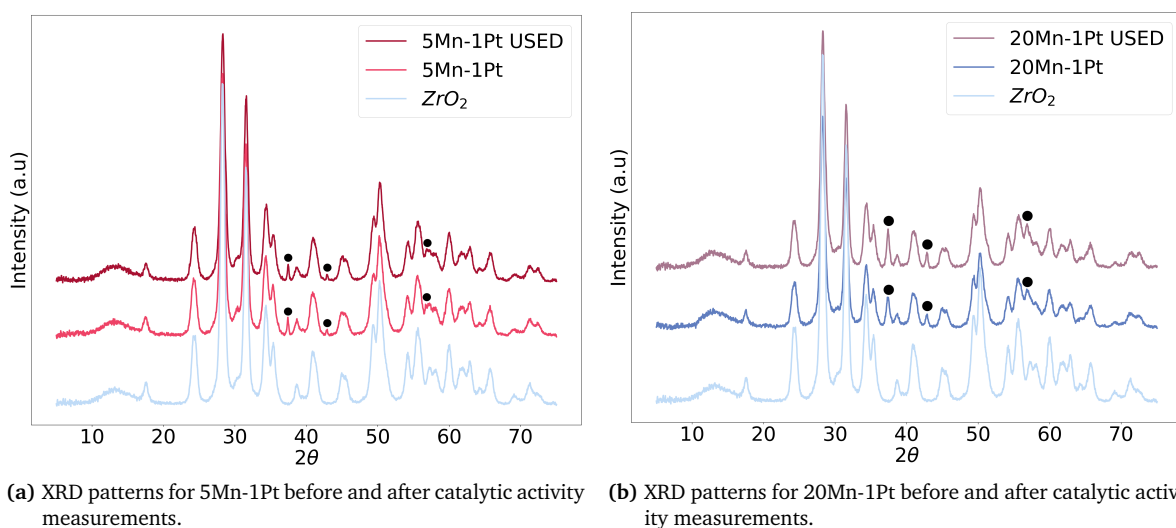
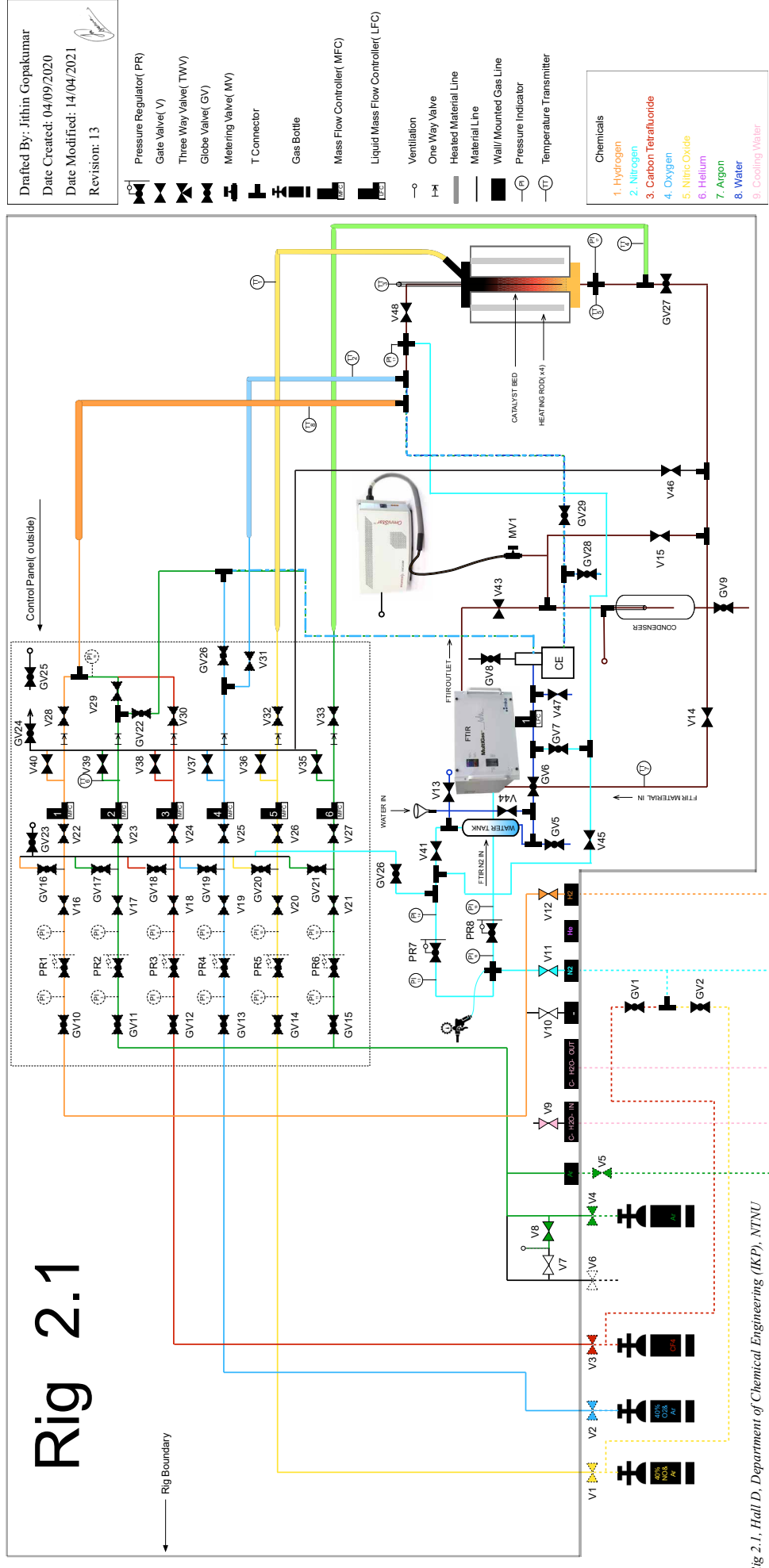


Figure C.14: XRD patterns of 5Mn-1Pt and 20Mn-1Pt before and after catalytic activity measurements. The settings were 40 kV and 40 mA with a wavelength of 1.54060 Å employing Cu α radiation. γ -MnO₂ (●) is indicated with a dot and Mn₂O₃ (★) is indicated with a star.

Appendix D

Flow Scheme of Rig 2.1

Rig 2.1



Rig 2.1, Hall D, Department of Chemical Engineering (IKP), NTNU

Appendix E

Risk Assessment



ID	40056	Status	Date
Risk Area	Risikovurdering: Helse, miljø og sikkerhet (HMS)	Created	07.09.2020
Created by	Sunniva Vold	Assessment started	09.09.2020
Responsible	Sunniva Vold	Measures decided	
		Closed	

Risk Assessment:**CAT, Master student, 2020, Sunniva Vold**

Valid from-to date:

9/7/2020 - 9/7/2023

Location:

Kjemi 5, Hall D, Gløshaugen, Sem Sælands Vei 4

Goal / purpose

To study the oxidation kinetics of nitric oxide (NO) using different catalysts.
Make different catalysts and characterize them by using different characterization techniques.

Background

Gasses Involved in the process mainly consists of NO, NO₂, O₂, H₂, and N₂.

Reaction Conditions:

1. The typical feed for the process consists of 10% NO, 6% O₂, and 15% H₂O. 2. Argon (Ar) is used as the inert gas in the process.
3. Pressure 1–10 bar; and
4. Temperature 150 – 450 degrees C.
5. Catalyst weight: 500mg

An FTIR instrument is used in the setup for gas analysis. When this is in use, liquid nitrogen is required and will be poured in manually.

Gas detectors are placed inside the setup for measuring NO and H₂. Additionally, three portable detectors for H₂, NO & NO₂ is also present inside the setup.

Water is introduced into the feed stream using a Controlled Evaporator Mixer (CEM). The water vapor generation system contains N₂ pressured water tank fitted with a filter (15 µm) at the outlet, a liquid flow controller (typical flow range = 2 g/h), also carrier gases O₂ and Ar, a temperature-controlled mixer and evaporation device.

Description and limitations



The research activities will be carried out as part of the Catalysis group at IKP, NTNU.

The project will start with the synthesis of different catalysts, followed by characterization, and then test the made catalysts in the reactor where NO to NO₂ oxidation occurs.

Preparation of Catalyst:

In the preparation of the catalysts, the preparation method will be the Incipient Wetness Method.

Incipient Wetness Method:

Active Material: Manganese

Promoters: Platinum, Silver

Support: Zirconia

List of chemicals: Pt(IV)(NO₃)₄ solution, Pt 15% w/w, ZrO₂, Mn(NO₃)₂, AgNO₃,

The support material will be calcined before catalyst synthesis.

Zirconia is pre-calcined at 650 degrees C for two hours in the presence of synthetic air, with a temperature ramp rate of 10 degrees C /min. The precursor solution is added dropwise to the calcined support and dried at 120 degrees C (usually kept overnight). The dried catalyst will be calcined again with a dry airflow (170 Ncm³/min) and heating at 10 degrees C /min ramp rate, which is held for 2 hours and subsequently cooled inside the calcination reactor.

The temperature used for the latter calcination is based on the different active material:

Mn - Ambient to 400 degrees C (held for 6 hrs)

Several characterization techniques will be used to characterize the prepared catalysts and study their surface-specific and temperature-related properties. Few listed methods are BET/BJH, TPR, XRD, Chemisorption, TGA, and SEM.

Location of Activity measurements: ChemHallD 2nd floor at rig 2.1 and the preparation lab on the 1st floor in ChemHallD.

Prerequisites, assumptions and simplifications

Prerequisites:

1. The setup users must undergo proper training by authorized personnel
2. Protective equipment like gloves, lab coat, and goggles, etc should be used all the time
3. The lab scheduler must be updated when in use
4. Apparatus card to be up to date

Steps for setup switch off procedure

1. The immediate closure of all the gas bottles in use
2. Cutting off the electricity to the whole setup. (In case of emergency, an emergency button located on the setup will be activated for safety)

Safety measures related to spreading of Covid-19 infection:

1. Wash hands before you start the experiment and after when you exit the lab;
2. Use of nitrile gloves, and goggles in the lab;
3. Disinfection with ethanol (strength: 70% or more) on all surfaces you are in contact with (before and after the use), specifically door knobs – card reader with code panel, keyboard, mouse, screen, desk, and FTIR;
4. Avoid direct contact with your face before cleansing your hands;
5. Keep 1m distance from colleagues and other personnel at all times.
6. All lab activities are pre-planned and updated in the IKP activity 2020 Teams group for enabling other setup users to be aware of common lab usage.

Attachments



Argon.pdf
Pt(IV) nitrate solution, Pt 15 ww.pdf
Oxygen.pdf
ZrO2.pdf
NO_Flowscheme_Colour_Coded.pdf
CobaltNitrate.pdf
OSHA3990.pdf
Nitric Oxide.pdf
Hydrogen.pdf
AgNO3.pdf
Mn(NO3)2.pdf
Ce(NO3)2.pdf
NO_Wiringscheme_Colour_Coded.pdf
NOx_Apparatus_Card_Jithin (2).doc
NO2.pdf
null.pdf
PrintMSDSAction.do.pdf
CO-msds.pdf

References

[Ingen registreringer]

Summary, result and final evaluation

The summary presents an overview of hazards and incidents, in addition to risk result for each consequence area.

Hazard: Working in the Lab and at campus During Covid-19 Pandemic

Incident: Interactions with Colleagues and Other Personnel

Consequence area: Helse
Risk before measures: Risiko after measures:

Incident: Using the same Tools and Equipment

Consequence area: Helse
Risk before measures: Risiko after measures:

Hazard: Characterization Techniques

Incident: BET/BJH

Consequence area: Helse
Risk before measures: Risiko after measures:

Incident: TPR/TPD

Consequence area: Helse
Risk before measures: Risiko after measures:

Incident: XRD

Consequence area: Helse
Risk before measures: Risiko after measures:

Incident: XPS



Consequence area: Helse
Risk before measures: Risiko after measures:

Incident: Chemisorption with CO


Consequence area: Helse
Ytre miljø Risiko after measures:
Materielle verdier Risiko after measures:

**Hazard: Characterization Techniques****Incident: Chemisorption with CO**



Omdømme

Risk before
measures: Risiko after
measures:**Hazard: Use of High Pressure Gases****Incident: Inert Gas Leak****Consequence area:** HelseRisk before
measures: Risiko after
measures:


Ytre miljø

Risk before
measures: Risiko after
measures:



Materielle verdier

Risk before
measures: Risiko after
measures:**Incident: Expansion and Depletion of Oxygen - Uncontrollable****Consequence area:** HelseRisk before
measures: Risiko after
measures:



Ytre miljø

Risk before
measures: Risiko after
measures:



Materielle verdier

Risk before
measures: Risiko after
measures:**Incident: Inhalation of inert gases due to leaks****Consequence area:** HelseRisk before
measures: Risiko after
measures:

Ytre miljø

Risk before
measures: Risiko after
measures:**Incident: Pressure Disk Burst****Consequence area:** HelseRisk before
measures: Risiko after
measures:

Ytre miljø

Risk before
measures: Risiko after
measures:**Hazard: Catalyst Chemicals****Incident: Pt(IV)(NO₃)₄****Consequence area:** HelseRisk before
measures: Risiko after
measures:

**Hazard: Catalyst Chemicals****Incident: Pt(IV)(NO3)4**

Ytre miljø

Risk before
measures: Risiko after
measures:

Materielle verdier

Risk before
measures: Risiko after
measures:**Incident: ZrO2****Consequence area: Helse**Risk before
measures: Risiko after
measures:**Incident: Mn(NO3)2****Consequence area: Helse**Risk before
measures: Risiko after
measures:**Incident: AgNO3****Consequence area: Helse**Risk before
measures: Risiko after
measures:

Ytre miljø

Risk before
measures: Risiko after
measures:**Hazard: Use of Reactant Gases - NO, H2 and NO2****Incident: Gas Leak****Consequence area: Helse**Risk before
measures: Risiko after
measures:

Ytre miljø

Risk before
measures: Risiko after
measures:**Incident: Fire****Consequence area: Helse**Risk before
measures: Risiko after
measures:

Ytre miljø

Risk before
measures: Risiko after
measures:

Materielle verdier

Risk before
measures: Risiko after
measures:**Incident: Explosion****Consequence area: Helse**Risk before
measures: Risiko after
measures:



Hazard: Use of Reactant Gases - NO, H2 and NO2

Incident: Explosion

Ytre miljø	Risk before measures:		Risiko after measures:	
Materielle verdier	Risk before measures:		Risiko after measures:	
Omdømme	Risk before measures:		Risiko after measures:	

Incident: Formation of NOx gases and Inhalation to respiratory system

Consequence area: Helse	Risk before measures:		Risiko after measures:	
Ytre miljø	Risk before measures:		Risiko after measures:	

Hazard: Heated Surfaces

Incident: Skin Burns

Consequence area: Helse	Risk before measures:		Risiko after measures:	
--------------------------------	-----------------------	--	------------------------	--

Hazard: Electricity/Power cuts

Incident: Ventilation Cut

Not to be analyzes.

Hazard: Calcination

Incident: Accident related to high temperatures

Consequence area: Helse	Risk before measures:		Risiko after measures:	
Materielle verdier	Risk before measures:		Risiko after measures:	

Final evaluation

Organizational units and people involved

A risk assessment may apply to one or more organizational units, and involve several people. These are listed below.

Organizational units which this risk assessment applies to

- Institutt for kjemisk prosesssteknologi

Participants

Estelle Marie M. Vanhaecke

Karin Wiggen Dragsten

Anne Hoff

Magnus Rønning

Jithin Gopakumar

Readers

[Ingen registreringer]

Others involved/stakeholders

[Ingen registreringer]

The following accept criteria have been decided for the risk area Risikovurdering: Helse, miljø og sikkerhet (HMS):

Helse



Materielle verdier



Omdømme



Ytre miljø



Overview of existing relevant measures which have been taken into account

The table below presents existing measures which have been taken into account when assessing the likelihood and consequence of relevant incidents.

Hazard	Incident	Measures taken into account
Working in the Lab and at campus During Covid-19 Pandemic	Interactions with Colleagues and Other Personnel	Personal Safety Measures - Covid-19
	Interactions with Colleagues and Other Personnel	Personal Safety Measures - Covid-19
	Using the same Tools and Equipment	Personal Safety Measures - Covid-19
	Using the same Tools and Equipment	Personal Safety Measures - Covid-19
Characterization Techniques	BET/BJH	Personal measures
	BET/BJH	Safety Measures
	TPR/TPD	Personal measures
	TPR/TPD	Instrument/method training
	TPR/TPD	Gas detection
	TPR/TPD	HSE Documentation
	TPR/TPD	Safety Measures
	XRD	Personal measures
	XRD	Instrument/method training
	XRD	HSE Documentation
	XRD	Dust Mask
	XRD	Safety Measures
	XPS	Personal measures
	XPS	Instrument/method training
XPS	HSE Documentation	
XPS	Safety Measures	
Use of High Pressure Gases	Chemisorption with CO	Gas detection
	Chemisorption with CO	Gas Handling
	Inert Gas Leak	Fume hood
	Inert Gas Leak	Local exhaust
	Inert Gas Leak	Gas detection
	Inert Gas Leak	Ventilation
	Expansion and Depletion of Oxygen - Uncontrollable	
	Inhalation of inert gases due to leaks	Gas detection
Catalyst Chemicals	Inhalation of inert gases due to leaks	Ventilation
	Inhalation of inert gases due to leaks	Gas Handling
	Pressure Disk Burst	HSE Documentation
	Pt(IV)(NO ₃) ₄	Personal measures



Catalyst Chemicals	Pt(IV)(NO ₃) ₄	Ventilation
	Pt(IV)(NO ₃) ₄	Safety Measures
	ZrO ₂	Personal measures
	ZrO ₂	Safety Measures
	Mn(NO ₃) ₂	Personal measures
	Mn(NO ₃) ₂	Fume hood
	Mn(NO ₃) ₂	Dust Mask
	Mn(NO ₃) ₂	Ventilation
	Mn(NO ₃) ₂	Safety Measures
	AgNO ₃	Personal measures
	AgNO ₃	Safety Measures
	Use of Reactant Gases - NO, H ₂ and NO ₂	Gas Leak
Gas Leak		Gas detection
Gas Leak		Ventilation
Gas Leak		Gas Handling
Gas Leak		Safety Measures
Fire		Gas detection
Fire		Ventilation
Fire		Gas Handling
Fire		Safety Measures
Explosion		Personal measures
Explosion		Fume hood
Explosion		Gas detection
Explosion		HSE Documentation
Explosion		Ventilation
Explosion		Gas Handling
Explosion		Safety Measures
Explosion		Working Regulations at NTNU (after working hours)
Formation of NO _x gases and Inhalation to respiratory system		Personal measures
Formation of NO _x gases and Inhalation to respiratory system		Ventilation
Heated Surfaces		Skin Burns
	Skin Burns	Instrument/method training
	Skin Burns	HSE Documentation
Calcination	Accident related to high temperatures	Personal measures
	Accident related to high temperatures	Instrument/method training
	Accident related to high temperatures	Safety Measures

Existing relevant measures with descriptions:

**Personal measures**

Safety goggles mandatory in all laboratories
Lab coat

Gloves - while handling and refilling liquid nitrogen in the MKS-FTIR gaz analyzer.

Fume hood

[Ingen registreringer]

Local exhaust

[Ingen registreringer]

Instrument/method training

[Ingen registreringer]

Gas detection

Where it is installed
Portable detectors if not installed

HSE Documentation

The laboratory will always be equipped with a room card and the instrument should have an updated copy of the risk assessment, operating instructions, and apparatus card.

The manuals will include emergency stop procedures for the setup. The phone number of the rig in charge personnel will be provided.

Dust Mask

Reduces risk of inhalation of particles when exposed to the materials used.

Ventilation

The setup/rig is enclosed inside a cabinet with proper ventilation equipment.

Gas Handling

Any changes to the gas bottles will be performed by authorized personnel.

Existing gas bottles will be checked for leaks near the bottle mouth.

There is NO gas detector installed in the rig cabinet.

There are portable detectors capable of measuring NO, H2 and NO2 (used mainly for leak testing).

Safety Measures

Gas & Fire alarm is present in Kjemi 5 Hall D

A fire extinguisher is available for all lab users.

Emergency shower/eye washer is available for all lab users.

Ventilation: All off-gases from the reactor are directed to the ventilation system present in the lab.

Working Regulations at NTNU (after working hours)

NTNU students and employees are not allowed to work alone after 7 pm and during the weekends.

Working after 19:00 or on the weekends, you need to be at least 2 in the lab or in the building with regular check-ups (every 30 minutes). Both of the people need to have access to the labs.



Personal Safety Measures - Covid-19

Disinfect the common surfaces, such as computer keyboard, mouses, machine surfaces, and panels.
Disinfection to be carried out using ethanol (strength: 70% or higher).
Distance from other personnel (approx. 2m).

Risk analysis with evaluation of likelihood and consequence

This part of the report presents detailed documentation of hazards, incidents and causes which have been evaluated. A summary of hazards and associated incidents is listed at the beginning.

The following hazards and incidents has been evaluated in this risk assessment:

- **Working in the Lab and at campus During Covid-19 Pandemic**
 - Interactions with Colleagues and Other Personnel
 - Using the same Tools and Equipment
- **Characterization Techniques**
 - BET/BJH
 - TPR/TPD
 - XRD
 - XPS
 - Chemisorption with CO
- **Use of High Pressure Gases**
 - Inert Gas Leak
 - Expansion and Depletion of Oxygen - Uncontrollable
 - Inhalation of inert gases due to leaks
 - Pressure Disk Burst
- **Catalyst Chemicals**
 - Pt(IV)(NO₃)₄
 - ZrO₂
 - Mn(NO₃)₂
 - AgNO₃
- **Use of Reactant Gases - NO, H₂ and NO₂**
 - Gas Leak
 - Fire
 - Explosion
 - Formation of NO_x gases and Inhalation to respiratory system
- **Heated Surfaces**
 - Skin Burns
- **Calcination**
 - Accident related to high temperatures

Detailed view of hazards and incidents:

Hazard: Working in the Lab and at campus During Covid-19 Pandemic

Incident: Interactions with Colleagues and Other Personnel

Cause: Covid-19 Symptomatic People to Others

Likelihood of the incident (common to all consequence areas): **Very likely (5)**

Kommentar:

It is very likely to have conversations and be close to other people at the university, and when the virus is contagious you can easily have the virus.

Consequence area: Helse

Assessed consequence: **Large (3)**

Comment: [Ingen registreringer]

Risk:**Incident: Using the same Tools and Equipment**

Cause: Common equipment

Likelihood of the incident (common to all consequence areas): **Very likely (5)**

Kommentar:

Personnel can forget after or before the experiment to clean the surfaces they come in contact with.

Consequence area: Helse

Assessed consequence: **Large (3)**

Comment: [Ingen registreringer]

Risk:



Hazard: Characterization Techniques

Incident: BET/BJH

Cause: Spills on Skin

Likelihood of the incident (common to all consequence areas): **Less likely (2)**

Kommentar:

The characterization requires the use of liquid nitrogen, but with the right safety equipment it is not likely to spill on skin. Proper gloves has to be used.

Consequence area: Helse

Assessed consequence: **Large (3)**

Comment: Liquid Nitrogen:
H281 - CONTAINS REFRIGERATED GAS; MAY CAUSE CRYOGENIC BURNS
OR INJURY

Risk:



**Incident: TPR/TPD**

Cause: Spills on Skin

Cause: Inhalation/ingestion during preparation

Cause: The reactor breaks

Cause: Skin Burns

Likelihood of the incident (common to all consequence areas): **Less likely (2)**

Kommentar:

In this characterization techniques a small u-shaped glass is used as a reactor. It is important to not have too high pressure so it does not break. When the pressure is controlled at no more than 4-5 bars, it is not likely that the reactor will break.

The gas used is normally Hydrogen, but due to gas detection it is not likely that it will cause any inhalation or ignite fire.

The temperature is high, but it is not likely to have skin burns when this is controlled and when the safety measure is used.

Consequence area: Helse

Assessed consequence: **Large (3)**

Comment: [Ingen registreringer]

Risk:

Incident: XRD

Cause: Spills on Skin

Cause: Radiation exposures (eyes)

Likelihood of the incident (common to all consequence areas): **Less likely (2)**

Kommentar:

In the XRD-lab there is special closed holders for your sample if you are working with hazardous chemicals. You'll need special training to use these holders, and the sample preparation have to be done in a fume hood. The recollection of your sample and initial cleaning of the sample holder after measurement must be done in a fume hood as well. With this safety measures it is not likely to have chemicals spilled on the skin.

When working with Cobalt, a mask should be used so the likelihood for inhalation is low.

The propbaility for eye radiation is low when the XRD is working as is should, and normally it is not run when the students are present.

Consequence area: Helse

Assessed consequence: **Large (3)**

Comment: If the catalyst is spilled on your skin, there is different hazardous statements involved. See the section "Chemicals".

Radiation exposure on the eye is damaging.

Risk:**Incident: XPS**

Cause: Spills on Skin

Cause: Radiation exposures (eyes)

Likelihood of the incident (common to all consequence areas): **Less likely (2)**

Kommentar:

It is not likely to spill the catalyst on the skin when the personal safety measures is done.

Consequence area: Helse

Assessed consequence: **Large (3)**

Comment: If the catalyst is spilled on your skin, there is different hazardous statements involved. See the section "Chemicals".

Risk:

Incident: Chemisorption with CO

Chemisorption with CO is carried out to measure the metal dispersion of Pt in the catalysts containing Pt.

Cause: Inhalation

Cause: Fire

Likelihood of the incident (common to all consequence areas): **Unlikely (1)**

Kommentar:

There are several CO detectors at the lab, and when using the gas, a leak test is always performed with a CO detector. The likelihood of inhalation is, therefore, small.
The explosion may occur if the gas bottle is heated, but fire alarms will detect fire and therefore the likelihood for fire is also small.

Consequence area: Helse

Assessed consequence: **Very large (4)**

Comment: H331 - TOXIC IF INHALED
H360 - MAY DAMAGE FERTILITY OR THE UNBORN CHILD
H372 - CAUSES DAMAGE TO ORGANS (CENTRAL NERVOUS SYSTEM) THROUGH PROLONGED OR REPEATED EXPOSURE

Risk:

**Consequence area: Ytre miljø**

Assessed consequence: **Very large (4)**

Comment: H220 - EXTREMELY FLAMMABLE GAS
H280 - CONTAINS GAS UNDER PRESSURE; MAY EXPLODE IF HEATED
CGA-HG04 - MAY FORM EXPLOSIVE MIXTURES WITH AIR
CGA-HG10 - ASPHYXIATING EVEN WITH ADEQUATE OXYGEN

Risk:

**Consequence area: Materielle verdier**

Assessed consequence: **Very large (4)**

Comment: H220 - EXTREMELY FLAMMABLE GAS
H280 - CONTAINS GAS UNDER PRESSURE; MAY EXPLODE IF HEATED

If the gas explodes, will this will damage other material in the lab.

Risk:

**Consequence area: Omdømme**

Assessed consequence: **Large (3)**

Comment: If a person is poisoned or if the gas explodes, this will harm the reputation of NTNU.

Risk:





Hazard: Use of High Pressure Gases

Incident: Inert Gas Leak

Cause: Loose connections in the gas pipes

Likelihood of the incident (common to all consequence areas): **Likely (3)**

Kommentar:

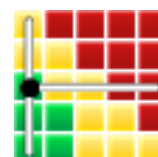
When a leak test is done, an inert gas is used. It is likely that it is a leak, but the inert gas is used because it is not dangerous.

Consequence area: Helse

Assessed consequence: **Small (1)**

Comment: [Ingen registreringer]

Risk:

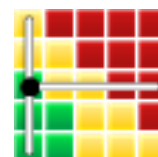


Consequence area: Ytre miljø

Assessed consequence: **Small (1)**

Comment: [Ingen registreringer]

Risk:



Consequence area: Materielle verdier

Assessed consequence: **Small (1)**

Comment: [Ingen registreringer]

Risk:



Incident: Expansion and Depletion of Oxygen - Uncontrollable

Likelihood of the incident (common to all consequence areas): **Less likely (2)**

Kommentar:

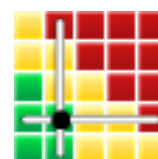
[Ingen registreringer]

Consequence area: Helse

Assessed consequence: **Medium (2)**

Comment: [Ingen registreringer]

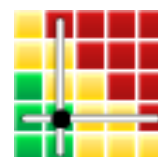
Risk:

**Consequence area: Ytre miljø**

Assessed consequence: **Medium (2)**

Comment: [Ingen registreringer]

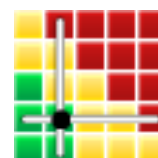
Risk:

**Consequence area: Materielle verdier**

Assessed consequence: **Medium (2)**

Comment: [Ingen registreringer]

Risk:



Incident: Inhalation of inert gases due to leaks

Cause: Inhalation

Likelihood of the incident (common to all consequence areas): **Likely (3)**

Kommentar:

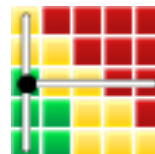
Proper ventilation is present and leakage test is done regularly.

Consequence area: Helse

Assessed consequence: **Small (1)**

Comment: [Ingen registreringer]

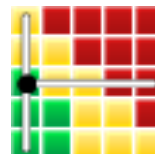
Risk:

**Consequence area: Ytre miljø**

Assessed consequence: **Small (1)**

Comment: [Ingen registreringer]

Risk:

**Incident: Pressure Disk Burst**

Cause: Gas release into the box from the ventilation inlet

Likelihood of the incident (common to all consequence areas): **Less likely (2)**

Kommentar:

[Ingen registreringer]

Consequence area: Helse

Assessed consequence: **Large (3)**

Comment: [Ingen registreringer]

Risk:





Consequence area: Ytre miljø

Assessed consequence: **Large (3)**

Comment: [Ingen registreringer]

Risk:



Hazard: Catalyst Chemicals

Incident: Pt(IV)(NO₃)₄

Cause: Spills on Skin

Cause: Inhalation/ingestion during preparation

Cause: Splash into the eyes

Likelihood of the incident (common to all consequence areas): **Less likely (2)**

Kommentar:

When working with the chemical, there is a chance to spill this on the skin. With the proper use of personal safety equipment, and working in a lab with ventilation etc, the likelihood for spillage or inhalation is low.

Consequence area: Helse

Assessed consequence: **Large (3)**

Comment: Causes severe skin burns and eye damage.
Causes serious eye damage.
May cause an allergic skin reaction.

Risk:**Consequence area: Ytre miljø**

Assessed consequence: **Large (3)**

Comment: May intensify fire; oxidizer.

Risk:**Consequence area: Materielle verdier**

Assessed consequence: **Large (3)**

Comment: May be corrosive to metals.

Risk:

Incident: ZrO2

Cause: Spills on Skin

Cause: Inhalation/ingestion during preparation

Cause: Splash into the eyes

Likelihood of the incident (common to all consequence areas): **Less likely (2)**

Kommentar:

When working with the chemical, there is a chance to spill this on the skin. With the proper use of personal safety equipment, and working in a lab with ventilation etc, the likelihood for spillage or inhalation is low.

Consequence area: Helse

Assessed consequence: **Small (1)**

Comment: No Hazards characteristics

Risk:**Incident: Mn(NO3)2**

Cause: Spills on Skin

Cause: Inhalation/ingestion during preparation

Cause: Splash into the eyes

Likelihood of the incident (common to all consequence areas): **Less likely (2)**

Kommentar:

When working with the chemical, there is a chance to spill this on the skin. With the proper use of personal safety equipment, and working in a lab with ventilation etc, the likelihood for spillage or inhalation is low.

Consequence area: Helse

Assessed consequence: **Large (3)**

Comment: Causes serious eye irritation.
May cause respiratory irritation.
Irritating to skin.

Risk:

**Incident: AgNO3**

Cause: Spills on Skin

Cause: Inhalation/ingestion during preparation

Cause: Splash into the eyes

Cause: Washed out in the sink

Likelihood of the incident (common to all consequence areas): **Less likely (2)**

Kommentar:

When working with the chemical, there is a chance to spill this on the skin. With the proper use of personal safety equipment, and working in a lab with ventilation etc, the likelihood for spillage or inhalation is low.

The chemical will not be spilled in the sink, but will be thrown in a special waste for further treatment. This makes it unlikely that it will end up in the nature.

Consequence area: Helse

Assessed consequence: **Very large (4)**

Comment: H272 - May intensify fire; oxidizer
H314 - Causes severe skin burns and eye damage
H410 - Very toxic to aquatic life with long lasting effects

Risk:**Consequence area: Ytre miljø**

Assessed consequence: **Very large (4)**

Comment: H410 - Very toxic to aquatic life with long lasting effects

Risk:

Hazard: Use of Reactant Gases - NO, H2 and NO2

Incident: Gas Leak

Cause: Loose connections to/from the reactor

Likelihood of the incident (common to all consequence areas): **Less likely (2)**

Kommentar:

There is a possibility that there will be a leakage in the system, but before every experimental run, a gas leak detection will be done. This makes it less likely that the reactant gases will leak. The experiment is also happening inside a ventilated box with gas detectors.

Consequence area: Helse

Assessed consequence: **Very large (4)**

Comment: NO: May cause or intensify fire; oxidizer.
Contains gas under pressure; may explode if heated.
Fatal if inhaled.
Symptoms may be delayed.
Causes severe skin burns and eye damage.
Causes serious eye damage.

H2:
Extremely flammable gas.
May form explosive mixtures with air.
Contains gas under pressure; may explode if heated.
May displace oxygen and cause rapid suffocation.
Burns with invisible flame

NO2: May cause or intensify fire; oxidizing.
H314 Causes severe skin burns and eye damage.
H412 Harmful to aquatic life with long lasting effects.

Risk:



Consequence area: Ytre miljø

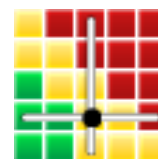
Assessed consequence: **Large (3)**

Comment: NO: May cause or intensify fire; oxidizer.
Contains gas under pressure; may explode if heated.

H2:
Extremely flammable gas.
May form explosive mixtures with air.
Contains gas under pressure; may explode if heated.
May displace oxygen and cause rapid suffocation.
Burns with invisible flame

NO2: May cause or intensify fire; oxidizing.
H412 Harmful to aquatic life with long lasting effects.

Risk:



**Incident: Fire**

Likelihood of the incident (common to all consequence areas): **Less likely (2)**

Kommentar:

The gas detector will detect small amount of gasses and will shutoff all the MFC.

Also, gasses are not combustibile themselves but they aid in combustion. So these things are less likely to lead to the fire incidents

The gases will be detected if they start leaking, and the amount of gas will not be big enough to ignite a fire. There will not be any flames used un the experiment.

Consequence area: Helse

Assessed consequence: **Very large (4)**

Comment: [Ingen registreringer]

Risk:**Consequence area: Ytre miljø**

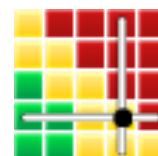
Assessed consequence: **Very large (4)**

Comment: [Ingen registreringer]

Risk:**Consequence area: Materielle verdier**

Assessed consequence: **Very large (4)**

Comment: [Ingen registreringer]

Risk:

**Incident: Explosion**

Cause: High temperatures

Cause: Loose connections to/from the reactor

Likelihood of the incident (common to all consequence areas): **Less likely (2)**

Kommentar:

Proper leakage tests and ventilation can avoid any explosions in the setup.

Consequence area: Helse

Assessed consequence: **Very large (4)**

Comment: An explosion could cause serious injuries if you are near.

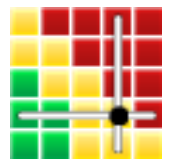
Risk:

**Consequence area: Ytre miljø**

Assessed consequence: **Very large (4)**

Comment: An explosion will most likely release dangerous gases, or cause a fire which again release dangerous gases.

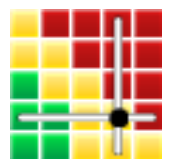
Risk:

**Consequence area: Materielle verdier**

Assessed consequence: **Very large (4)**

Comment: Material will be damaged if an explosion happen.

Risk:

**Consequence area: Omdømme**

Assessed consequence: **Very large (4)**

Comment: An explosion will be covered in the news, and it will not be good for NTNUs reputation.

Risk:



**Incident: Formation of NOx gases and Inhalation to respiratory system**

Cause: (uten tittel)

Likelihood of the incident (common to all consequence areas): **Less likely (2)**

Kommentar:

It is not likely that NOx gases will form because the system is heated and isolated. There is also gas detectors which will trigger the gas alarm if the gas level is too high.

Consequence area: Helse

Assessed consequence: **Very large (4)**

Comment: [Ingen registreringer]

Risk:

**Consequence area: Ytre miljø**

Assessed consequence: **Very large (4)**

Comment: [Ingen registreringer]

Risk:





Hazard: Heated Surfaces

Incident: Skin Burns

Likelihood of the incident (common to all consequence areas): **Less likely (2)**

Kommentar:

[Ingen registreringer]

Consequence area: Helse

Assessed consequence: **Large (3)**

Comment: [Ingen registreringer]

Risk:



Hazard: Calcination

Incident: Accident related to high temperatures

Cause: Uncontrolled high temperature

Cause: Skin burns

Likelihood of the incident (common to all consequence areas): **Unlikely (1)**

Kommentar:

During the calcination method, you have to deal with different temperatures. Sometimes the wanted temperatures are high, and the maximum temperature possible in the calcination oven is over 1000 degrees celcius. When the instructions are followed, and when you wait to touch any sample until it is cooled, it is not likely to have a skin burn, or a uncontrolled high temperature.

Consequence area: Helse

Assessed consequence: **Large (3)**

Comment: If some warm parts are in contact with your skin, the skin burn can be damaging for the skin.

Risk:



Consequence area: Materielle verdier

Assessed consequence: **Large (3)**

Comment: Uncontrolled high temperatures will destroy material who is not made for the high temperatures.

Risk:





Overview of risk mitigating measures which have been decided:

Below is an overview of risk mitigating measures, which are intended to contribute towards minimizing the likelihood and/or consequence of incidents:

Overview of risk mitigating measures which have been decided, with description:



Detailed view of assessed risk for each hazard/incident before and after mitigating measures

